Study on Properties of Plastic Scintillators for Designing a Tissue- Equivalent LET Spectrometer

TRAN NGUYEN THUY NGAN

Doctor of Philosophy

Department of Accelerator Science
School of High Energy Accelerator Science
SOKENDAI (The Graduate University for Advanced Studies)

THE GRADUATE UNIVERSITY FOR ADVANCED STUDIES

SCHOOL OF HIGH ENERGY ACCELERATOR SCIENCE

DEPARTMENT OF ACCELERATOR SCIENCE

Study on Properties of Plastic Scintillators for Designing a Tissue-Equivalent LET Spectrometer

BY

TRAN NGUYEN THUY NGAN

THESIS FOR THE DEGREE OF DOCTOR OF PHILOSOPHY

Acknowledgments

This thesis would not have been completed without the support of several individuals.

Foremost, I would like to express my sincere gratitude to my supervisor Prof. Shinichi Sasaki for the continuous support of my Ph.D. study, for his patience, motivation, enthusiasm, and immense knowledge. His guidance helped me in all the time of research and writing of this thesis. I could not have imaged having a better mentor for my Ph.D. study.

It gives me great pleasure in acknowledging Prof. Toshiya Sanami, Prof. Yuji Kishimoto, Prof. Eido Shibamura, Prof. Hideo Hirayama for supporting me in study and research. Besides, I would like to thank the rest of my thesis committee Prof. Yoshihito Namito and Prof. Kiwamu Saito for spending their time to read, help me realize my mistakes, and give me precious advice to improve my thesis.

Last but not least, I am deeply indebted and thankful to my parents, all my family members, and my friends for their constant support and solicitude during my study.

List of tables

List of figures

CHAPTER 1 INTRODUCTION

1.1. Background and motivation

In general, the effect of irradiation can be quantified by the absorbed dose *D*, which is defined as the total energy absorbed per unit mass of the absorber. The historical unit of the absorbed dose was the *rad* (1 rad = 100 ergs/g); then, the *rad* has been replaced by *gray*-Gy (1 Gy = 1 J/kg = 100 rad). Although the absorbed dose represents the chemical or physical effects created in a material due to the irradiation, it does not indicate the radiation's specification [1,2]. The information on radiation species is needed to evaluate the damage due to irradiation because the same absorbed dose cannot assure the same biological effects created. The biological effects depend not only on the total energy deposited but also on the radiation species because the way in which the energy of radiation is deposited along the path in a material is not similar if the kind of the radiation is different. Then, to evaluate the biological effects created in the same absorbing material due to different radiation species with the same deposited energy, the dose equivalent *H* is employed.

The dose equivalent *H* (Sv) is defined as the product of the absorbed dose *D* and a quality factor *Q* relating to radiation species and its energy: $H = DQ$. For example, *Q* is equal to 1 in the case of photons for all energies, while *Q* is equal to 20 in the case of alpha particles and heavy charged particles [1,2]. However, for unknown radiation, the absorbed dose *D* can be measured but there is no information obtained for the quality factor *Q*.

The quality factor *Q* is given as a function of the linear energy transfer (LET). For a mixed radiation field or in the measurement regardless of the radiation species, the dose

equivalent can be calculated from D and Q (LET). The LET is nearly identical to the specific energy loss (dE/dx). However, the LET (keV/μm) is practically the energy deposited locally per unit track length due to ionization and excitation, and it does not include the bremsstrahlung [1,2].

Moreover, if the dosimeter is constructed with a tissue-equivalent material, the obtained dose equivalent is more useful for personal radiation protection.

Space radiation consists of galactic cosmic rays (GCR), geomagnetic trapped particles, solar energetic particles (SEP) and their secondary particles. The amount of the dose equivalent in space reaches 1 mSv per day, which is comparable with that received on the ground in one year. The main components of doses in space are primary charged particles (protons and heavy ions) and secondary neutrons produced by the interaction between cosmic rays and the spacecraft materials. Thus, astronauts would face the risk of intense radiation exposure.

The operation of the high energy and power accelerators requires the observation and maintenance of radiation safety in the environment around the accelerators. Small amounts of radioactivity are generated in the environment of accelerator during its operation, and a mixed radiation field consisting of gamma rays, neutrons and charged particles with a wide range of energies is formed around the accelerators. The monitoring of such radiation and radioactivity, as well as the measurement of the radiation dose due to them, are the important task to maintain the radiation protection in the accelerator facilities. However, it is normally difficult to measure precisely a small amount of radioactivity produced in accelerator environments such as tunnel air, cooling water, and structures of accelerators, or to determine radiation dose of the mixed radiation field.

Particularly, there is a little of dosimeters which are usable for mixed radiation as well as some complicated methods using a combination of several detector systems are employed.

Regarding the measurement of radiation dose in space, a Tissue Equivalent Proportional Counter (TEPC) [3,4], which is a simple gas proportional counter made of tissue equivalent plastics and filled with tissue-equivalent gas, has been used by NASA as a standard space dosimeter. In TEPC, the lineal energy (the deposited energy divided by the mean chord length of the detector) is measured instead of the LET since no position information is available. The lineal energy does not represent the LET precisely. The dose obtained with TEPC is reported to be inconsistent with those measured with real LET spectrometers [5].

Real-time Radiation Monitoring Device (RRMD) [6,7] is an active LET spectrometer which utilizes silicon semiconductor detectors. RRMD has been used as real-time monitoring of space radiation which can achieve measurements of the LET distribution, particle count rates, rates of absorbed dose and dose equivalent. However, RRMD is not made of tissue equivalent materials and does not have a sensitivity to neutrons.

Recently, PS-TEPC (Position Sensitive Tissue Equivalent Proportional Chamber) [8] has been developed as a space dosimeter with the property of sensitivity to the position. PS-TEPC is a dosimeter based on LET measurement, which can measure energies and tracks of radiation simultaneously, give us the radiation dose for any kinds of radiation without knowing their species. There would be problems related to its long-term stable operation because of employing complicated electronics circuits, deterioration in the gas mixture, and higher high-voltage systems to obtain gas gains which may lead to discharge.

An ideal tissue-equivalent dosimeter based on LET measurement should have the following properties: an active (real-time) detector with isotropic sensitivity, having the sensitivity to detect many radiation types as well as the incident position of radiation (position sensitivity), being formed as simply as possible with tissue-equivalent materials, being stable and long-term operation [3].

Thus, a tissue-equivalent dosimeter based on LET measurement gives the potentials to obtain the dose equivalent directly regardless of radiation species and can be used in a mixed radiation field.

In this study, plastic scintillators are selected as the candidate material because of their beneficial properties [1,2]:

- Plastic scintillators are inexpensive materials which have the flexibility in shape and size. They can be machined into the shapes of cylinders, rods, or flat sheets, etc.

- Plastic scintillators have high scintillation yields and very fast decay time constant of about 2 – 3 ns.

- Plastic scintillators have the effective atomic number and density close to those of water and human tissues because their main component is hydrocarbon molecules.

- Plastic scintillators can respond to various radiation species (photons, charged particles, and neutrons).

On the other hand, plastic scintillators also have demerits:

- The non-proportionality between light yield and deposited energy, especially at low energy region.

- The light yield is affected by the quenching effect when irradiated with charged particles.

- The response of plastic scintillators to charged particles shows the particle-species dependency at the high specific energy loss dE/dx.

1.2. Objectives of this study

In order to obtain LET, the deposited energy and track length of radiation in the spectrometer must be measured simultaneously. The light yield and deposited energy in plastic scintillator due to different radiation species need to be examined. Considering the track length determination in the spectrometer, the feasibility of using plastic scintillators in measuring the position sensitivity of incident radiations into the spectrometer is studied.

Based on the results of energy and position sensitivity measurements, the conceptual design for the tissue-equivalent LET spectrometer using plastic scintillators, and principles of determining the deposited energy and position of incident radiation in this spectrometer are proposed.

1.3. Methodology used in this study

In this study, three $2''\phi \times 2''L$ cylindrical plastic scintillators EJ-200, EJ-212, EJ-252 [9] are used to examine the light yield due to incident gamma rays.

EJ-200 and EJ-212 are commercially available, both of them have the density and the effective atomic number close to those of water and human tissues. Besides, EJ-252 is an air-equivalent scintillator and is a potential candidate for developing an air-equivalent dosimeter. These plastic scintillators are selected to check whether there are any differences in their behaviors or not.

The absolute light yield of plastic scintillators is evaluated as W_s which is defined as the average energy required to produce one scintillation photon in a scintillator. The W_s is determined as the result of deposited energy divided by the number of scintillation photons generated in a scintillator. For incident gamma rays, the deposited energy corresponding to the maximum Compton electron energy (Compton edge) is used in the W_s determination.

Compton scattering which is the dominant interaction in plastic scintillators results in a Compton continuum in the energy distribution; hence, the deposited energies are difficult to determine precisely. The scintillation efficiency defined as the relative light yield per unit energy deposited by electrons (called as "electron response") of plastic scintillators has been examined by using Compton Coincidence Technique.

For determining the deposited energy, an energy resolution is one of the essential factors which must be evaluated, and the light yield is an important factor in consideration of the energy resolution. In this study, the energy resolution of plastic scintillators is evaluated from the results of the electron response and W_s measurement.

The pulse height distribution for 60-keV gamma rays from an ^{241}Am is measured with plastic scintillator detectors. This pulse height distribution corresponds to the photopeak as the result of the interaction with low energy gamma rays. Then, the width of this photopeak is also used to evaluate the energy resolution of plastic scintillators.

In order to examine the response of plastic scintillators to charged particles, a square-aligned rod system made of the NE-102 plastic scintillator (equivalent to EJ-212) is irradiated by heavy ions generated from an accelerator at HIMAC (H – 230 MeV, Si – 800 MeV/u, and C – 400 MeV/u). The light yields are measured and the deposited energies are calculated using the SRIM2008 code.

The feasibility of detecting the incidence position of radiation of plastic scintillators is examined by using square-aligned plastic scintillator rods (the rods of 10 cm and 30 cm in length are used), and multi-segmented photomultiplier tubes (PMTs) are attached to both ends of the rods. The 30 cm plastic scintillator rod wrapped in aluminized mylar reflector is irradiated with alpha (^{241}Am) particles to study the nature of the transparency of light in the rod. The 10 cm plastic scintillator rod is irradiated with beta particles (^{90}Sr/^{90}Y) to examine the signal obtained with different reflectors (teflon tape, aluminized mylar sheet, and black tape) and the signal as a function of distance from the source to the PMT. Additionally, the signal as a function of distance from the source to the PMT is studied by using the measured data of C (400 MeV/u).

Theories and relating studies for properties of plastic scintillators and LET spectrometers are presented in Chapter 2. The method description and experimental procedure of light yield, deposited energy, energy resolution, and feasibility of detecting the incidence position of radiation of plastic scintillators are presented in Chapter 3. Then, experimental results and discussion are presented in Chapter 4. In Chapter 5, the conceptual design and operation principles of a tissue-equivalent LET spectrometer are described. The conclusion of the study is shown in Chapter 6.

References

[1] G. F. Knoll, Radiation Detection and Measurement, 4th ed., John Wiley & Sons, United States of America, 2010.

[2] W. R. Leo, Techniques for Nuclear and Particle Physics Experiments – A how to Approach", 2nd ed., Springer-Verlag, New York, 1994.

[3] S. Sasaki, K. Saito, H. Tawara, T. Nagayoshi, Y. Fujita, T. Doke, K. Terasawa, K. Miuchi, H. Matsumoto, and Y. Uchihori, Development of Position-sensitive Tissue Equivalent Proportional Chamber for Space Dosimetry, 2007 IEEE Nuclear Science Symposium Conference Record, 2007, 1826 – 1829.

[4] G. D. Badhwar, F. A. Cucinotta, L. A. Braby, A. Konradi, Measurements on the shuttle of the LET spectra of galactic cosmic radiation and comparison with the radiation transport model, Radiation Research 139 (3), 1994, 344 – 351.

[5] S. Sasaki, Development of a New Space Dosimeter Based on LET Measurements for Heavy Charged Particles, International Journal of Microgravity Science and Application 28 (3), 2011, 67 – 73.

[6] T. Doke, T. Fuse, K. Hara, T. Hayashi, J. Kikuchi, S. Suzuki, K. Terasawa, Measurement of Linear Energy Transfer Distribution at CERN-EU High-Energy Reference Field Facility with Real-Time Radiation Monitoring Device III and Its Comparison with Dosimetric Telescope, Japanese Journal of Applied Physics 43 (6A), 2004, 3576 – 3581.

[7] T. Sakaguchi, T. Doke, N. Hasebe, T. Hayashi, T. Kashiwagi, J. Kikuchi, S. Kono, S. Nagaoka, T. Nakano, T. Takagi, K. Takahashi, LET distribution measurement with a new real time radiation monitoring device – III onboard the Space Shuttle STS-84, Nuclear Instruments and Methods in Physics Research A 437, 1999, 75 – 78.

[8] Y. Kishimoto, S. Sasaki, K. Saito, K. Takahashi, T. Doke, K. Miuchi, T. Fuse, A. Nagamatsu, Y. Uchihori, H. Kitamura, K. Terasawa, "Basic performance of a position-sensitivity tissue-equivalent proportional chamber (PS-TEPC), Nuclear Instruments and Methods in Physics Research A 732, 2013, 591 – 594.

[9] http://www.eljentechnology.com/index.php/products/plastic-scintillators.

CHAPTER 2 THEORIES AND RELATING STUDIES FOR PROPERTIES OF PLASTIC SCINTILLATORS AND THE DEVELOPMENT OF LET SPECTROMETERS

In this chapter, some important characteristics and properties of plastic scintillators as a radiation detector material are overviewed which include scintillation mechanisms, light yields, temperature dependence, and radiation damage properties of plastic scintillators. Theoretical or experimental studies on the plastic scintillators relating to this research are also reviewed. In the last section, the so far studies relating on Linear Energy Transfer (LET) spectrometers are presented.

2.1. Overview of plastic scintillators

Plastic scintillators are categorized as organic scintillators which are aromatic hydrocarbon compounds consisting of linked or condensed benzene ring structures. Particularly, plastic scintillators compose of an organic scintillator dissolved in a solvent that can be subsequently polymerized to a solid solution. The most popular solvents are polyvinyl-toluene, polyphenyl-benzene, and polystyrene. Some common primary organic scintillators (solutes) are 2-phenyl-5-(4-biphenylyl)-1,3,4 oxadiazole (PBD), p-terphenyl and 2,5-diphenyloxazole (PPO), which are dissolved in concentrations typically on the order of 10 g/l. Additionally, a secondary solute such as 1,4-di-[-2-(5-phenyloxazolyl)]-benzene (POPOP) is added in a tiny portion to play as a wavelength shifter. The wavelength shifter's function is to absorb the light produced by the primary solute and re-emit it at a longer wavelength to be more compatible with the spectral sensitivity of a photomultiplier tube or to minimize bulk self-absorption in a large plastic scintillator [1,2].

Scintillation light in plastic scintillators arises from transitions made by the free valence electrons of the molecules. These delocalized electrons are not associated with any particular atom in the molecule and occupy those are known as the π-molecular orbitals. A typical energy diagram for these orbitals is shown in Fig.2.1. S_0 denotes the ground state which is a singlet state. The levels above this state are the excited singlet states (S^*, S^{**}, …) and lowest triplet state (T_0) and its excited levels (T^*, T^{**}, …). Also associated with each electron level is a fine structure which corresponds to excited vibrational modes of the molecule. The energy spacing between electron levels is on the order of a few eV whereas that between vibrational levels is of the order of a few tenths of eV [1].

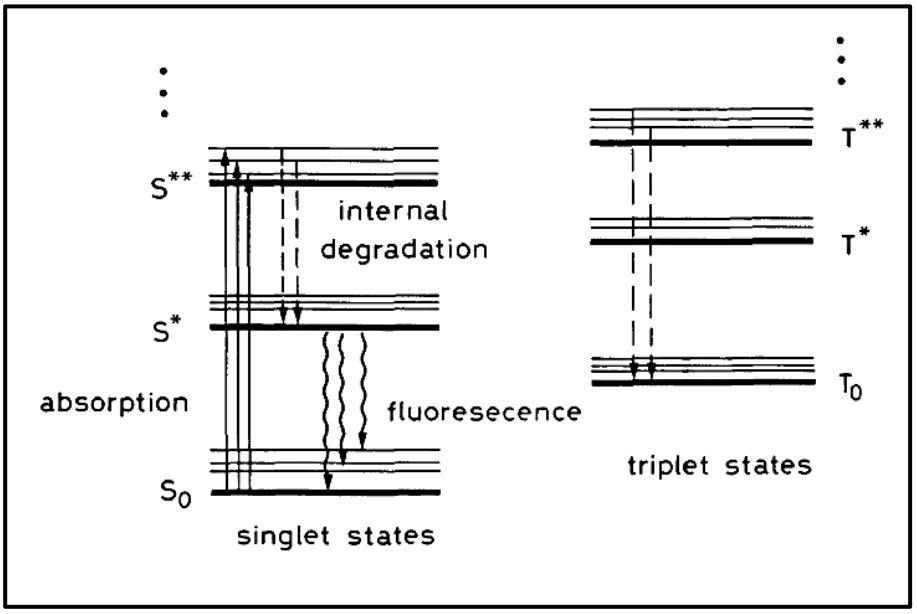

Fig.2.1. Energy level diagram of an organic scintillator molecule [1].

Ionization energy from penetrating radiation excites both the electron and vibrational levels as shown by the solid arrows in Fig.2.1. The singlet excitations generally decay immediately (≤ 10 ps) to S^* state without the emission of radiation, a process which is known as internal degradation. There is a high probability of making a

radiative decay from S^* to one of the vibrational states of S_0 (wavy lines) within a few nanoseconds time. This is the normal process of fluorescence. S^* decays to excited vibrational states of S_0, with the emission of radiation energy less than that required for the transition $S_0 \rightarrow S^*$ also explains the transparency of the scintillators to their own radiation [1].

For the triplet excited states, a similar internal degradation process occurs which brings the system to the lowest triplet state. While transitions from T_0 to S_0 are possible, however, they are highly forbidden by multipole selection rules. Instead, the T_0 state decays mainly by interacting with another excited T_0 molecules to leave one of the molecules in the S^* state; then, radiation is emitted by the S^* [1],

$$T_0 + T_0 \rightarrow S^* + S_0 + photons.$$

This light comes after a delay time characteristic of the interaction between the excited molecules and is the delayed or slow component of scintillator light. The contribution of this slow component to the total light output is only significant in certain organic materials [1].

Plastic scintillators produce high light outputs and offer a fast signal with a decay time constant of about 2 – 3 ns [1,2].

The major advantage of plastic scintillators is their flexibility in shape and size. They can be easily machined to cylinders, rods, blocks, large sheets, and small diameter fibers. Besides, plastic scintillators can be damaged by organic solvents such as acetone and other aromatic compounds [1]. However, plastic scintillators are resistant to water, pure methylal, silicone grease, and lower alcohols. Thus, it is advised to wear cotton or terylene gloves to handle bare plastic scintillators because the body acids from hands can cause cracking of the scintillators after a period of time [1].

2.1.1 Temperature dependence

The light output of plastic scintillators is practically independent of temperature between – 60°C and 20°C. At 60°C, the light output is 95% as compared to the value in the range of – 60°C and 20°C [1].

A study on the temperature dependence of the plastic scintillator detector was performed by Zhao-Min Wang et al. [3]. A plastic scintillator detector was used as the main sub-detector in the Dark Matter Particle Explorer (DAMPE) project. For this purpose, the plastic scintillator detector was operated over a large temperature range from – 10°C to 30°C. Thus, the temperature dependence of a scintillator bar (180 mm x 28 mm x 10 mm) coupled to a photomultiplier tube at each end and settled in a thermal chamber was examined. The temperature inside the chamber was changed from 3°C to 42°C, and the detector was irradiated with a ^{207}Bi source. As a result, the temperature dependence of the outputs mainly came from the photomultiplier tube, and the plastic scintillator was not sensitive to the observed temperature range.

Four different scintillators BCF-10 and BCF-60 (polystyrene base), BC-404 (polyvinyl-toluene base) and RP-200A (PMMA base) were studied for the dependence of their light yield on temperature by Peralta [4]. The plastic scintillator detectors were exposed to a 50 kVp X-ray beam, and the data were obtained for the temperature ranging from 0°C to around 50°C. BCF-10, BCF-60, and RP-200A presented a small temperature dependence, while BC-404 showed a negligible temperature dependence within the measured range.

2.1.2. Radiation damage

Plastic scintillators would suffer from the degradation in the scintillation output due to radiation damage. Significant degradation in light yield has been observed for cumulative gamma-ray exposures of 10^3 or 10^4 Gy, whereas a little decrease in light output with doses as high as 10^5 Gy can be observed for other radiation-resistant-formulation scintillators [2].

The radiation damage in polyvinyl-toluene plastic scintillators due to charged particles at different stopping powers and ion doses has been studied by Torrisi [5]. The detector was irradiated with He (100 keV), H (50 – 350 keV, 24 MeV, and 60 MeV), and Ar (300 keV). The stopping power was calculated by TRIM simulation program. The results indicated that the radiation damage effect increases with the stopping power of the incident particle as well as the ion dose. The damage produced a decrease in scintillation yield because the irradiation causes the polymer modification. The black color of the polymer caused by 100-keV He at a dose of 10^{14} ions/cm^2 which corresponding to 10 MGy. The scintillation yield reduction was about 15% due to 60-MeV H (stopping power 1.1 keV/μm) at a dose of 1 kGy, and a similar degradation was obtained due to 300 keV H (stopping power 65.8 keV/μm) at 60 kGy dose and 300-keV Ar (stopping power 705 keV/μm) at 500-kGy dose.

The radiation damage to the scintillation properties of four commercial plastic scintillators (EJ-200, EJ-208, EJ-260, and BC-408) following the irradiation with 6 MeV proton beam has been studied by Jivan et al. [6]. The scintillators maintained their transmission character for low doses (about 0.8 MGy), but a loss in absorption correlating to the fluor absorption region occurred and led to a loss in light yield. At dose exposures higher than 8 MGy, more changes in the scintillators were observed such as visible dis-

coloration progressing from yellow to brown, formation of an absorptive component shifting to higher wavelengths, increasing loss to the light yield. Then, the scintillators showed recovery of transmission character within 4 weeks after irradiation. Among the samples, EJ-260 and EJ-208 exhibited the most tolerance against radiation damage effects to their optical properties.

The radiation damage properties of plastic scintillators BC-404, BC-408, and EJ-200 were experimentally studied by Zhao Li et al. [7]. The scintillators were irradiated with ^{60}Co (1 Ci and 5 MCi) at the dose rate of 8.3×10^{-3} Gy/min and 52.7 Gy/min; hence, the corresponding dose was 0.57 Gy and 1.4×10^{4} Gy. The transmittance was not influenced by the irradiation at a dose less than 600 Gy. However, the scintillator samples were destroyed at a dose rate of 52.7 Gy/min when the dose reached 1.4×10^{4} Gy, the transmittance decreased substantially. The shape of the emission spectra of scintillator samples was unchanged after the irradiation. At 600 Gy, the light yield loss was 14.1% for BC-408, 13.4% for BC-404, and 10.6% for EJ-200. Additionally, there were no signs of recovery after 100 hours.

2.1.3. Light output

The light output of a scintillator represents the efficiency for ionization energy into photons conversion. The light output is also important to determine the resolution of a scintillator. Moreover, the light output corresponding to different radiation species is different even at the same deposited energy [1].

High energy electrons produced only a weak excitation and low ionization density along their path within a scintillator. Then, the individual molecular excitations and ionizations are spaced several molecular distances apart along the particle path, and the

interactions between them can be negligible. In such cases, it is assumed that the fluorescent light emitted per unit track length *dL/dx* is proportional to the specific energy loss *dE/dx* as the response of plastic scintillators,

$$\frac{dL}{dx} = S\frac{dE}{dx}, \quad (2.1)$$

where *S* is the normal scintillation efficiency. However, this linear relation is not always assured. The response of the scintillator depends not only on the specific energy loss but also on the radiation species. For organic scintillators, non-linearity is observed for electrons at energies below 125 keV. The degree of non-linearity becomes more noticeable at lower energies for heavier particles or slow electrons, *dE/dx* is increased compared with that for fast electrons, and the fluorescence increases non-linearly with the energy.

Birks [8] has proposed a semi-empirical model to explain this behavior. The non-linearity in the response is suggested as the quenching effect. A high ionization density along the track of particle leads to this quenching from damaged molecules and the scintillation efficiency is reduced. The density of damaged molecules is then presented as *B* (*dE/dx*), where *B* is a proportionality constant; and *k* is the fraction that leads to quenching,

$$\frac{dL}{dx} = \frac{S\frac{dE}{dx}}{1 + kB\frac{dE}{dx}} \quad . \quad (2.2)$$

The light output data reported for anthracene, stilbene, NE-213, NE-102 and Pilot-B to electrons and protons, and NE-230 to electrons and deuterons were analysed by Craun and Smith [9]. The data were fitted to determine the parameters relating to the

semi-empirical equation proposed by Birks. Particularly, for NE-102 which is the widely used plastic scintillator, the light output corresponding to electrons was approximately 6 times higher than the one due to protons at 1 MeV.

The response of a NE-102 scintillator to He (150 MeV/u), C (290 MeV/u), Ne (400 MeV/u), Si (490 MeV/u) and Ar (550 MeV/u) has been studied by Matsufuji et al. [10]. NE-102 has taken a role as a ΔE detector in ΔE-E measurements where a BGO detector was used as an E detector. Based on the obtained results of light yield and deposited energy in the NE-102 detector, the *dE/dx* and *dL/dx* relation was derived as shown in Fig.2.2. It indicated the existence of a universal quenching in high-*dE/dx* region which is independent of the particle species.

Recently, the response to gamma rays and neutrons of plastic scintillator EJ-200 has been studied by Tkaczyk et al. [11] for the purpose of using EJ-200 as an active shield to reduce the neutron background caused by cosmic rays. The light outputs and energies of recoil electrons corresponding to Compton edge positions determined from the theoretical distribution obtained from MCNP simulations were used to obtain the response to gamma rays from ^{137}Cs, ^{232}Th, and ^{238}PuC sources. For the response to mono-energetic neutrons (4.0 – 6.5 MeV, 17.5 – 19.0 MeV, and 1.3 – 3.2 MeV), the high energy region corresponding to the maximum output which was delivered by protons (the results from a head-on elastic scattering on hydrogen) with an energy that equaled the incident neutron energy. The light output as a function of energy for electrons showed a non-linearity in the low energy region. Besides, the light output function for protons below 20 MeV was about 3 times smaller compared to the one for electrons and was strongly non-linear.

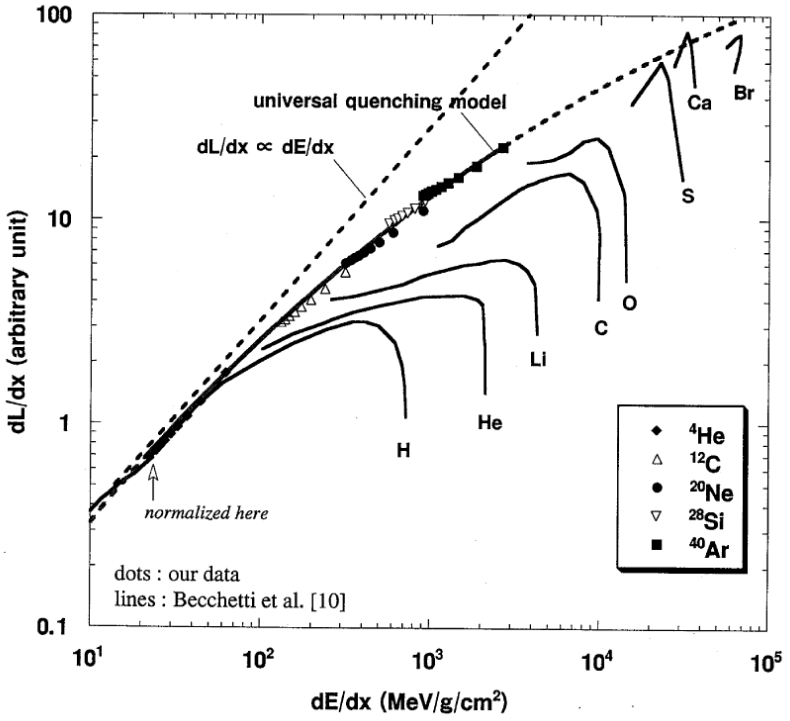

Fig.2.2. dL/dx as a function of dE/dx at the entrance surface of the NE-102 scintillator [10].

There are three main mechanisms for interactions of gamma rays in a matter: photoelectric absorption, Compton scattering, and pair production. Particularly, a plastic scintillator is a low atomic number material, and Compton scattering is the dominant interaction. Therefore, it is difficult to precisely determine the energy in a Compton continuum distribution or make the energy calibration. For plastic scintillators, Compton edge energies are used to make the energy calibration, and the Compton edge positions in the measured spectra are determined by comparing the measured spectrum with the result obtained by Monte Carlo calculation.

Valentine and Rooney have designed a Compton spectrometer [12] and benchmarked a Compton Coincidence Technique [13] to study the light yield non-

linearities and intrinsic energy resolution of inorganic scintillators for detecting gamma rays. They proposed a coincidence method to record a nearly monoenergetic internal electron source inside the scintillator of the primary detector only when its pulse is in coincidence with the one generated by a second detector. This internal electron source was sufficient to study the non-linearity between the deposited energy and the light yield as well as the intrinsic energy resolution because it was not influenced by the surface effect and it was monoenergetic compared with the electrons results in the gamma-ray photopeaks. The proposed Compton Coincidence Technique (CCT) employed a combination of two detectors operating in coincidence. The experimental set up is shown in Fig.2.3. The first detector was exposed to a collimated beam of mono-energetic gamma rays of known energy E_γ from a source. Some gamma rays undergo a Compton scatter interaction within the detector, transferring energy E_e to an electron. If a Compton scattered gamma ray had no further interaction, then it was emitted from the scintillator with an energy E_γ, at an angle of θ, given by,

$$E'_\gamma = \frac{E_\gamma}{1 + \frac{E_\gamma}{m_0 c^2}(1 - cos\theta)}, \quad (2.3)$$

$$E_e = E_\gamma - E'_\gamma, \quad (2.4)$$

where m_0 is the rest mass of an electron, and c is the speed of light.

The second detector placed at a specific angle θ was used to record the scattered gamma ray. The relative light yield per unit energy of the recoil electron generated in the scintillator as the result of the Compton scattering was defined as the "electron response" and was used to study the non-linearity firstly for NaI(Tl) irradiated with 662-keV gamma rays.

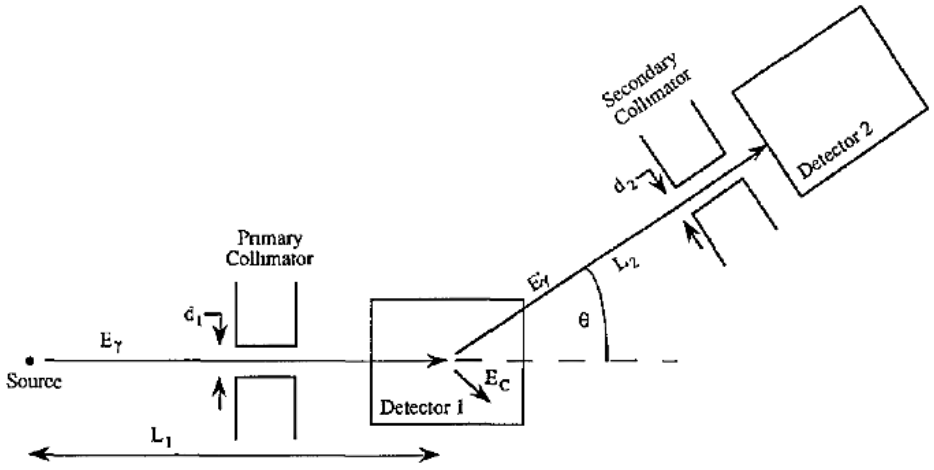

Fig.2.3. Experiemtal setup for Compton Coincidence Technique measurement [12].

Limkitjaroenporrn et al. [14] firstly employed the Compton Coincidence Technique measurement to study the non-proportionality in electron response of a plastic scintillator NE-102 irradiated with 662-keV gamma rays. A NaI(Tl) detector was used as the second detector. The electron response was determined for measured electron energies from 28 keV to 436 keV when the scattering angle was changed. The NE-102 showed a good proportionality of light yield at energies between 90 keV and 436 keV, and there was a decrease in the light yield of about 20% upon lowering the electron energy to 28-keV.

The electron response (relative light yield per unit energy) of plastic scintillator BC408 (equivalent to EJ-212) has been measured in the energy range of 10 keV up to 4-MeV via the Wide Angle Compton Coincidence (WACC) technique by Swiderski et al. [15]. WACC has been developed based on the CCT with the advantage that weak

radioactive sources can be used without collimators. A *40 mm ∅ × 50 mm L* BC-408 was irradiated with gamma rays from ^{137}Cs, ^{65}Zn, and Pu-Be sources placed at different angles. The electron response was determined from the light yields and energies corresponding to Compton edge electrons as shown in Fig.2.4. The electron response kept increased beyond 500 keV, and the electron response at 10 keV was about 70% compared with the one at 500 keV.

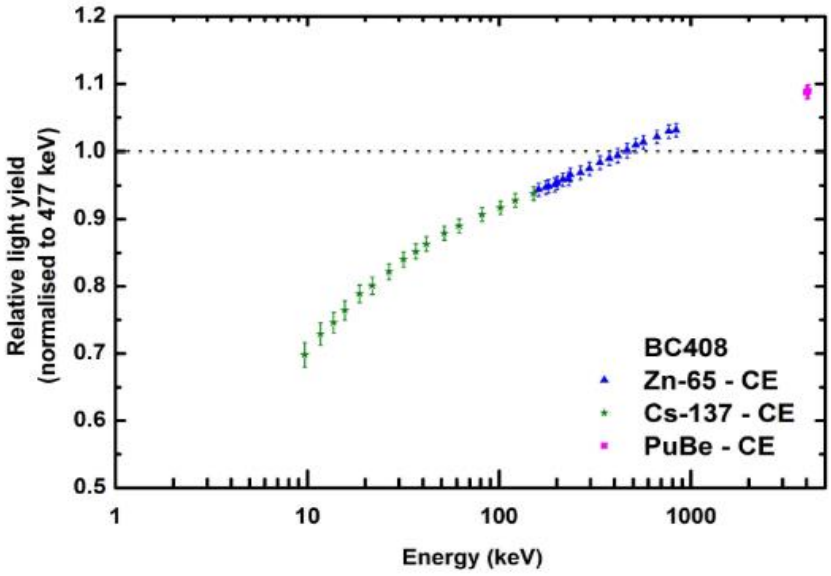

Fig.2.4. Nonproportionality of the light yield measured for a BC-408 plastic scintillator [15].

2.2. Studies on LET spectrometer so far made

The linear energy transfer (LET) is nearly identical to the specific energy loss (*dE/dx*). However, the LET (keV/μm) is practically the energy deposited locally per unit track length due to ionization and excitation, and it does not include the bremsstrahlung [1,2]. Based on the LET distribution, the quality factor *Q*, which relates to the determination of the dose equivalent $H = DQ$, can be obtained because *Q* can be

expressed as a function of LET (where *D* is the absorbed dose). Several LET spectrometers which have been studied and developed are mentioned as follows:

A tissue-equivalent proportional counter (TEPC) has been developed by Badhwar [16] and this system was used on Shuttle missions in 1993. The system consisted of a cylindrical detector (1.78 cm long and 1.78 cm in diameter) simulating a 2 μm diameter site which was bounded by tissue-equivalent plastic, and the detector was filled with low-pressure propane gas. The full lineal energy spectra were recorded where the lineal energy was the deposited energy divided by the mean chord length of the detector. Because the position information could not be determined, the LET was evaluated by assuming that the LET was equal to the lineal energy. The dose obtained with TEPC is reported to be inconsistent with those measured with real LET spectrometers [17].

A real-time Radiation Monitoring Device (RRMD-III) has been constructed and used onboard the Space Shuttle mission STS-84 [18]. The device consisted of three double-sided silicon strip detector (DSSDs). RRMD-III measured directly the LET distributions contributed by galactic cosmic ray (GCR) particles and trapped protons over the range of 0.2 – 600 keV/μm. The differential LET distributions obtained by RRMD-III aboard STS-84 were compared with those obtained by TEPC aboard STS-81 at the same observing orbits. The data showed that the LET distributions for GCR particles between two devices agreed well above 6 keV/μm. In the range from 1 to 6 keV/μm, there was the discrepancy in the data between two devices, the flux of TEPC is always higher than that of RRMD-III. This indicated that the assumption in TEPC that the LET was equal to the lineal energy was not correct.

Recently, a space dosimeter Position Sensitivity Tissue Equivalent (PS-TEPC) has been developed [19]. Then, the real-time LET and the equivalent dose were measured.

The detector of PS-TEPC is based on a time projection chamber (TPC) made of tissue equivalent materials, where a micro pixel chamber (μ-PIC) is used as a two-dimensional position sensor. By using the PS-TEPC, three-dimensional tracks of radiation as well as its energy can be measured to obtain LET from the measured energy and the track length of radiation simultaneously. PS-TEPC can be used for radiation dose management onboard the ISS and future manned space missions since it can precisely measure the doses due to various charged particles covered under a wide range of the LET energy spectrum.

References

[1] W. R. Leo, Techniques for Nuclear and Particle Physics Experiments – A how to Approach, 2nd ed., Springer-Verlag, New York, 1994.

[2] G. F. Knoll, Radiation Detection and Measurement, 4th ed., John Wiley & Sons, United States of America, 2010.

[3] Zhao-Min Wang, Yu-Hong Yu, Zhi-Yu Sun, Ke Yue, Duo Yan, Yong-Jie Zhang, Yong Zhou, Fang Fang, Wen-Xue Huang, Jun-Ling Chen, Temperature dependence of the plastic scintillator detector for DAMPE, Chinese Physics *C* 41 (1), 016001, 2017, 1 – 7.

[4] L. Peralta, Temperature dependence of plastic scintillators, Nuclear Instruments and Methods in Physics Research A 883, 2018, 20 – 23.

[5] L. Torrisi, Radiation damage in polyvinyltoluene (PVT), Radiation Physics and Chemistry 63, 2002, 89 – 92.

[6] H. Jivan, J. E. Mdhluli, E. Sideras-Haddad, B. Mellado, R. Erasmus, and M. Madhuku, Radiation damage effects on the optical properties of plastic scintillators, Nuclear Instruments and Methods in Physics Research B 409, 2017, 224 – 228.

[7] Z. Li, W. Chong, H. Yuekun, Z. Xiaojian, S. Feng, S. Zhijia, W. Jinjie, A. Zhenghua, X. Yuda, Z. Ziping, W. Yifang, Properties of plastic scintillators after irradiation, Nuclear Instruments and Methods in Physics Research A 552, 2005, 449 – 455.

[8] J. B. Birks, The Theory and Practice of Scintillation Counting, Pergamon Press, Great Britain, 1964.

[9] R. L. Craun, D. L. Smith, Analysis of response data for several organic scintillators, Nuclear Instruments and Methods 80, 1970, 239 – 244.

[10] N. Matsufuji, T. Kanai, H. Komami, T. Kohno, The response of a NE-102 scintillator to passing-through relativistic heavy ions, Nuclear Instruments and Methods in Physics Research A 437, 1999, 346 – 353.

[11] A. H. Tkaczyk, H. Saare, C. Ipbuker, F. Schulte, P. Mastinu, J. Paepen, B. Pedersen, P. Schillebeeckx, G. Varasano, Characterization of EJ-200 plastic scintillators as active background shield for cosmogenic radiation, Nuclear Instruments and Methods in Physics Research A 882, 2018, 960 – 104.

[12] J. D. Valentine, B. D. Rooney, Design of a Compton spectrometer experiments for studying scintillator non-linearity and intrinsic energy resolution, Nuclear Instruments and Methods in Physics Research A 353, 1994, 37 – 40.

[13] B. D. Rooney, J. D. Valentine, Benchmarking the Compton Coincidence Technique for Measuring Electron Response Non-Proportionality in Inorganic Scintillators, IEEE Transactions on Nuclear Science 43, 1996, 1271 – 1276.

[14] P. Limkitjaroenporrn, J. Kaewkhao, P. Limsuwan, W. Chewpraditkul, Nonproportionality of electron response using CCT: Plastic scintillator, Applied Radiation and Isotopes 68, 2010, 1780 – 1784.

[15] L. Swiderski, R. Marcinkowski, M. Moszynski, W. Czarnacki, M. Szawlowski, T. Szczesniak, G. Pausch, C. Plettner, K. Roemer, Electron response of some low-Z scintillators in wide eneryg range, Journal of Instrumentation 7, 2012, 1 – 10.

[16] G. D. Baghwar, F. A. Cucinotta, L. A. Braby, A. Konradi, Measurements on the Shuttle of the LET Spectra of Galactic Cosmic Radiation and Comparison with the Radiation Transport Model, Radiation Research, 139, 1994, 344 – 351.

[17] S. Sasaki, Development of a New Space Dosimeter Based on LET Measurements for Heavy Charged Particles, International Journal of Microgravity Science and Application 28 (3), 2011, 67 – 73.

[18] T. Sakaguchi, T. Doke, N. Hasebe, T. Hayashi, T. Kashiwagi, J. Kikuchi, S. Kono, S. Nagaoka, T. Nakano, T. Takagi, K. Takahashi, S. Takahashi, LET distribution measurement with a new real-time radiation monitoring device-III onboard the Space Shuttle STS-84, Nuclear Instruments and Methods in Physics Research A 437, 1999, 75 – 87.

[19] Y. Kishimoto, S. Sasaki, K. Saito, K. Takahashi, T. Doke, K. Miuchi, T. Fuse, A. Nagamatsu, Y. Uchihori, H. Kitamura, K. Terasawa, Basic performance of a position-sensitive tissue-equivalent proportional chamber (PS-TEPC), Nuclear Instruments and Methods in Physics Research A 732, 2013, 591 – 594.

CHAPTER 3 EXPERIMENT

Chapter 3 describes the methods, experimental setups, and procedures used for the studies of the absolute light yields, the scintillation efficiency as a function of electron energy, the energy resolutions, and position sensitivity in plastic scintillators. The methods to obtain the light output and the resolutions for heavy charged particles are also given in this chapter.

3.1. Experiment for determining the absolute light yield in plastic scintillators

3.1.1. Plastic scintillators used in the study

The cylindrical plastic scintillators with a size of $2''\phi \times 2''L$ EJ-200, EJ-212, and EJ-252 (manufactured by ELJEN Technology [1]) are used for the light yield measurements. All the used plastic scintillators are commercially available. EJ-200 has important properties which are the long attenuation length and fast timing; hence, EJ-200 is generally used in Time-of-Flight (TOF) measurement. EJ-212 is a general purpose scintillator for use in geometries from thin films to cast sheets, rods, and ingots. Both of them have the density and the effective atomic number close to those of water and human tissues. EJ-252 is an air-equivalent scintillator and is a potential candidate for developing an air-equivalent dosimeter. Three different plastic scintillators are examined to see whether there are any differences in their behaviors or not. The cylindrical shape of the scintillator is chosen in order to compare light yields with each other or with other inorganic scintillators and to apply an existing simulation code to evaluate the light collection efficiency in a scintillator. The specifications of the used plastic scintillators are shown in Table.3.1. [1].

Table.3.1. Physical constants of plastic scintillators used in this study [1].

Properties	**EJ-200**	**EJ-212**	**EJ-252**
Light output (% Anthracene)	64	65	46
Scintillation efficiency* (photon/MeV)	10000	10000	-
Wavelength of maximum emission (nm)	425	423	423
Light attenuation length (cm)	380	250	200
Decay time of main component (ns)	2.1	2.4	2.4
Refractive index	1.58	1.58	1.58
Polymer base	Polyvinyltoluene		
Number of Hydrogen atom per cm^3 ($\times 10^{22}$)	5.17	5.17	5.19
Number of C atom per cm^3 ($\times 10^{22}$)	4.69	4.69	4.73
Number of arsenic atom per cm^3 ($\times 10^{19}$)	-	-	5.42
Density (g/cm^3)	1.023	1.023	1.037
Temperature range	-20°C to 60°C		
Light yield vs.Temperature	At 60°C, light yield = 95% of that at 20°C; no change from -60°C to 20°C		

* Values are taken from the manufacturer's catalog, are not established and recognized widely.

3.1.2. Determination of absolute light yields

3.1.2.1. Methods

The absolute light yield is characterized by the number of scintillation photons generated in a scintillator. In this section, the absolute light yield of a plastic scintillator is measured for the incident gamma rays. The absolute light yield is determined as W_s(eV) which is defined as the average energy required to produce one scintillation photon in the plastic scintillator. The concept of W_s is similar to the *W-value* which is the average energy to create an ion pair by an incident particle to the gas.

There are three main mechanisms for interactions of gamma rays in a matter: photoelectric absorption, Compton scattering, and pair production. Particularly, a plastic scintillator is a low atomic number material, and Compton scatterings are the dominant interactions from the energy of about 100 keV. Therefore, it is difficult to determine precisely the energy in a Compton continuum distribution.

W_s (eV) is obtained as a result of the deposited energy E from incident gamma rays divided by the number of scintillation photons N_{sp} generated in a scintillator [2] as follows

$$W_s = \frac{E}{N_{sp}} . \qquad (3.1)$$

N_{sp} is calculated based on the number of photoelectrons N_{pe} generated at the photocathode of a photomultiplier tube (PMT) as follows

$$N_{sp} = \frac{N_{pe}}{F_{collect} \times F_{convert}} , \qquad (3.2)$$

where $F_{collect}$ is the collection efficiency of photons from the scintillator at the photocathode, $F_{convert}$ is the effective conversion efficiency of photons arriving at the photocathode to photoelectrons, where the effects of incident angles of photons are taken into account.

The absolute value of the number of photoelectrons N_{pe} regardless of the PMT gain can be measured when the PMT was operated as a Photodiode mode (PD-mode) where the total gain of the PMT is assumed to be unity. The setup of the PD-mode is shown in Fig.3.1. [2].

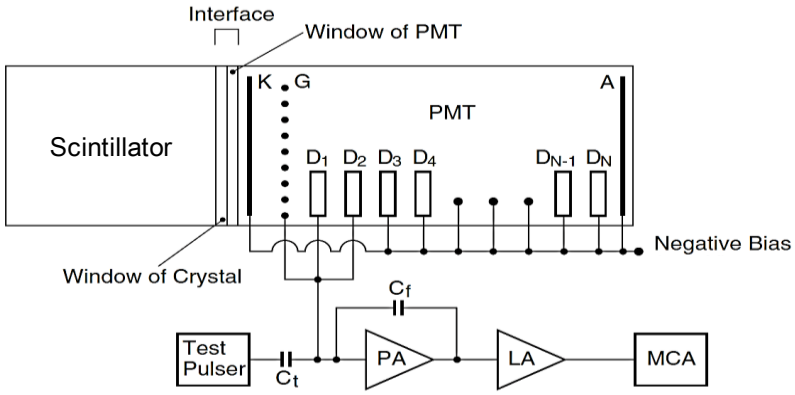

Fig.3.1. Block diagram of an experimental system in PD-mode [2]. The grid (G), the first dynode (D_1), and the second dynode (D_2) in the PMT were connected to act as a collector electrode. The photocathode, the other dynodes (D_N), and an anode (A) were connected to act as a biasing electrode. The system was calibrated with a charge terminator (C_T) and a test pulser to convert pulse height into the number of photoelectrons.

The grid (G), the first dynode (D_1) and the second dynode (D_2) in the PMT were connected to act as a collector electrode. The photoelectrode, the other dynodes (D_N), and an anode (A) were connected to act as a biasing electrode. The charge signals from the collector were fed into a charge sensitive preamplifier, further amplified by a linear amplifier, and analyzed with a multichannel analyzer system (MCA). The detector was irradiated with gamma rays, and the corresponding pulse height was recorded by the MCA. The system was calibrated with a charge terminator (C_T) and a test pulser to convert the pulse height into the number of photoelectrons.

By the PD-mode measurement, the N_{pe} of a inorganic scintillator detector irradiated by known energy gamma-rays is evaluate from the pulse height of the corresponding

photopeak in the measured pulse height distribution [2] while the N_{pe} of a plastic scintillator detector cannot be directly obtained via the same method because it is difficult to determine the pulse height precisely in the continuum distribution. Therefore, N_{pe} of plastic scintillator detector was determined relatively via the N_{pe} of a reference detector. A CsI(Tl) scintillator with a size of $2''\phi \times 2''L$ was used as a reference scintillator instead of the widely used NaI(Tl) scintillator. The CsI(Tl) scintillator has appropriate properties such as less hygroscopic and better stability for temperature variation than NaI(Tl) [3]. Moreover, the light yield measured for CsI(Tl) seems almost established while there are fluctuations in those for NaI(Tl) so far [3].

The collection efficiency of photons at the photocathode $F_{collect}$ is calculated using Monte Carlo codes (EGS4-SPC4) [4]. The transport of a photon in the plastic scintillator from its generation to termination is traced by SPC4. The following eight processes are considered for the photon transport in a cylindrical-shape scintillator as shown in Fig.3.2 [2].

1) Absorption by the reflector,
2) Absorption by the scintillator,
3) Reflection at the reflector,
4) Reflection at the window,
5) Refraction at the window or scintillator interface,
6) Escape from the PMT-scintillator system,
7) Absorption by the photocathode, and
8) Reflection at the photocathode.

The calculation was performed with the EGS4-SPC4 source code [2,4] after some modifications. The modifications need to be made in the input files were the incident

energy of gamma rays, the refractive index for scintillators, the refractive index for window material, the absorption factor of the reflector material, the size (diameter and height) of the cylindrical scintillator, the diameter of the photocathode, and the thickness of the window.

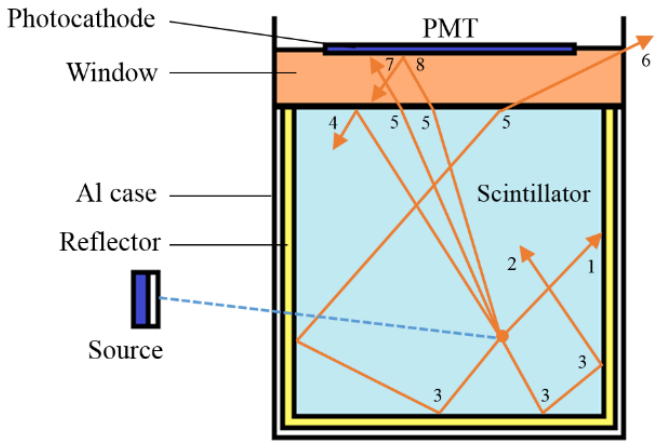

Fig.3.2. Photon tranport in a cylindrical scinitllator [2].

The effective conversion efficiency of photons to photoelectrons at the photocathode $F_{convert}$ is the result of the average quantum efficiency for the scintillation spectrum of the scintillator for each PMT-$\langle Q_m \rangle$ and the correction factor $\langle F \rangle$ for the angular variation of photons incident to the photocathode.

$$F_{convert} = \langle Q_m \rangle \times \langle F \rangle , \quad (3.3)$$

$$\langle Q_m \rangle = \frac{\int q_e(\lambda) I(\lambda) d\lambda}{\int I(\lambda) d\lambda} , \quad (3.4)$$

where $q_e(\lambda)$ is the spectral quantum efficiency of a PMT measured individually by the manufacturer, and $I(\lambda)$ is the scintillation intensity at wavelength λ in the scintillator. $q_e(\lambda)$ is measured by irradiating the PMT window at a right angle with monochromatic light [2,5,6], while photons can hit the PMT with an incident angle φ between 0° and 90°. Therefore, the angular variation of the quantum efficiency of the PMT needs to be determined, and the correction factor $\langle F \rangle$ for the angular variation of photons incident

to the photocathode was determined. The emission spectrum of EJ-200 and spectrum quantum efficiency of the PMT Hamamatsu R375 (serial number SB4349) used in this study are shown in Fig.3.3.

To determine the correction factor $\langle F \rangle$, the effective quantum efficiencies $\langle Q_{m\_effective} \rangle$ of the PMT R375 for photons from three LED lights with the wavelength of 470 nm, 525nm, and 640 nm were calculated by averaging the photon to photoelectron conversion efficiency over the distribution of photons incident to the photocathode as a function of incident angle $f(\varphi)$ obtained by SPC4, as shown in Fig.3.4 [2,5,6]. In this calculation, $\langle Q_{m\_effective} \rangle$ at φ between 0° and 90° was determined from the measured values of $\langle Q_{m\_effective} \rangle$ at φ equalling to 15°, 30°, 45°, 60°, and 75° by interpolating and extrapolating, where the singular point near 42° was taken into account because the SPC4 calculation showed the highest frequency of photon distribution at this incident angle. The correction factor $\langle F \rangle$ for each of the three LED wavelengths is the ratio between $\langle Q_{m\_effective} \rangle$ and $q_e(\lambda)$ [2,5,6]. $\langle F \rangle$ for the plastic scintillator (wavelength of maximum emission is 425 nm) was selected as $\langle F \rangle$ for LED wavelengths 470 nm. Similarly, $\langle F \rangle$ for the CsI(Tl) scintillator (wavelength of maximum emission is 540 nm) was selected as $\langle F \rangle$ for LED wavelengths 525 nm.

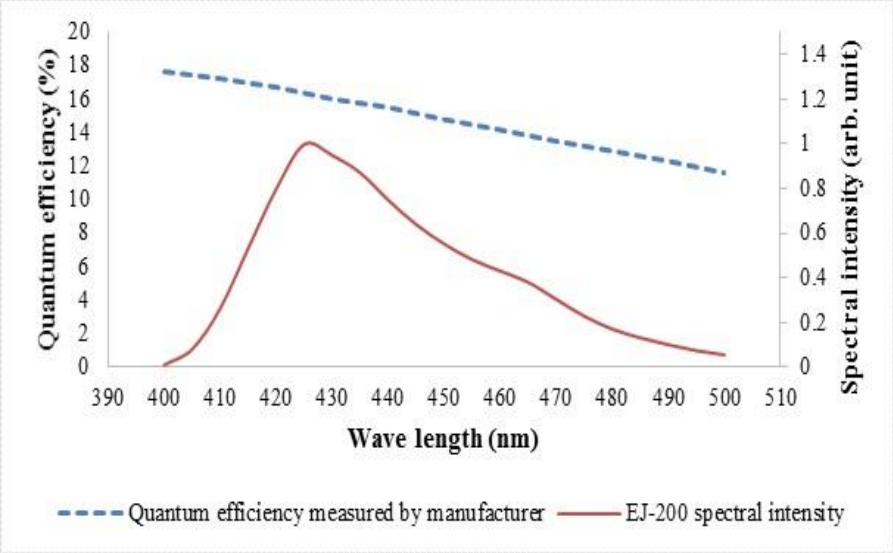

Fig.3.3. The emission spectrum of EJ-200 and spectral quantum efficiency of the photocathode of the PMT Hamamatsu R375.

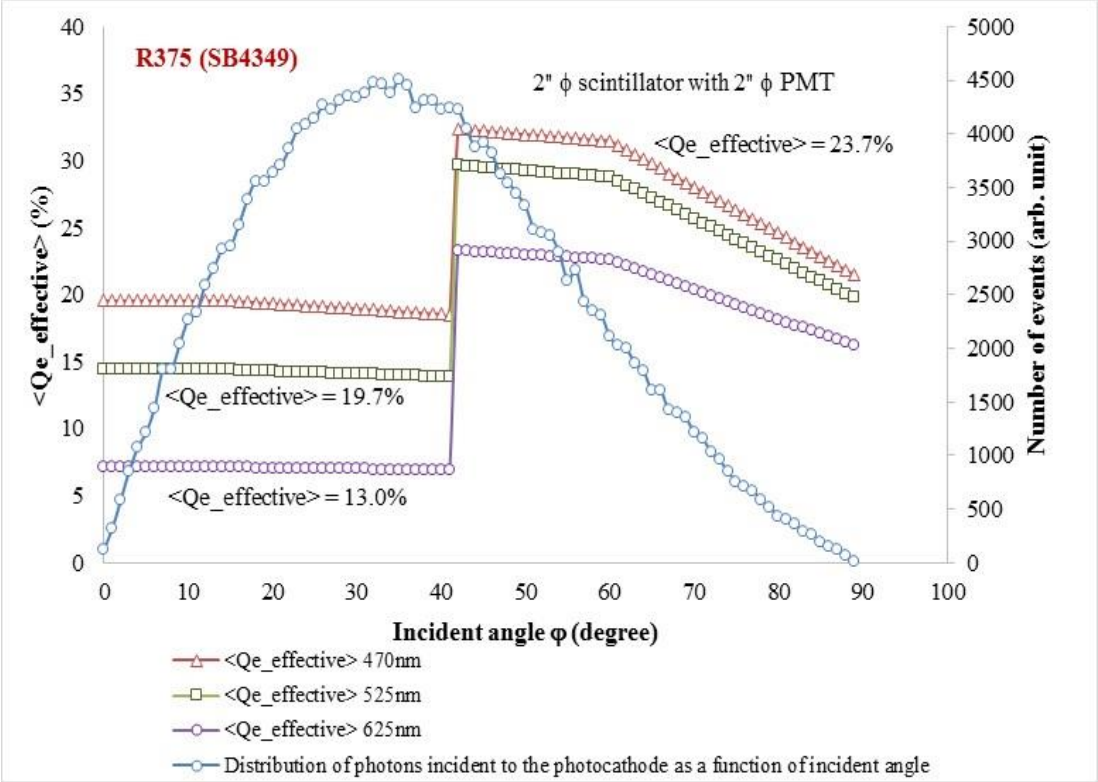

Fig.3.4. The effective quantum efficiency of PMT Hamamatsu R375 for three LED wavelengths and the distribution of photon as a function of the incident angle.

3.1.2.2. Measurement of N_{pe} for CsI(Tl) detector by PD-mode

Firstly, the N_{pe} for CsI(Tl) detector was determined via the PD-mode measurement. A $2''\phi \times 2''L$ CsI(Tl) scintillator was coupled to a $2''\phi$ PMT (Hamamatsu R375, S/N:SB4349). The spectral quantum efficiency of the photocathode of this PMT was measured identically as a function of wavelength by the manufacturer. The high voltage for the PMT was – 120 V. This operating high voltage was selected because the output signal approached a saturation point and it did not increase when the high voltage increased. The charge signals from the collector were fed into a charge sensitive preamplifier (Clear Pulse 5210B), further amplified by a linear amplifier (Ortec 671), and analyzed with the MCA (Seiko EG&G 7600).

The CsI(Tl) detector was irradiated with gamma rays from ^{137}Cs, ^{22}Na, and ^{60}Co sources. The pulse height was obtained as the photopeak's centroid in the distribution spectrum by fitting Gaussian. The centroid of the photopeak was then converted into the number of photoelectrons by using the combination of a charge terminator and a test pulser. The charge terminator was calibrated as 3770 electrons per 1000 test pulse dial by the employed test pulser. During the experiment, the amplifier's shaping time was set as 10.0 μs.

3.1.2.3. Measurement of N_{pe} for plastic scintillators

In order to determine N_{pe} for plastic scintillators relatively from N_{pe} for CsI(Tl), the light yields from the two detectors were compared when CsI(Tl) and plastic scintillator were sequentially coupled to the same PMT working at the same high voltage in the normal operation (PMT-mode).

The CsI(Tl) or plastic scintillator was coupled to the same PMT (Hamamatsu R375),

to which a high voltage of + 600 V was applied. The output signals from the PMT were fed into a pre-amplifier (Clear Pulse 5548), and further amplified by the main amplifier (Clear Pulse 4417) whose shaping time was to 10.0 μs and 0.5 μs in the case of CsI(Tl) and plastic scintillator measurement, respectively. Then, the signals were fed to and analyzed with an analog-to-digital converter ADC (Nikiglass A3400).

The CsI(Tl) detector was irradiated with gamma rays from ^{137}Cs, ^{22}Na, and ^{54}Mn sources placed at a distance of 10 cm from the detector. Each measurement was taken in 600 s and pulse height distribution spectra were obtained. The light yield was determined by fitting the photopeak in the distribution spectrum with a Gaussian function.

The plastic scintillator detector was also irradiated with gamma rays from ^{137}Cs, ^{22}Na, and ^{54}Mn in a similar manner to the CsI(Tl). In this case, however, the light yield corresponding to the Compton edge (Compton maximum energy) in the distribution has to be measured instead of photopeak, because the photopeaks in plastic scintillators for these gamma rays are not observed. Thus, it is necessary to determine the light yield for recoil electrons having Compton maximum energy given by equation 3.5 which are caused by the Compton scattering at 180^o in plastic scintillators [3]. For this purpose, a second detector was introduced together with the plastic scintillator detector in face-to-face geometry. The light yield in plastic scintillator detector was determined by selecting their events which were coincident with the events corresponding to scattered photons absorbed by the second detector.

$$E'_{\gamma}(\theta = 180^o) = \frac{E_{\gamma}}{1 + 2\frac{E_{\gamma}}{m_0 c^2}}, \qquad (3.5)$$

$$E_e(\theta = 180^o) = E_{\gamma} - E'_{\gamma}(\theta = 180^o), \qquad (3.6)$$

where E_γ (keV) is the energy of incident gamma rays to the plastic scintillator detector, $E\gamma'$ (keV) is the energy of the scattered gamma rays going next to the second detector after the scattering at the angle θ, and E_e (keV) is the energy of recoil electron in the plastic scintillator. The experimental setup to determine the Compton edge of plastic scintillators is shown in Fig.3.5.

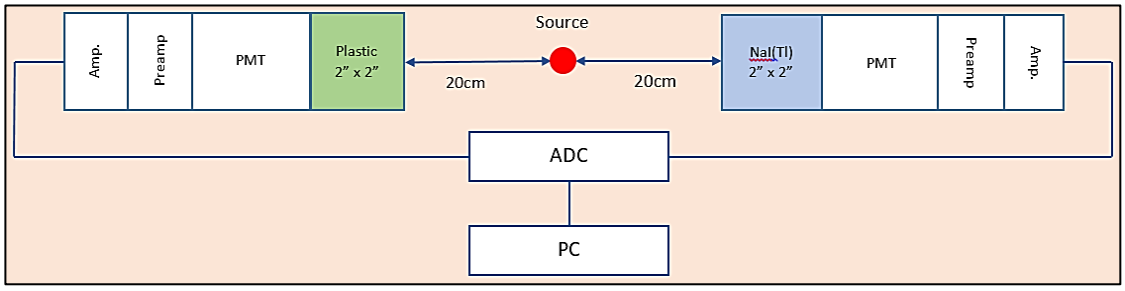

Fig.3.5. Experimental setup for Compton edge measurement for plastic scintillators.

The second detector is a $2''\phi \times 2''L$ NaI(Tl) scintillator coupled to a $2''\phi$ PMT Hamamatsu R878, and operated in an applied high voltage of +650 V. A NaI(Tl) scintillator was selected to realize faster timing measurement. The distance between the NaI(Tl) and plastic scintillator the was set to 40 cm and the radioactive sources mentioned above was placed in the middle between these two detectors. The output signals from the PMT were fed into a pre-amplifier (Clear Pulse 5626), further amplified by the main amplifier (Clear Pulse 4417) with a shaping time of 1.0 μs. The signals were analyzed with an analog-to-digital converter (Nikiglass A3400). The measurement for each radioactive source was taken in 24 hours due to the rate of coincidence events was quite low.

The pulse height distribution spectra obtained for the plastic scintillator detector as the results of coincidence was in the shape of a Gaussian function. Then, the light yield was determined as the peak centroid obtained by fitting Gaussian. The light yields of

CsI(Tl) and plastic detectors were converted into test pulse dial at the same scale. By comparing the light yield of two detectors and using the N_{pe} measured for CsI(Tl) detector, the N_{pe} for plastic scintillator detector was calculated.

3.2. Determination of scintillation efficiency per unit energy deposited by the recoil electron (Electron response)

3.2.1. Method

The electron response is defined as the relative light yield per unit energy deposited by electrons. As mentioned previous, Compton scattering, which is the dominant interaction in plastic scintillators for incident gamma rays, results in a Compton continuum in the energy and pulse height distribution spectrum. To determine the energy deposited by Compton electrons, the Compton Coincidence Technique (CCT) was employed.

The CCT measurement employs a combination of a target detector and a reference detector operating in coincidence [7,8]. A gamma ray of known energy, E_γ (keV), incidents firstly to the target detector, experiences the Compton scattering and transfers a fraction of the incident energy E_γ (keV) to a recoil electron as E_e (keV). If the scattered gamma ray has no further interaction, it is emitted from the scintillator with an energy $E_{\gamma'}$ (keV) at an angle of θ. The scattered gamma ray will travel to the reference detector where the full absorption occurs. By selecting the coincidence events between two detectors, the energy deposited by a recoil electron E_e in the target detector can be calculated via measuring the energy of the scattered gamma ray at a particular angle. The energy of scattered gamma rays and energy of recoil electrons can be calculated by using equations 2.3 and 2.4.

The electron response is determined as the ratio of the relative light yield and the corresponding deposited energy of the recoil electron.

3.2.2. Measurement of energy deposition of recoil electrons with the CCT

The experimental setups of the CCT measurement are shown in Fig.3.6. and Fig.3.7 for the case of the NaI(Tl) scintillator and HPGe detector, respectively.

The target detector is a $2''\phi \times 2''L$ plastic scintillator (EJ-200, EJ-212, or EJ-252) coupled to a $2''\phi$ PMT (Hamamatsu R375). Throughout the CCT measurements, the NaI(Tl) scintillator was employed as the reference detector (2^{nd} detector) due to its simple operation. The measurements are also conducted using a high-purity germanium (HPGe) detector as a reference detector to measure the electron response of the plastic scintillator in the low energy region. The results obtained with two different reference detectors were compared each other.

A 662-keV gamma ray from a ^{137}Cs radioactive source, which was shielded with a lead box, was collimated by a lead collimator with a thickness of 5 cm and a hole of 1 cm in diameter. The collimator was placed a the distance of 20 cm from the source. The plastic scintillator was placed at a distance of 55 cm from the source. Two $3''\phi \times 3''L$ NaI(Tl) detector (Bicron model 3M3/3) were used as reference detectors in order to measure two different scattering angles at the same time. Each NaI(Tl) detector was placed at a distance of 60 cm from the surface of the plastic scintillator detector. Scattered gamma rays at the angles of 15^o, 20^o, 25^o, 30^o, 60^o, 110^o, and 120^o were measured by the first NaI(Tl) detector, and the second NaI(Tl) detector measured the scattered gamma rays at angles of 35^o, 45^o, 75^o, 90^o, 140^o, and 150^o.

In the measurements with the HPGe as the reference detector, the HPGe detector was placed at a distance of 40 cm from the surface of the plastic scintillator detector, and

a 3 cm in diameter lead collimator was additionally placed in front of the HPGe detector to reduce the background radiation. The scattered gamma rays at the angles of 20°, 25°, 30°, 35°, 45°, 60° and 75° were measured by this reference detector. Each measurement was performed in 24 hours because the rate of coincidence events was quite low.

The output signals of the plastic scintillator detector were fed into a pre-amplifier (Clear Pulse 5548), further amplified by the main amplifier (Clear Pulse 4417) whose shaping time constant was set to 0.5 μs. The output signals from NaI(Tl) detectors were amplified by another main amplifier (Clear Pulse 4417) with a time constant of 1.0 μs. The output signals of the HPGe detector were fed into a high voltage power supply (Ortec 659), further amplified by a main amplifier (Ortec 572) with a time constant of 6.0 μs. The signals from the main amplifiers were analyzed with the ADC (Nikiglass A3400).

By selecting the coincidence events between two detectors, a Gaussian shape peak can be obtained in the pulse height distribution spectrum of the plastic scintillator detector. The coincidence events were extracted based on the difference in the time stamp of the recorded data in the ADC. The width of the coincidence window is adjusted based on the time constants of main amplifiers; typically, the width of the coincidence window used for plastic and NaI(Tl) detector was 1.0 – 2.0 μs, and was 13.0 – 14.0 μs for coincidence between plastic and HPGe detectors.

A typical pulse height distribution, obtained at a scattering angle θ of 150° is shown in Fig.3.8. The coincidence peak was fitted with a Gaussian function to determine the centroid and the width (FWHM – Full Width at Half Maximum) in the pulse height distribution spectrum of the target and reference detectors.

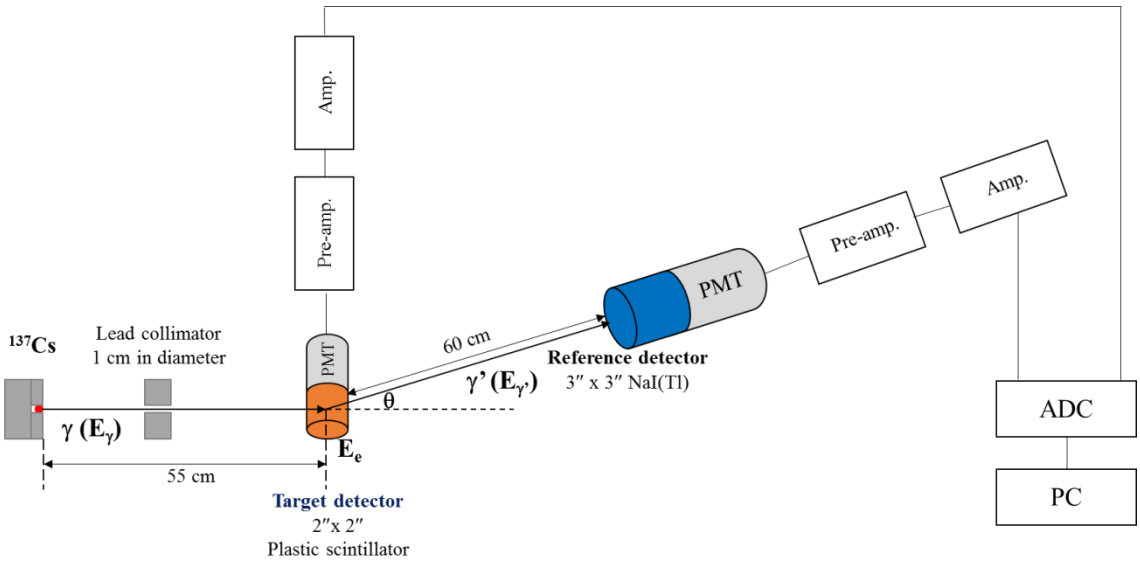

Fig.3.6. Experimental setup for CCT measurement using NaI(Tl) detector.

The energy E'_γ of a scattered gamma ray was determined by applying the corresponding peak centroid into the energy calibration equation of the reference detector. In order to perform the energy calibration of the detector systems, several radioactive sources emitting gamma rays were employed, and pulse height distribution spectra were obtained. By fitting the photopeaks with Gaussian functions, the peak centroids were determined and the relationship between peak centroids and corresponding energies (energy calibration) was established. Then, the energy of a recoil electron deposited in the plastic scintillator was calculated from equation 2.4.

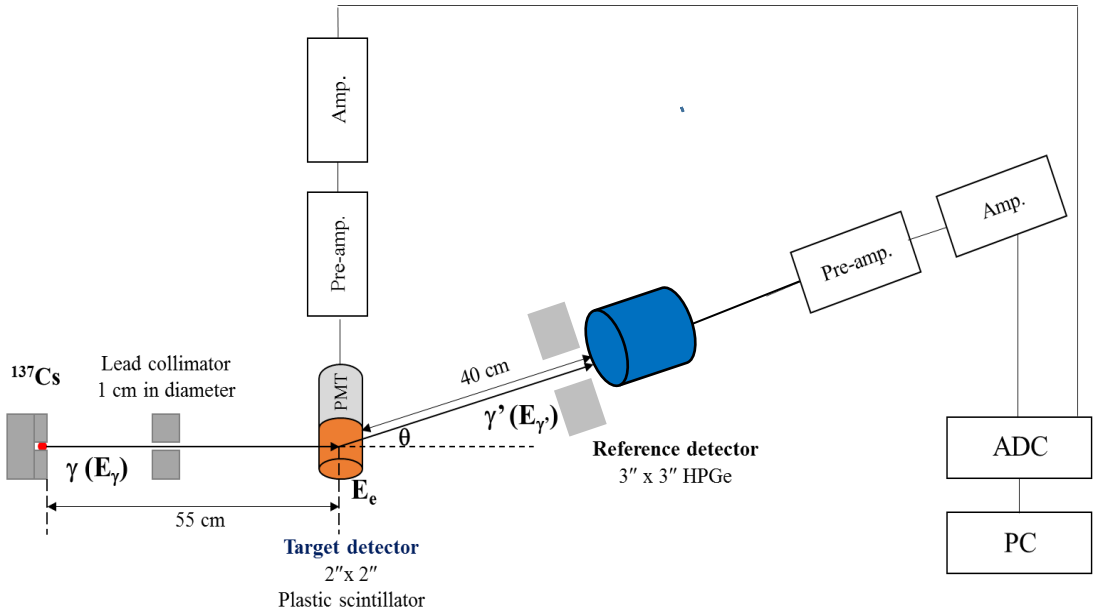

Fig.3.7. Experimental setup for CCT measurement using HPGe detector.

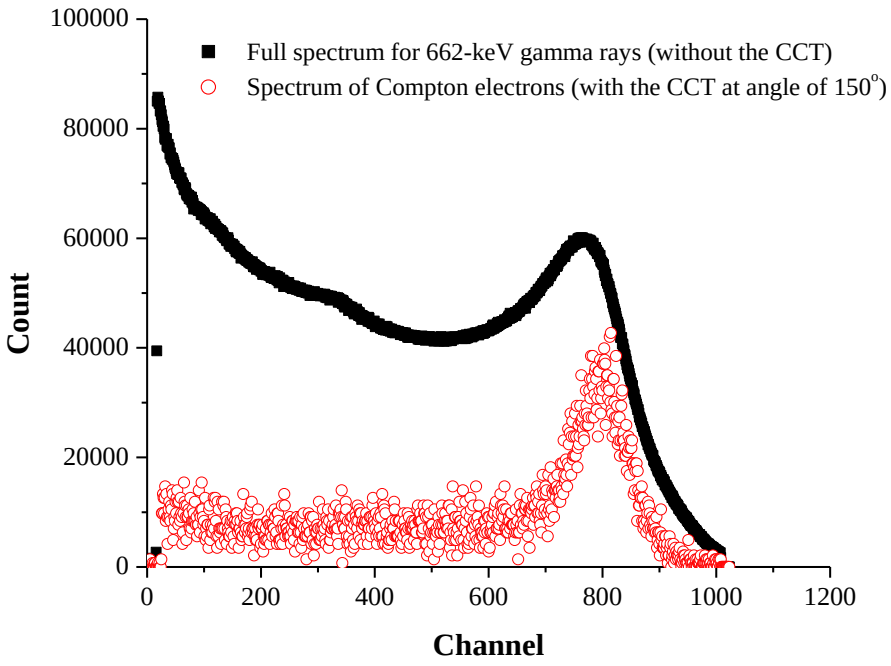

Fig.3.8. Typical pulse height distribution obtained in EJ-200.

3.3. Evaluation of energy resolution in plastic scintillators

Attempts to examine the energy resolutions for electrons in plastic scintillators were performed by using the data of the CCT measurements. The relative energy resolution is defined as a ratio of the full width at half maximum (FWHM) to the peak centroid obtained by Gaussian fitting for the coincidence peaks. The resolution obtained in the CCT measurement R is considered to be composed of two main components; a spread of electron energy in the plastic scintillator caused by the extent of solid angles subtended by the reference detectors from the target one in the CCT measurement δ_{CCT}, and a fluctuation generated in the energy deposition of recoil electrons in plastic scintillators δ_{sc}. Then the resolution in the CCT measurement may be written as follows,

$$R^2 = \delta_{CCT}^2 + \delta_{sc}^2 . \quad (3.7)$$

Here, δ_{sc} denotes the intrinsic resolution of plastic scintillators which is supposedly due to monochromatic recoil electrons and is evaluated as

$$\delta_{sc} = \sqrt{R^2 - \delta_{CCT}^2} \quad . \quad (3.8)$$

The intrinsic resolution includes the statistical fluctuation δ_{st} in the number of photoelectrons N_{pe} generated from the PMT photocathode [2], where $\delta_{st} = 2.35/\sqrt{N_{pe}}$. N_{pe} corresponding to the energy of a recoil electron measured in the CCT measurement is calculated from W_s with a correction for the electron response at each energy.

Since δ_{CCT} is complexly related to the solid angles between two detectors and cannot be given by simple calculations, δ_{CCT} was evaluated by simulations using the EGS5 code [9] for the experimental geometry in the CCT measurement. In addition, an energy resolution for 60-keV gamma rays from an ^{241}Am source was measured and compared with the resolution obtained with the CCT measurements.

3.4. Measurement of position sensitivity in plastic scintillator rod system

3.4.1. Plastic scintillators used in the study

The incidence position of radiation into the detector as well as its trajectory need to be measured in order to determine the track length of radiation inside the detector. Thus, the dependence of a plastic scintillator detector's outputs on the incident position of the radiation was examined by performing the following measurements.

NE-102 plastic scintillator (equivalent to EJ-212) was selected as the scintillator material for these measurements because it is a widely used plastic scintillator and has the shorter light attenuation length compared with that of EJ-200 as shown in Table.3.1. For the shape of the scintillator, a fiber shape has an advantage of fast timing and good transmitting of light, but does not give the information on the deposited energy; a sheet shape has a difficulty to give the position information; a long cylindrical shape is possible but some areas are insensitive to radiations due to its spherical surface in the use of combining together as a detector set.

For these reasons mentioned above, a rod geometry (rectangular parallelepipeds) was chosen. In this study, a rod made of EJ-212 having a square cross section of 0.9 cm x 0.9 cm was manufactured and a set of four rods was directly coupled to 4-segment PMTs (Hamamatsu R7600U-M4) at both ends. A set of four rods with one rod's length of 10 cm or 30 cm was prepared to investigate attenuation of scintillation lights from an incident point of radiation to PMTs at the ends. Particularly, 30 cm rods irradiated with alpha particles were employed to examine the nature of transparency of light in the rod, and only aluminized mylar reflector was used due to the strong energy attenuation of alpha particles while passing through matters. Separately, measurements for 10 cm rods irradiated with beta particles were performed with three different reflectors (aluminized

mylar sheet, teflon tape, and black tape) to examine the relationship between the irradiation position and outputs from PMTs at the ends and observe the difference in the outputs obtained from the reflectors. Experimental methods for beta particles and for alpha particles are basically similar but differ in collimating the radiation and taking data. The methods are given for two radiation sources in the following sections.

3.4.2. Measurements with alpha particles

The measurement was carried out for a plastic scintillator detector irradiated with alpha particles from an ^{241}Am source, E_α = 5.49 MeV (85% in intensity).

Polished square NE-102 rods with a size of 0.9 cm x 0.9 cm x 30 cm were used. Four rods unified as one set were coupled to multi-segment PMTs (Hamamatsu R7600U-M4) at both ends. The rod was wrapped in one layer of aluminized mylar sheet with a thickness of 1.5 μm. Due to the substantial attenuation of alpha particles in matter, only one layer of aluminized mylar sheet is applicable for this test. The ^{241}Am was placed on the plastic scintillator rod's reflector surface. The area of radiation material in the source which was created by evaporation on a copper foil has a size of 0.5 cm in diameter. The distance in air from the source to the plastic scintillator rod's reflector surface is approximately 0.3 cm. The measurements were performed by changing the position of the ^{241}Am source along the rod (nine points were marked on detector's supporter frame from one edge to another with a step of 3 cm), and the related pulse height spectra were recorded for each point. The experimental setup is shown in Fig.3.9. In operation, the ^{241}Am source irradiated one rod only. Due to the detector's configuration, four plastic scintillator rods were operated simultaneously but the output signals from the rod irradiated with alpha particles were recorded only because the alpha particles completely stop in the rod, where a track length of the alpha particles is estimated to be 35 μm

(SRIM2008) in the rod. The arranged order of the rods is shown in Fig.3.10.

In order to examine the influence due to the existence of the aluminized mylar reflector, such as a fluctuation in energy of alpha particles in it, a similar measurement was also performed under the bare plastic scintillator rod condition, in which no reflector materials were used for the same rod.

The output signals from the PMTs of the plastic scintillator detector were directly fed into an amplifier (Clear Pulse 4417) with a shaping time constant of 0.5 μs through a T-connector coupled to a 50 Ω terminator. The high voltage of – 800 V was applied for PMTs.

The pulse height distribution with a Gaussian shape was obtained. A typical pulse height distribution spectrum is shown in Fig.3.11. The pulse height for each position of the source was determined as the peak centroid by applying Gaussian fitting to the pulse height distribution. The pulse height was then converted from channel to test pulse dial. Finally, the relationship between the source positions and pulse height from PMTs was examined.

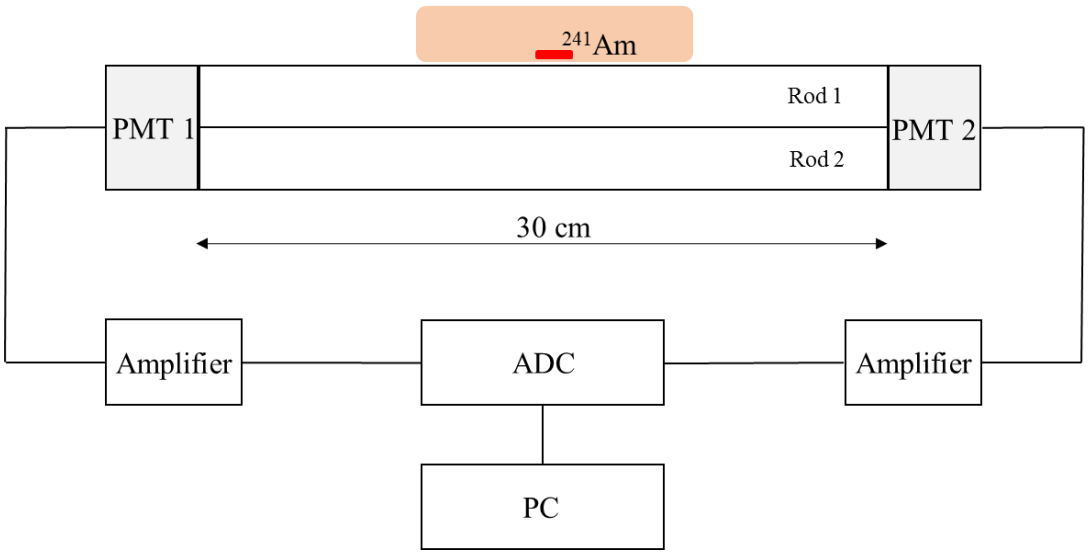

Fig.3.9. Experimental setup for position sensitivity using alpha particles.

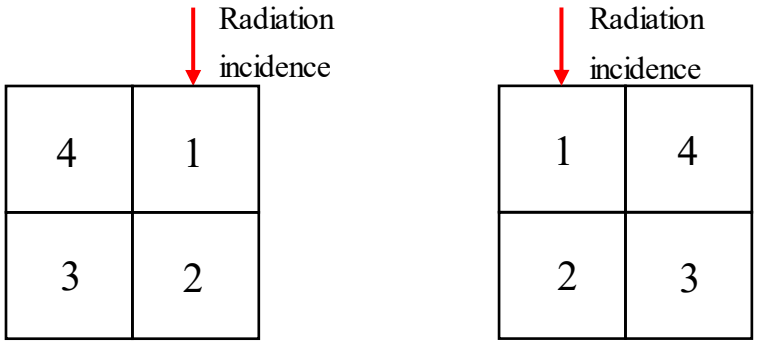

Fig.3.10. The arranged order of the plastic scintillator rods in the detector's configuration; a) the interface coupled to the PMT 1 and b) the interface coupled to the PMT 2.

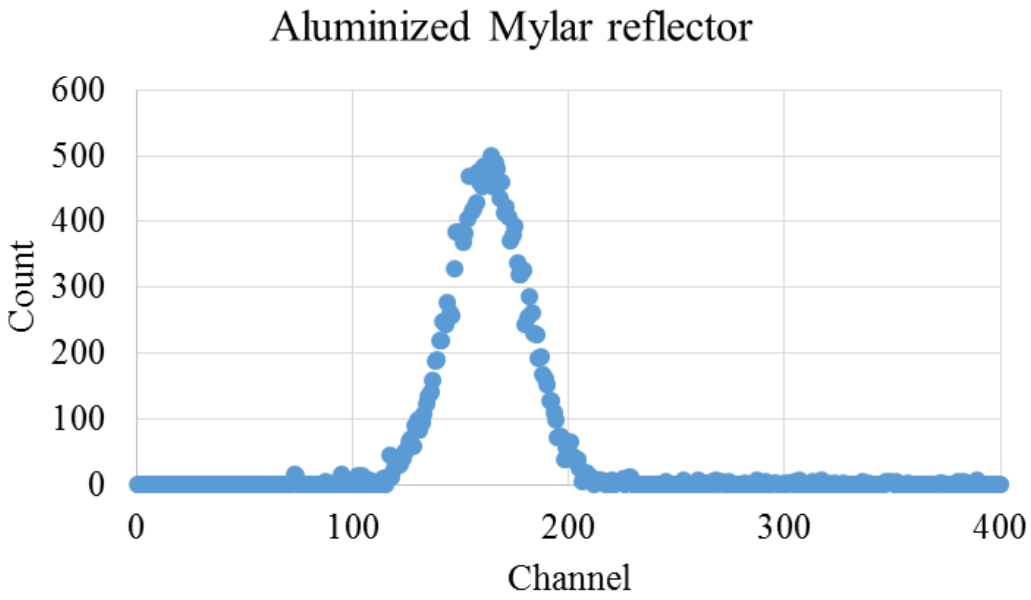

Fig.3.11. Pulse height distribution obtained from PMT 1 of the rod for the ^{241}Am placed at 3 cm from PMT 1.

3.4.3. Measurements with beta particles

The measurement was carried out for plastic scintillator rods irradiated with beta particles from a ^{90}Sr/^{90}Y source, which emits beta particles with the energies of 545.9 keV and 2279 keV.

Polished square NE-102 rods with a size of 0.9 cm x 0.9 cm x 10 cm were used.

Four rods unified as one set were coupled to 4-segment PMTs (Hamamatsu R7600U-M4) at the both ends. Three different reflectors: aluminized mylar sheets, teflon tapes, and black adhesive tapes, were used. An acrylic collimator having 2 cm thickness, which can fully stop 2279 keV beta particles, was put on the top surface of the detector's supporter frame, and the $^{90}Sr/^{90}Y$ was placed on the top surface of the collimator. The distance from the source to the plastic scintillator rod's reflector surface is approximately 4 cm in air. The measurements were performed by changing the position of the $^{90}Sr/^{90}Y$ source along the collimator where nine collimator holes with a diameter of 3 mm were set with a step of 1 cm. The related pulse height spectra were recorded for each point. The experimental arrangement was illustrated with Fig.3.12. The output signals from the PMTs of the plastic scintillator detector were fed directly into an amplifier (Clear Pulse 4417) with a shaping time constant of 0.5 μs through a T-connector coupled to a 50 Ω terminator. The high voltage of – 800 V was applied for PMTs. The gain of the amplifier was set differently for each reflector because the different thicknesses and materials of the reflectors contribute to the different attenuation of the beta particles. According to the ways of wrapping, the thickness of reflectors was estimated to be 1.5 μm for aluminized mylar sheet, or 0.25 mm for black adhesive sheet, where each rod was wrapped by one layer only. Teflon tape reflector, where the tape was wrapped around the rod from one end to the other for the two layers, and another layer was wrapped over four rods. The estimated thickness at the surface of radiation incidence and the gain set for the amplifier for each reflector are shown in Table.3.2. The acquisition time was set to 1200 s for each measurement.

Table.3.2. The thickness of reflectors and the amplifier setting.

	Aluminized mylar sheet	Teflon tape	Black adhesive sheet
Thickness of the reflector at radiation incident point	1.5 μm	0.3 mm	0.25 mm
Coarse gain set for the amplifier	8	8	32
Time constant of the amplifier	0.5 μs	0.5 μs	0.5 μs

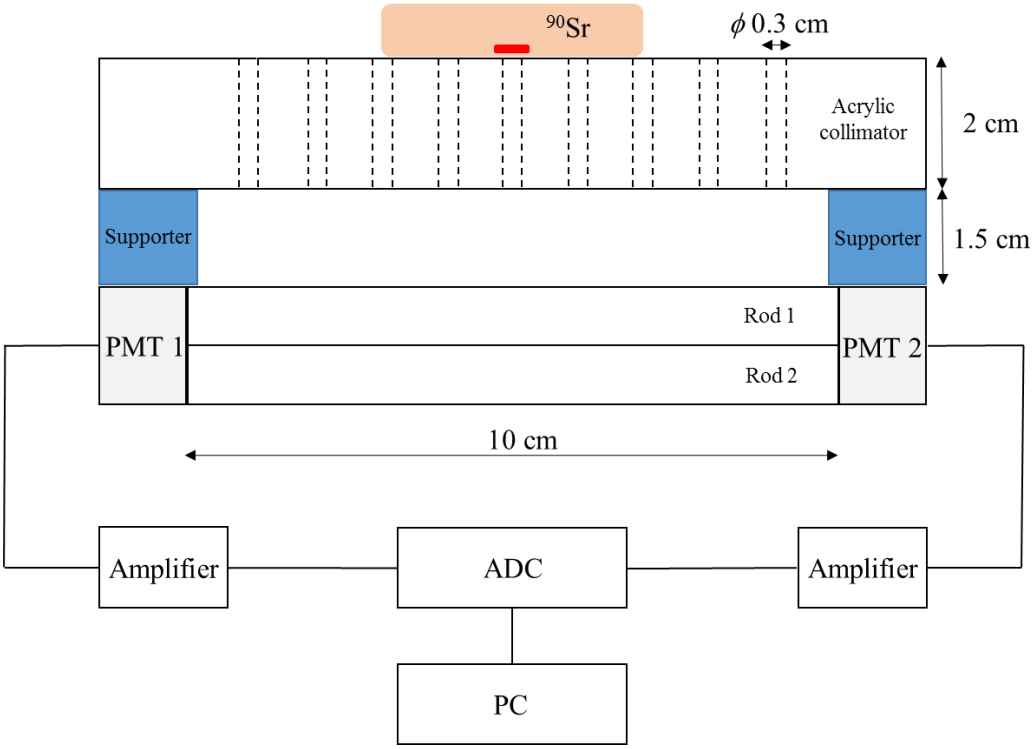

Fig.3.12. Experimental setup for position sensitivity using beta particles.

By considering the energy loss of 2279 keV beta particles from ^{90}Y after transversing the air and the reflector, the range of the beta particles in plastic scintillator material was calculated as approximately 1.1 cm. These beta particles possibly pass through rod 1 to rod 2 as depicted in Fig.3.12. By selecting only the coincidence events in both-end PMTs' output signals between rod 1 and rod 2, the events corresponding to deposited energies in rod 1 were extracted from the full recorded data.

The pulse height distribution obtained in rod 1 is a continuum distribution which is the typical distribution of measuring beta particles, and a typical distribution obtained for the $^{90}Sr/^{90}Y$ placed at 1 cm from PMT 1 is shown in Fig.3.13. To determine the pulse height corresponding to the maximum deposited energy, the linear portion of the curve was extrapolating to zero count. The pulse height was then converted from channel to test pulse dial. Finally, a relationship between the source positions and pulse height from PMTs was examined.

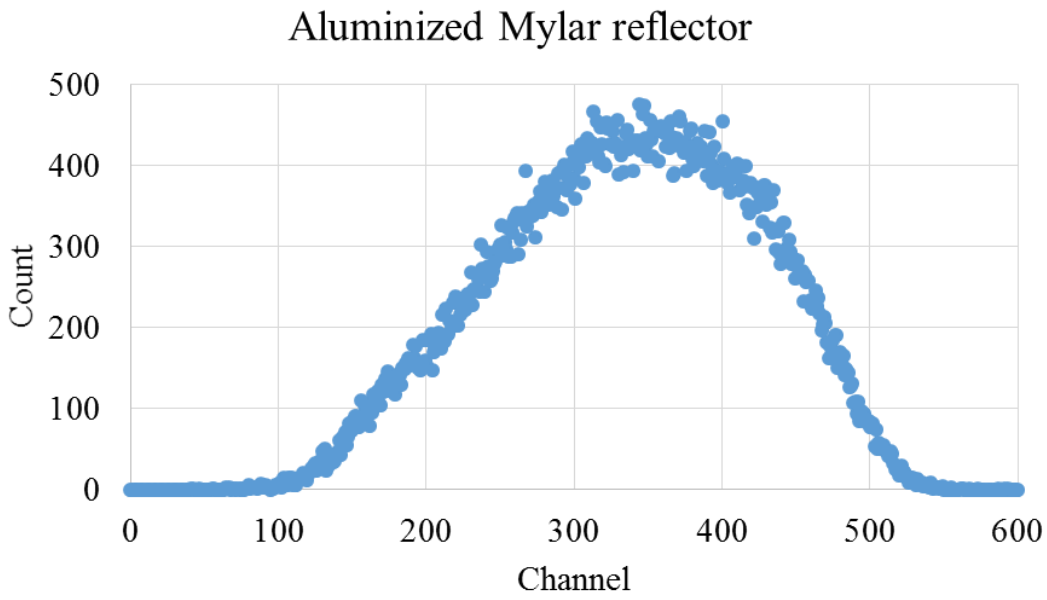

Fig.3.13. Pulse height distribution obtained from PMT 1 of rod 1 for the $^{90}Sr/^{90}Y$ placed at 1 cm from PMT 1 as the result of coincident technique.

3.5. Response of plastic scintillators for heavy charged particles

High energy heavy charged particles of H (230 MeV/u) and Si (800 MeV/u) from the PB2 beamline of HIMAC (Heavy Ion Medical Accelerator in Chiba) in National Institute of Radiological Sciences (NIRS) were used for studying the response of plastic scintillators to heavy charged particles. The detector system used in the measurement of beta particles mentioned above was employed (NE-102 rod with a size of 0.9 cm × 0.9

cm × 10 cm wrapped by aluminized mylar reflector). The experimental setup is shown in Fig.3.14. The detector was placed inside a light-proof black box for light shielding, and the black box was arranged after the detector and beam alignment set up. The detector system placed inside the light-proof black box is shown in Fig.3.15.

The beam of heavy charged particles with a size of 1 cm in diameter at the place of beam window incident at the normal angle to the center of the rod 1 (at a position of 5 cm from each PMT) as illustrated in Fig.3.16. The incidence position of ions beam was kept for the whole procedure. Several aluminum absorbers with different thicknesses were used to vary the energy of the heavy charged particles. The distance between the beam window and the detector system was 1 m in case of H and 4 m in case of Si. The pulse heights from both-end PMTs for rod 1 and rod 4 were measured. The applied high voltage for both-end PMTs was – 800 V in the measurement of H ions and – 600 V in the measurement of Si.

Other measurements were conducted for C (400 MeV/u) using the bio-experimental beamline in HIMAC. The same detector system at the H and Si measurements was used. In this case, the size of ion beams is expanded up to 10 cm in diameter at the place of the beam window, and the beam covered the surface area of the detector. Then, a trigger detector was additionally employed to examine the ion response of each rod as well as to position sensitivity. The trigger detector was an assembly of a 1 cm x 4 cm x 0.5 cm NE-102 coupling to a 1/2″ϕ PMT (Hamamatsu R4124). The applied voltages to both-end PMTs of the main detector were – 650 V. In order to determine incidence positions of beams, signals were selected using the trigger detector. The detector was moved so that the beam incident to several positions (2cm, 3cm, 4cm, 5cm, 6cm, 7cm, and 8cm along the rod). At each position, the trigger detector was placed so as to face a 0.5 x 1 cm^2 area

of the detector to the rod. By selecting the coincidence events between rod 1, rod 4 and trigger detector or between rod 2, rod 3 and trigger, the pulse height distributions of main plastic scintillator rods were recorded. The illustration for ions beam incident to plastic scintillator rod with trigger detector is shown in Fig.3.17.

Fig.3.14. Detector system used in measurement of response to heavy charged particles.

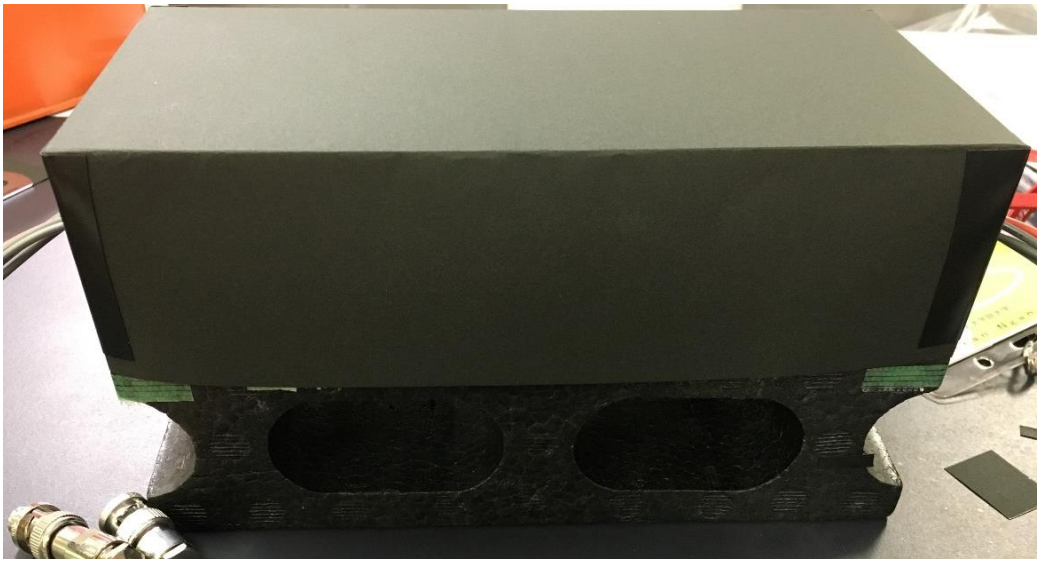

Fig.3.15. A light-proof box for light shielding where the detector sytem was placed inside.

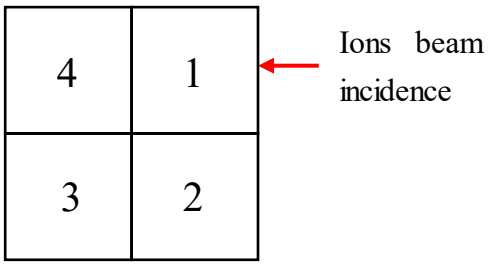

Fig.3.16. Illustration of ions beam incident to plastic scintillators.

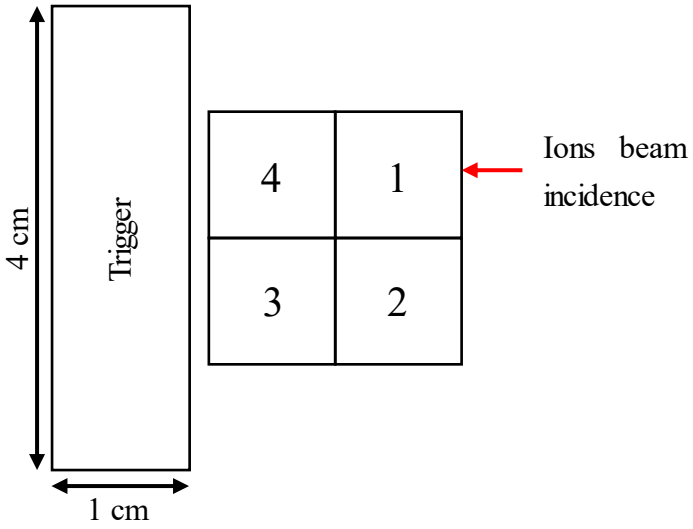

Fig.3.17. Illustration of ions beam incident to plastic scintillators and the arrangement of the trigger detector.

In order to calibrate the gains of PMTs as a function of applied high voltage. The PMTs were coupled to a $2''\phi \times 2''L$ NaI(Tl) scintillator, and the high voltage was adjusted to – 800 V, – 650 V, and – 600 V, respectively. The light outputs from the four segments of the PMTs were measured by irradiating the detector with gamma rays from ^{137}Cs, ^{22}Na, and ^{54}Mn sources. The light outputs corresponding to incident energies were obtained by fitting the photopeak in the pulse height distribution with Gaussian functions. Then, the

linear relation between the light output and energy was established for each high voltage set in each measurement. Besides, $2''\phi \times 2''L$ NaI(Tl) totally covered the area of four channels of the PMT, these measured data were used to compare the gain of each PMT channel.

References

[1] http://www.eljentechnology.com/index.php/products/plastic-scintillators.

[2] S. Sasaki, H. Tawara, K. Saito, M. Miyajima, and E. Shibamura, Average Energies Required per Scintillation Photon and Energy Resolutions in NaI(Tl) and CsI(Tl) Crystals for Gamma Rays, Japanese Journal of Applied Physics 45 (8A), 2006, 6420 – 6430.

[3] G. F. Knoll, Radiation Detection and Measurement, 4th ed., John Wiley & Sons, United States of America, 2010.

[4] W. R. Nelson, H. Hirayama and D. W. O. Rogers, The EGS4 Code System, SLAC265, Stanford University, Stanford, 1985.

[5] E. Shibamura, S. Sasaki, H. Tawara, K. Saito, M. Miyajima, Photon-to-electron conversion efficiency and reflectance of photomultiplier tubes as a function of incidence angle of photon, Nuclear Instruments and Methods in Physics Research A 567, 2006, 192 – 195.

[6] E. Shibamura, S. Sasaki, H. Tawara, K. Saito, M. Miyajima, Angular Response of Photomultiplier Tubes: Photon-to-Electron Conversion Efficiency and Reflectance, Japanese Journal of Applied Physics 45 (7), 2006, 5990 – 5995.

[7] J. D. Valentine, B. D. Rooney, Design of a Compton spectrometer experiment for studying scintillator non-linearity and intrinsic energy resolution, Nuclear Instruments and Methods in Physics Research A 353, 1994, 37 – 40.

[8] B. D. Rooney and J. D. Valentine, Benchmarking the Compton coincidence technique for measuring electron response nonproportionality in inorganic scintillators, IEEE Transactions on Nuclear Science 43 (3), 1996, 127 – 1276.

[9] H. Hirayama, Y. Namito, A.F. Bielajew, S.J. Wilderman and W.R. Nelson: SLAC-R-730, KEK Report 2005-8, 2005.

CHAPTER 4 RESULTS AND DISCUSSION

In this chapter, the experimental results obtained in this study are presented. The results include the absolute light yield in plastic scintillators, the electron response, and the energy resolution, the position sensitivity with using beta particles and alpha particles, and the response of plastic scintillators to energetic heavy charged particles. Discussions are also given for the results.

4.1. The absolute light yield of plastic scintillators

4.1.1. W_s in CsI(Tl) for 662-keV gamma rays

The number of photoelectrons N_{pe} measured for a $2''\phi \times 2''L$ CsI(Tl) scintillator in PD-mode was obtained to be 7657 ± 92 electron/MeV.

From the EGS4-SPC4, the collection efficiency $F_{collect}$ of photons at the photocathode of a PMT coupled to the CsI(Tl) scintillator was obtained to be 0.64 ± 0.03. The results of $F_{collect}$ show that 100 percent of the generated scintillation photon in a scintillator cannot be collected at the photocathode of the PMT because of several processes where a photon can undergo in a scintillator, which were mentioned in section 3.1. The correction factor $\langle F \rangle$ was determined to be 1.88 for CsI(Tl).

The W_s in CsI(Tl) for 662-keV gamma rays was determined. The data were compared with those obtained from other studies. W_s in CsI(Tl) was obtained as 15.1 ± 1.3 eV. Using the similar experimental setup, Sasaki et al. [1] determined W_s in CsI(Tl) as 13.3 ± 1.1 eV by assuming $F_{collect} = 0.55 \pm 0.03$, which was taken from the value for NaI(Tl). Applying the present $F_{collect}$ to the results by Sasaki et al., a value of 15.6 ± 1.3 eV as W_s in CsI(Tl) was obtained, which agrees well with our result. The value of W_s in CsI(Tl) was theoretically determined by Doke et al. [2] to be 13.7 or 14.8 eV, and

measured by Valentine et al. [3] as 15.4 eV. Both values are very close to the value determined in this study and indicate the validity of the method used to determined W_s.

The uncertainty in the measurement of W_s for CsI(Tl) evaluated in a similar manner of the other study [1] was totally ±8.6% including the uncertainty in the number of photoelectrons, the uncertainty in the collection efficiency, and the uncertainty in the conversion efficiency. The determination of uncertainty is given in detail in Table.4.1.

Table.4.1. Uncertainties in the measurement of W_s in CsI(Tl) [1].

(1) Uncertainty in Photoelectron number ±1.2% Reproducibility in measurement ±1% Calibration in charge ±0.5% Peak centroid determination in fitting ±0.3%
(2) Uncertainty in Conversion efficiency ±7.1% Spectral quantum efficiency ±5% Reflectance of PMT ±5% Peak centroid determination in fitting ±0.1% LED stability (reproducibility) ±0.25% Absolute reflectance with integrating sphere ±5% Quantum efficiency at an angle ±0.27% Peak centroid determination in fitting ±0.1% LED stability (reproducibility) ±0.25%
(3) Uncertainty in Collection efficiency ±4.7% Ambiguity in geometry (below) ±3% Reflectance of reflector ±3% Reflectance of PMY (for photons returning to crystal) ±2%
Total ±8.6%

4.1.2. W_s in plastic scintillators for gamma rays

The pulse height distributions in three plastic scintillators at the Compton maximum energy of electron are shown in Fig.4.1. (a)-(c). These distributions obtained for gamma rays from ^{137}Cs, ^{54}Mn, and ^{22}Na with the CCT measurement for a scattering angle of 180^{o}

where the target and the reference detectors were on either side of a radiation source in line (hereby it was called as the “face-to-face” measurement).

The Compton edge positions obtained from the measurement were compared with those obtained by fitting the full spectrum of plastic scintillators. The Compton edge position determination by the fitting is simply described as follows:

(1) Calculating the energy distribution of scattered electrons by a gamma ray with given energy.

(2) Adjusting horizontal factors to multiply the value of energy to fit the experimental horizontal value (channel number).

(3) Adjust vertical factors to multiply the value of energy distribution to fit the experimental vertical value (counts/channel).

(4) Making convolution with Gaussian function with adjusted FWHM. These parameters are adjusted so that the modified energy distribution is in the best agreement with pulse height spectrum near the peak channel.

A sample of Compton edge position’s determination by fitting is shown in Fig.4.2. The results of the comparison in EJ-200, EJ-212, and EJ-252 are shown in Table.4.2, Table.4.3, and Table.4.4 respectively. The results are in good agreement with each other approximately within 3%.

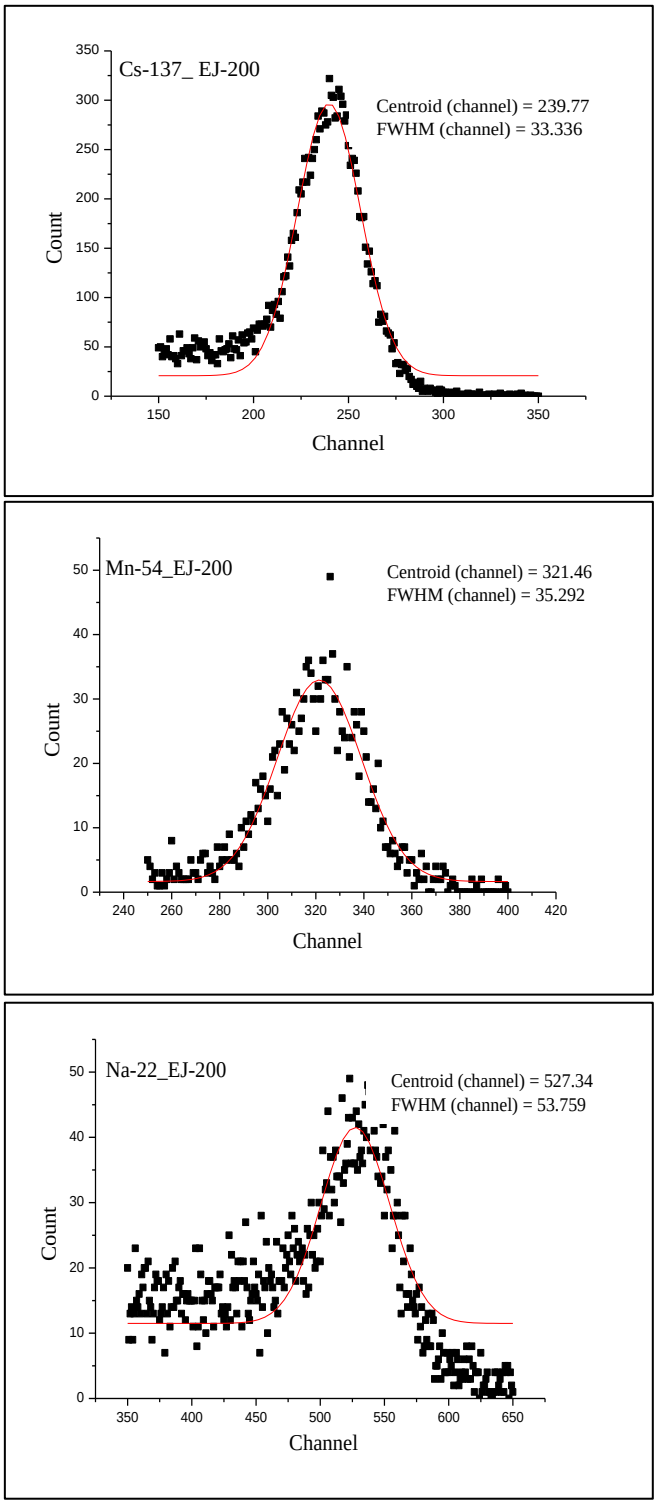

Fig.4.1.(a). Pulse height distributions corresponding to the Compton edge in EJ-200 obtained for gamma rays from ^{137}Cs, ^{54}Mn, and ^{22}Na with the face-to-face measurement (the CCT measurement for the scattering angle of 180°).

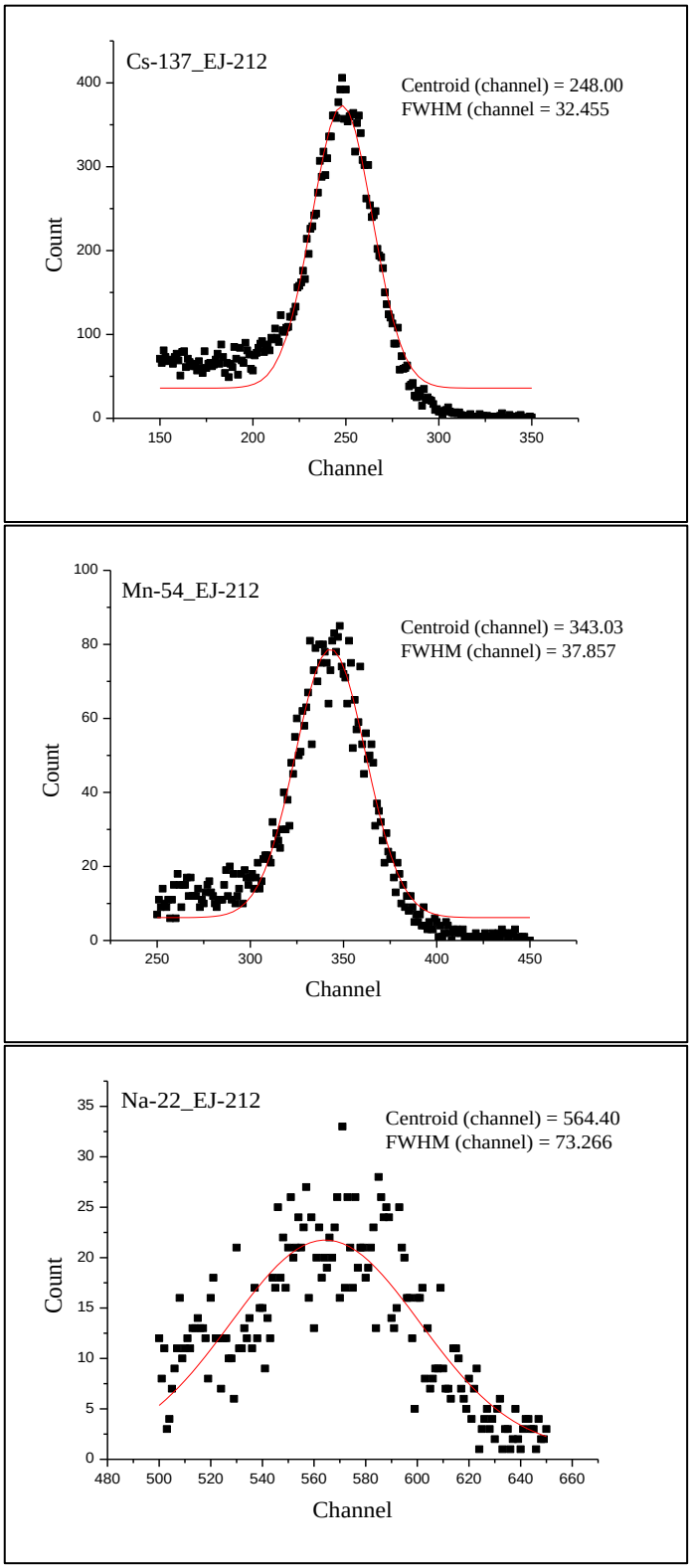

Fig.4.1.(b). Pulse height distributions corresponding to the Compton edge in EJ-212 obtained for gamma rays from ^{137}Cs, ^{54}Mn, and ^{22}Na with the face-to-face measurement (the CCT measurement for the scattering angle of 180°).

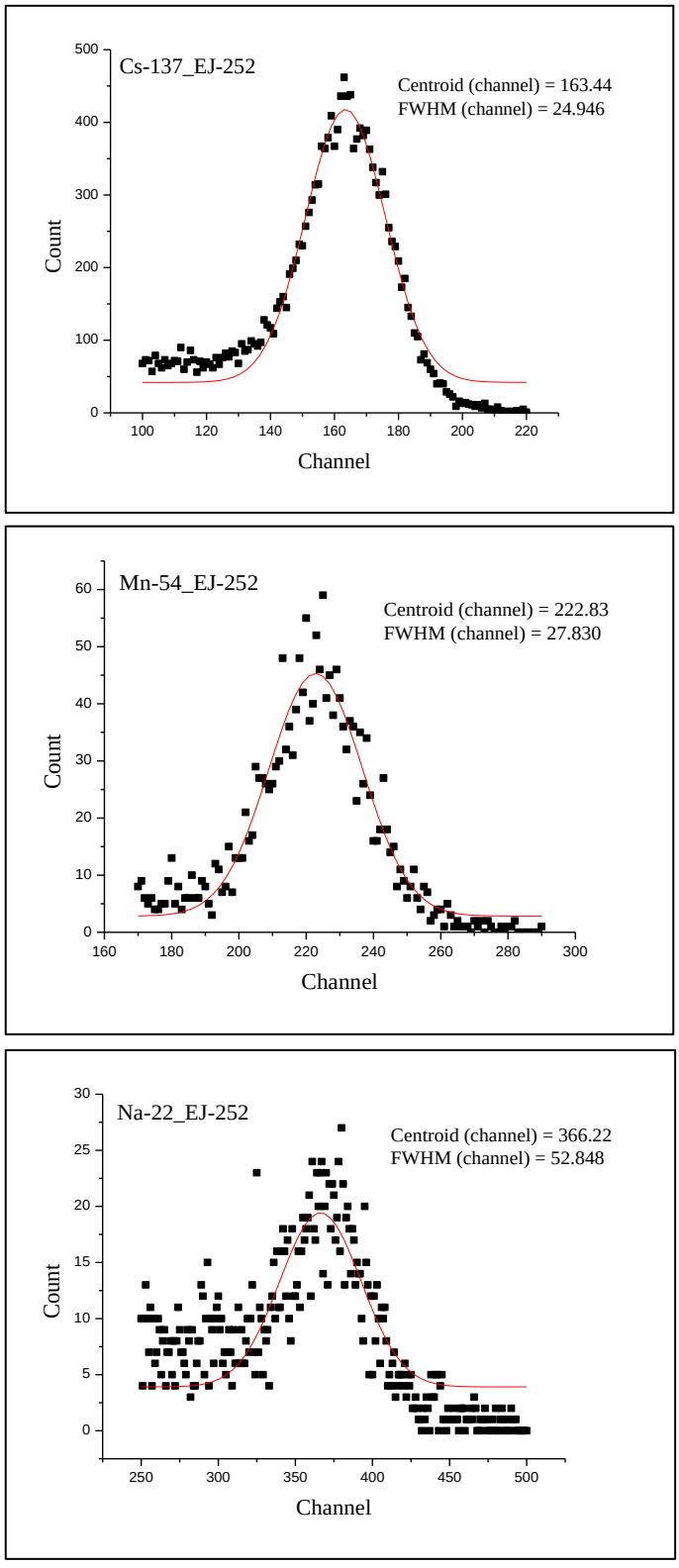

Fig.4.1.(c). Pulse height distributions corresponding to the Compton edge in EJ-252 obtained for gamma rays from ^{137}Cs, ^{54}Mn, and ^{22}Na with the face-to-face measurement (the CCT measurement for the scattering angle of 180°).

Table.4.2. Positions of the Compton edge in EJ-200 obtained with the face-to-face measurement and the fitting method.

	Radioisotope source	Compton edge energy (keV)	Compton edge position (channel)		
			Measured	Fitting	Difference (%)
EJ-200	^{137}Cs	477.3	240	247	2.93
	^{54}Mn	639.2	321	330	2.59
	^{22}Na	1061.7	527	546	3.42

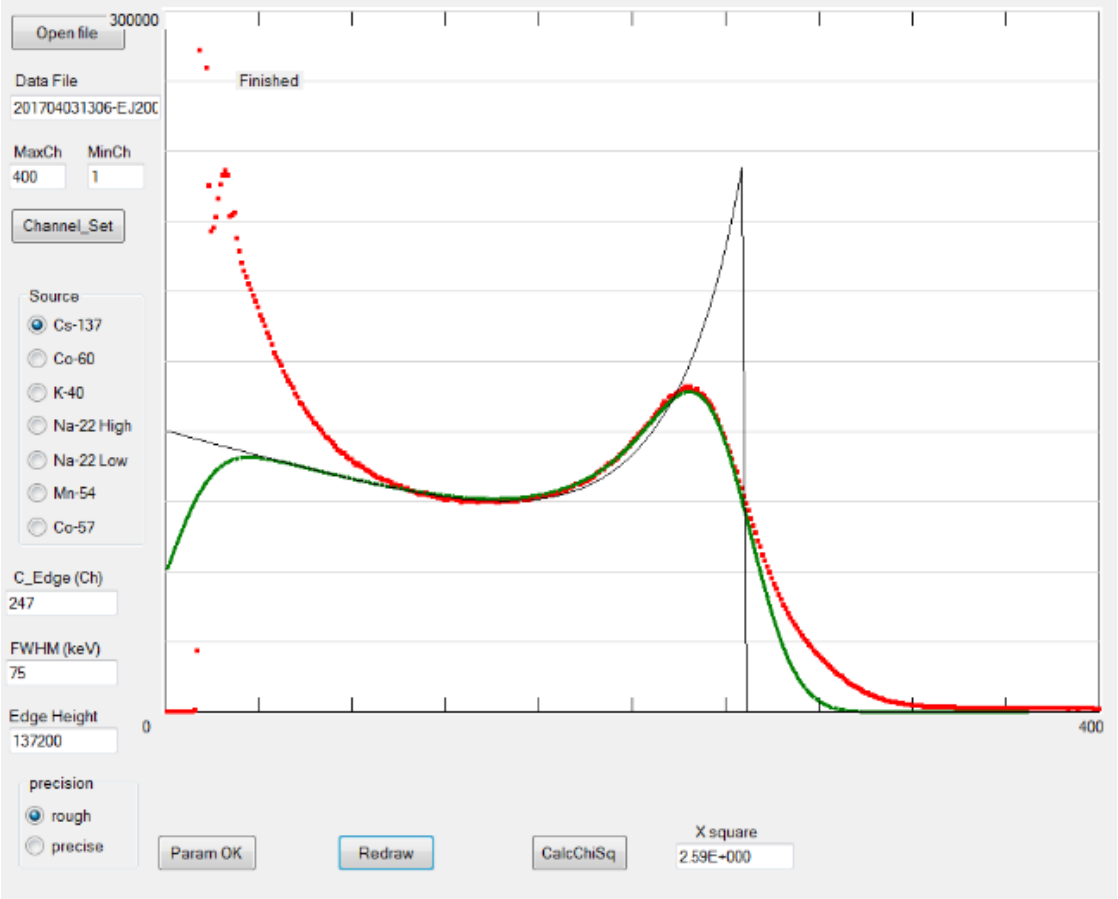

Fig.4.2. Compton edge postion in the measured pulse height distribution of EJ-200 (shown in red) was determined by fitting, the calculated distribution was shown in green.

The light yields in the plastic scintillator and the CsI(Tl) obtained with the same PMT (Hamamatsu R375) operated in the normal operation mode (PMT-mode) are shown in Table.4.5 and Table.4.6 where the relative light yields were converted into test pulse dials to normalize the gains of amplifier used in the measurements. Figures 4.3, 4.4, 4.5, and 4.6 indicates the light yields as a function of Compton maximum energy, and the linearity between them is quite well in any plastic scintillators.

The number of photoelectrons of plastic scintillator detector was obtained by comparing the light yields of plastic scintillator with those of CsI(Tl) and using the number of photoelectrons of CsI(Tl) detector obtained by the PD-mode measurement mentioned previously.

Table.4.3. Positions of the Compton edge in EJ-212 obtained with the face-to-face measurement and the fitting method.

	Radioisotope source	Compton edge energy (keV)	Compton edge position (channel)		
			Measured	Fitting	Difference (%)
EJ-212	^{137}Cs	477.3	248	256	3.13
	^{54}Mn	639.2	343	351	2.27
	^{22}Na	1061.7	564	582	3.02

From the EGS4-SPC4 calculation, the collection efficiency $F_{collect}$ of photons at the photocathode of a PMT coupled to the plastic scintillator was obtained to be 0.60 ± 0.03 while $F_{collect}$ for CsI(Tl) was 0.64 ± 0.03 as mentioned previously. The difference is mainly caused by the different peak wavelengths in emission spectra of the scintillators and different refractive index (1.58 and 1.79 for plastic scintillator and CsI(Tl) scintillator,

respectively). The correction factor $\langle F \rangle$ was determined to be 1.75 for plastic scintillator, while 1.88 for CsI(Tl) as mentioned previously.

Table.4.4. Positions of the Compton edge in EJ-252 obtained with the face-to-face measurement and the fitting method.

	Radioisotope source	Compton edge energy (keV)	Compton edge position (channel)		
			Measured	Fitting	Difference (%)
EJ-252	^{137}Cs	477.3	163	168	2.71
	^{54}Mn	639.2	223	227	1.84
	^{22}Na	1061.7	366	385	4.88

Table.4.5. Light yield of plastic scintillator operated in the normal operation mode of the PMT (Hamamatsu R375).

Radioisotope source	Compton Edge energy (keV)	Compton edge position (test pulse dial)		
		EJ-200	EJ-212	EJ-252
^{137}Cs	477.3	14	14	10
^{54}Mn	639.2	19	20	13
^{22}Na	1061.7	31	33	21

Table.4.6. Light yield CsI(Tl) detector working in the normal operation mode of the PMT.

Radioisotope source	Energy (keV)	Photopeak position (test pulse dial)
^{137}Cs	661.7	91
^{54}Mn	834.8	116
^{22}Na	511.0	71
	1274.5	178
^{60}Co	1173.2	163
	1332.5	186

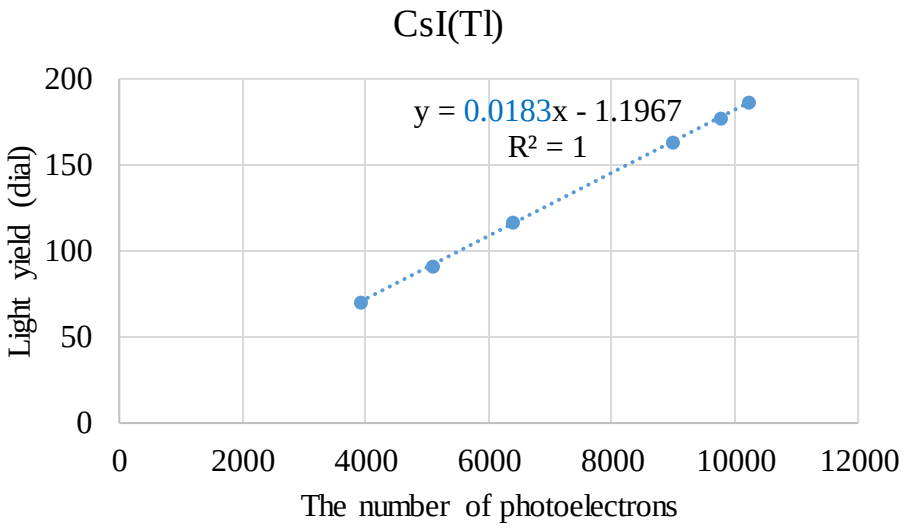

Fig.4.3. Light yield of CsI(Tl) detector as a function of photoelectron number.

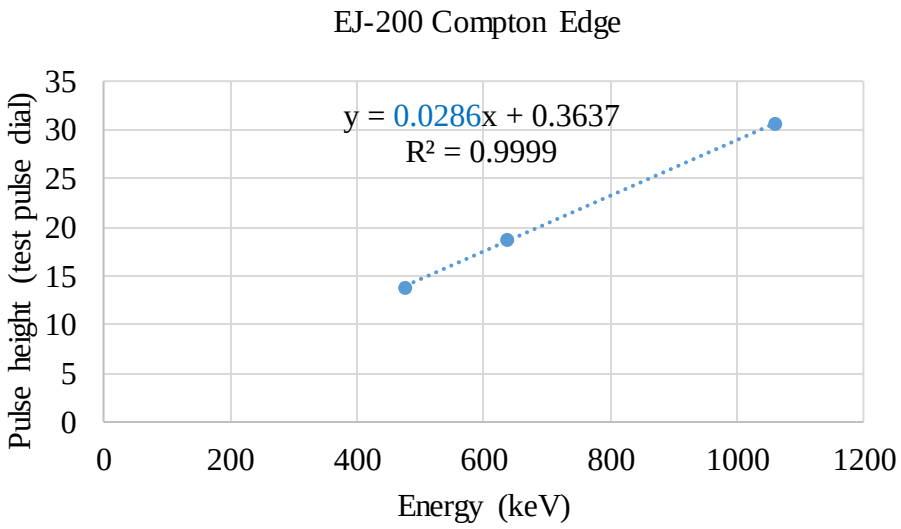

Fig.4.4. Light yield of EJ-200 detector as a function of energy.

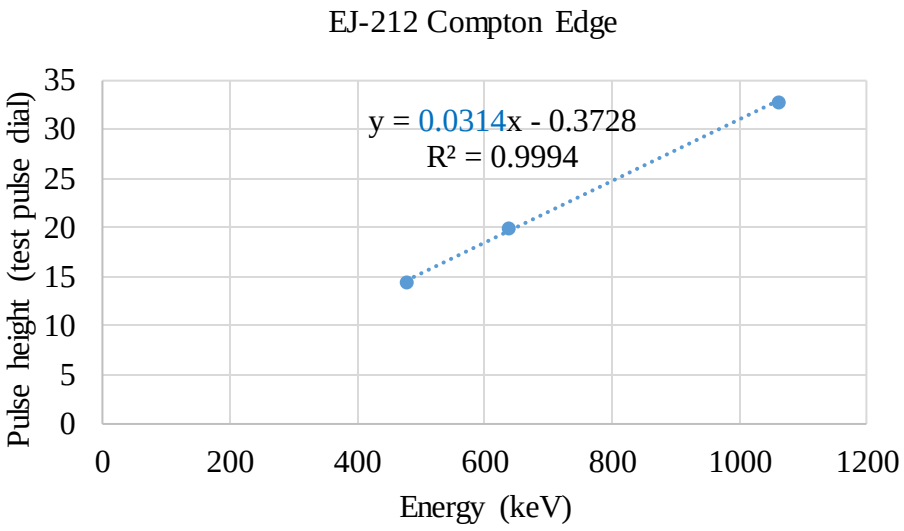

Fig.4.5. Light yield of EJ-212 detector as a function of energy.

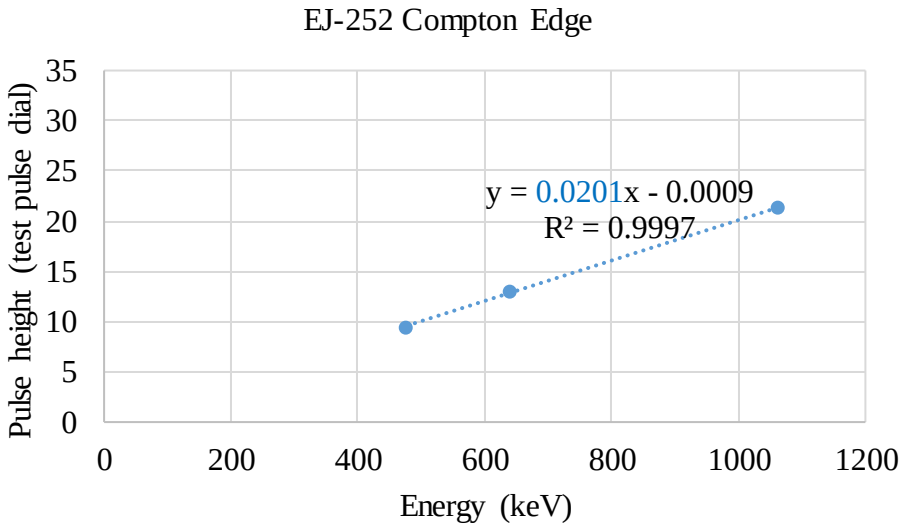

Fig.4.6. Light yield of EJ-252 detector as a function of energy.

The results of W_s in three plastic scintillators determined from the number of photoelectrons by using the parameters mentioned above are shown in Table.4.7.

Table.4.7. Light yield for plastic scintillators.

	Photoelectron/MeV	Photon/MeV	W_s (eV)
EJ-200	1563	9659	104 ± 9
EJ-212	1716	10718	93 ± 8
EJ-252	1098	6861	146 ± 13

The uncertainty in the measurement of W_s for plastic scintillators evaluated in a similar manner for those for CsI(Tl) was totally ± 8.7% due to the uncertainty in the photoelectron number was ± 1.9% instead of ± 1.2% because the photoelectron number of plastic scintillators was relatively determined from that of CsI(Tl).

The manufacturer introduces 10000 photon/MeV as the light output of the EJ-200 and EJ-212 in their catalogue [1], which means the value of W_s is 100 eV in them. However, there is no information referring to the determination of these values from the manufacturer; hence, the reason for the difference from our results cannot be sufficiently discussed. The W_s in EJ-252 is given for the first time.

4.2. The scintillation efficiency per deposit energy of electrons as a function of its energy (Electron response)

The electron response measured for three plastic scintillators are shown in Figs.4.8, 4.9, and 4.10, respectively. The electron response obtained with the NaI(Tl) detector are normalized to the data which was taken by averaging six data points in the energy range of 320 – 480 keV, while the data obtained with HPGe detector were normalized to that at the energy of 320 keV.

The relative light yield per electron energy in plastic scintillators approaches a saturated value in the high energy region, while indicates a reduction in the energy region

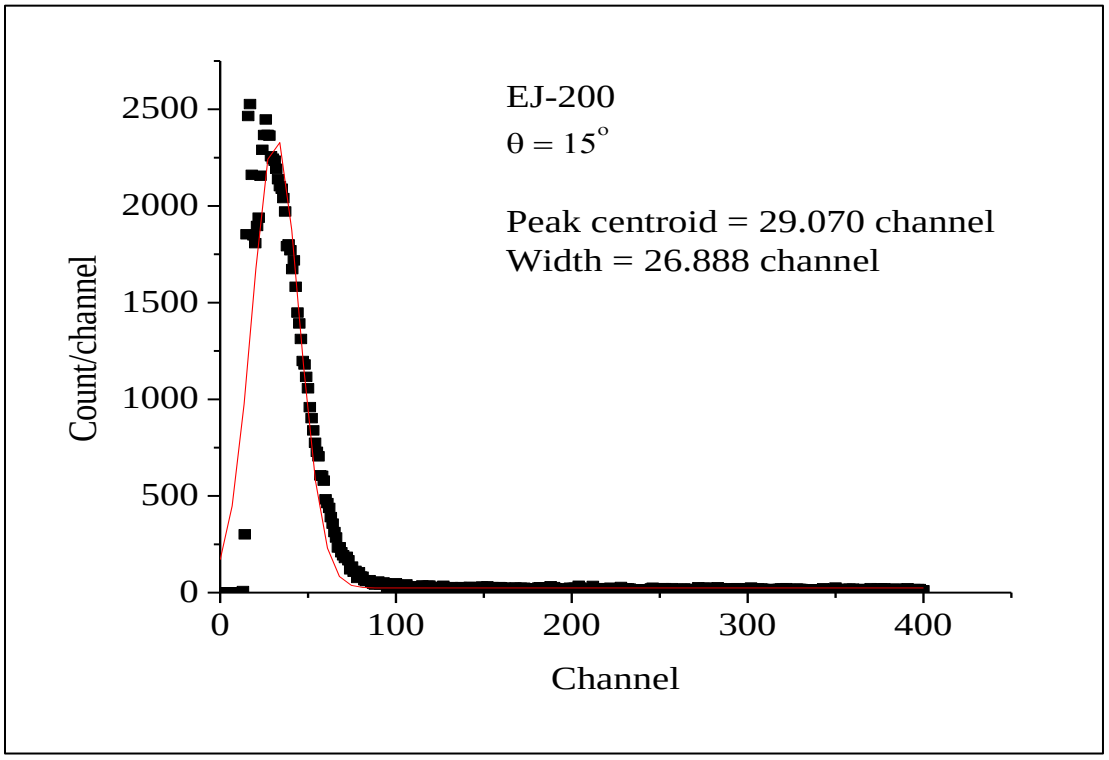

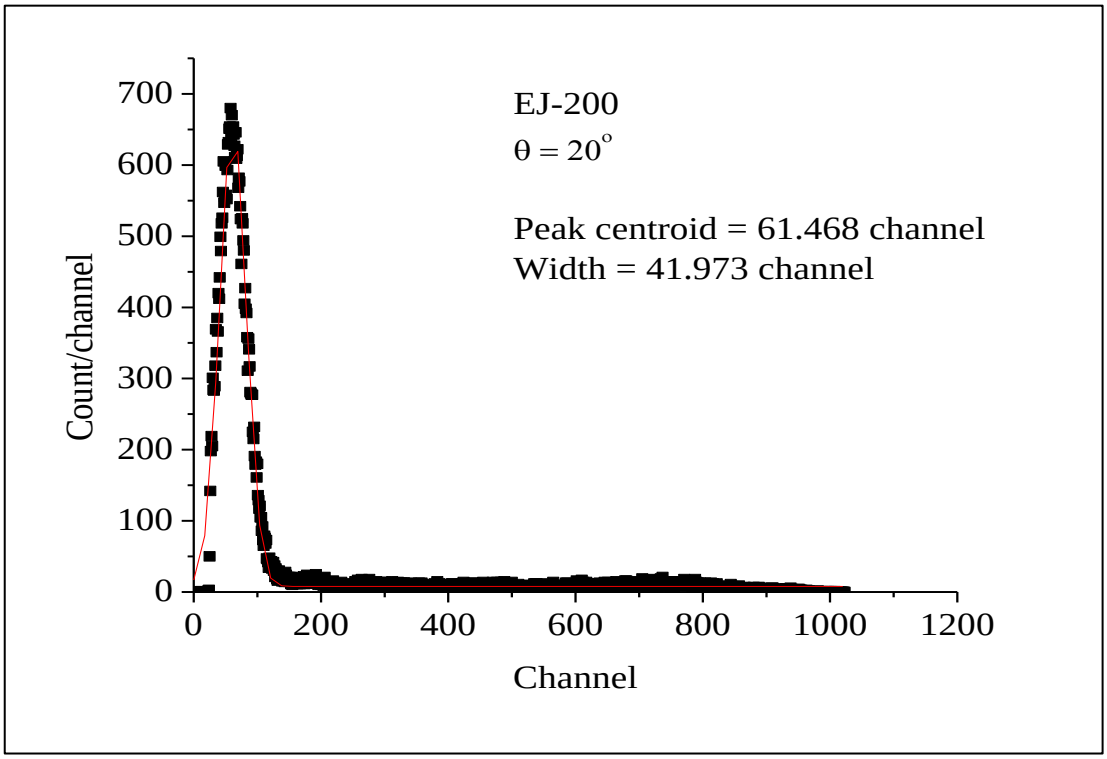

Fig.4.7.(a). The pulse height distribution from EJ-200 detector for the coincidence events with NaI(Tl) detector in CCT measurements.

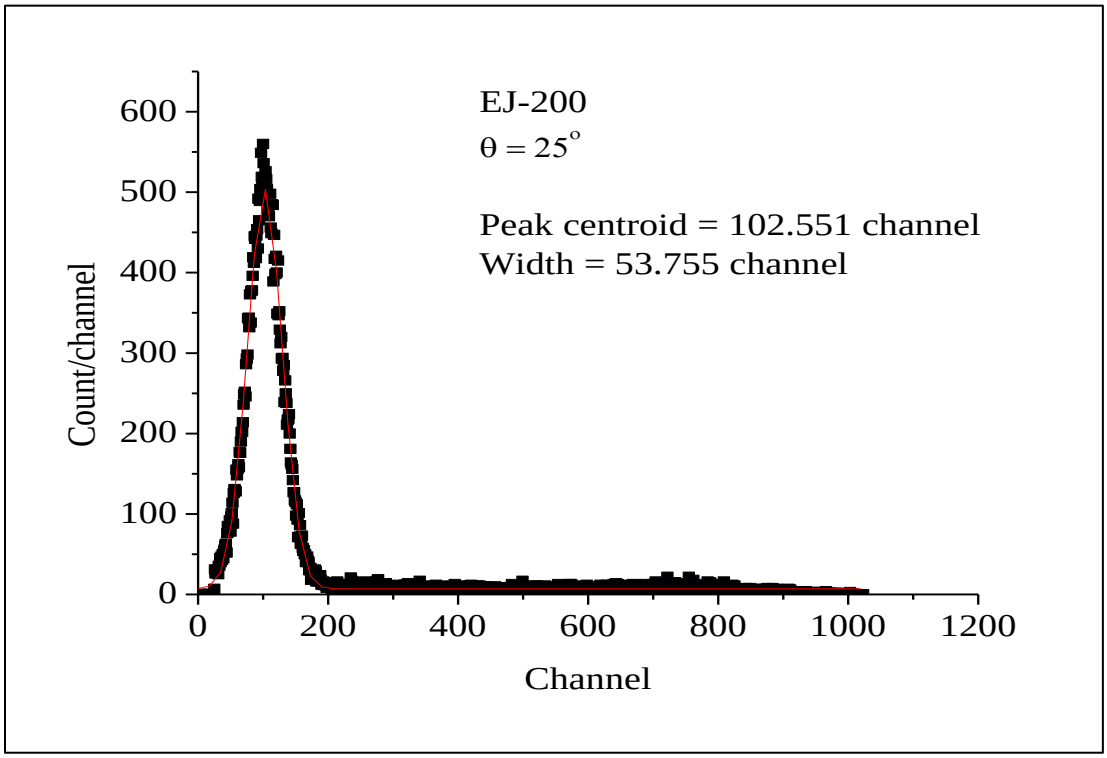

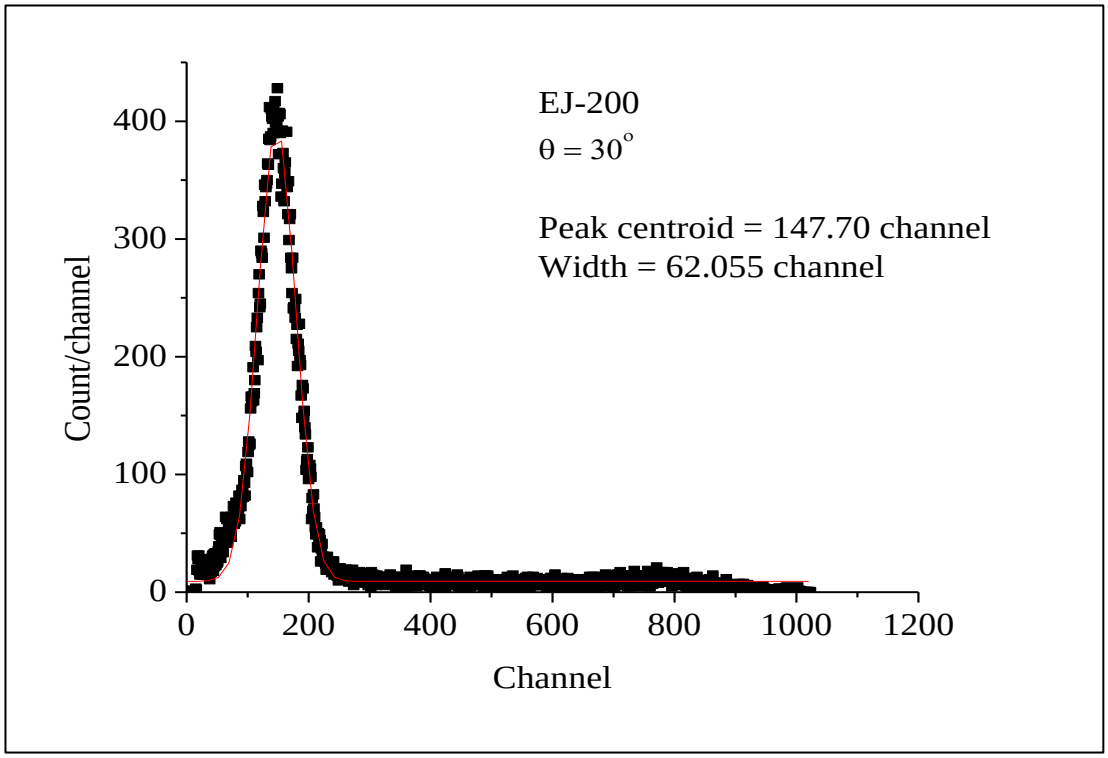

Fig.4.7.(b). The pulse height distribution from EJ-200 detector for the coincidence events with NaI(Tl) detector in CCT measurements.

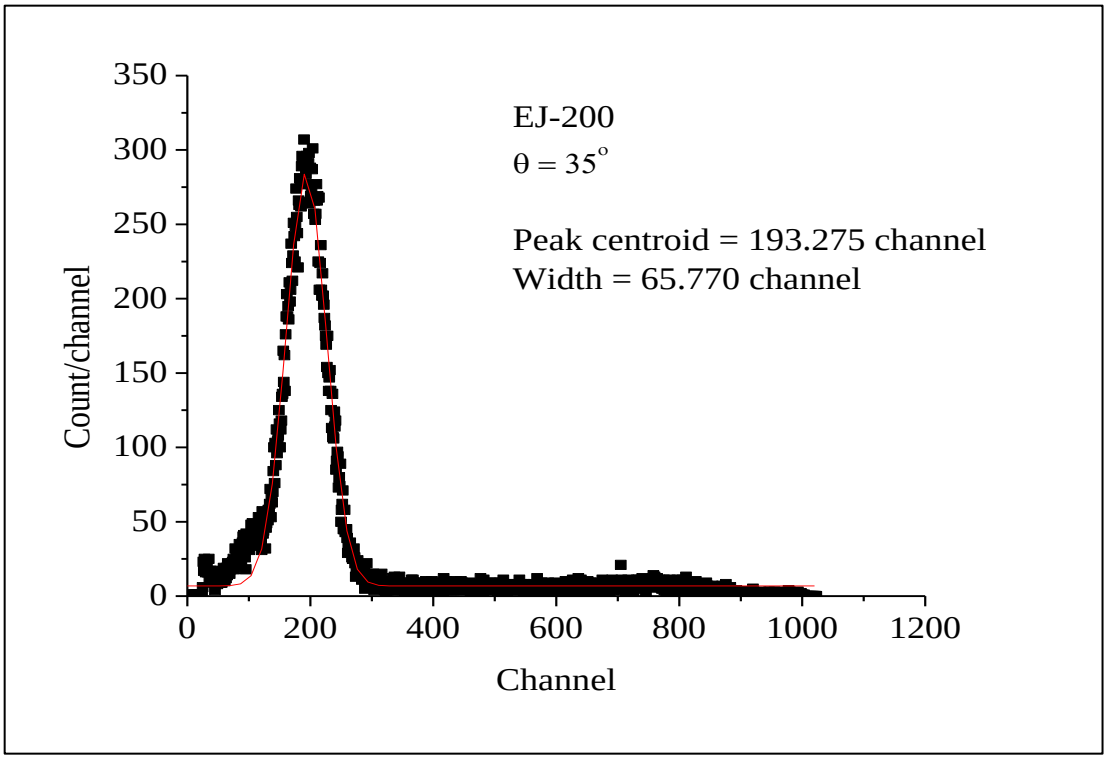

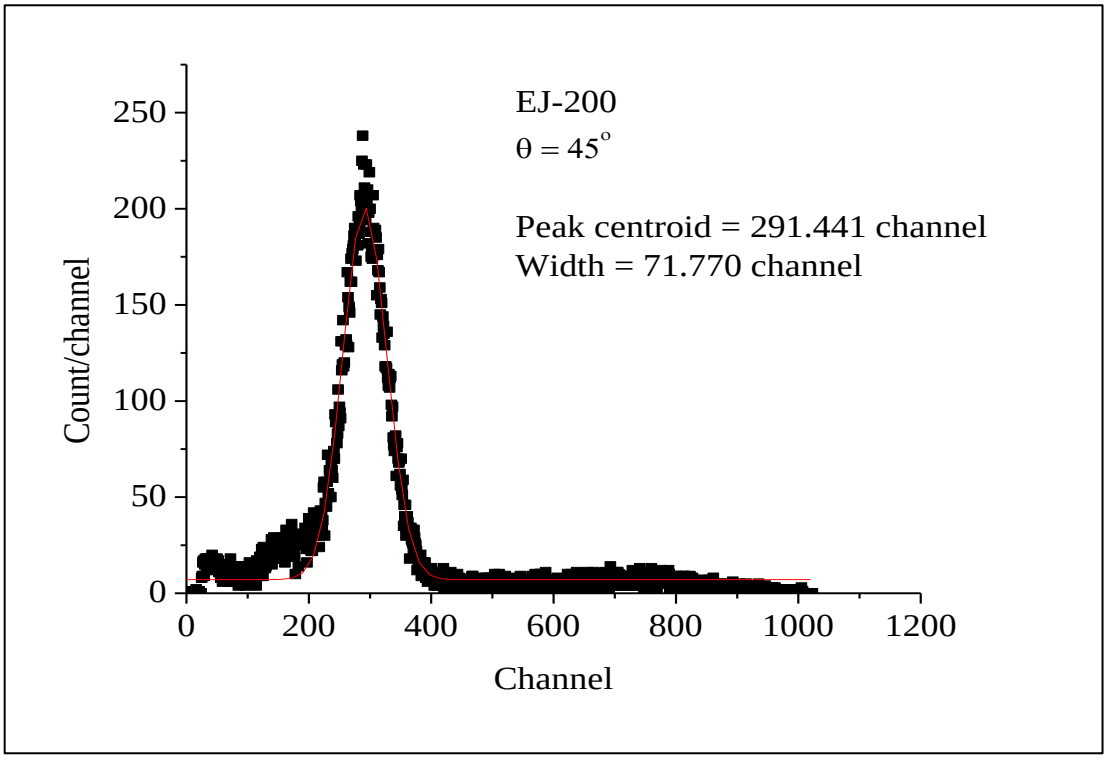

Fig.4.7.(c). The pulse height distribution from EJ-200 detector for the coincidence events with NaI(Tl) detector in CCT measurements.

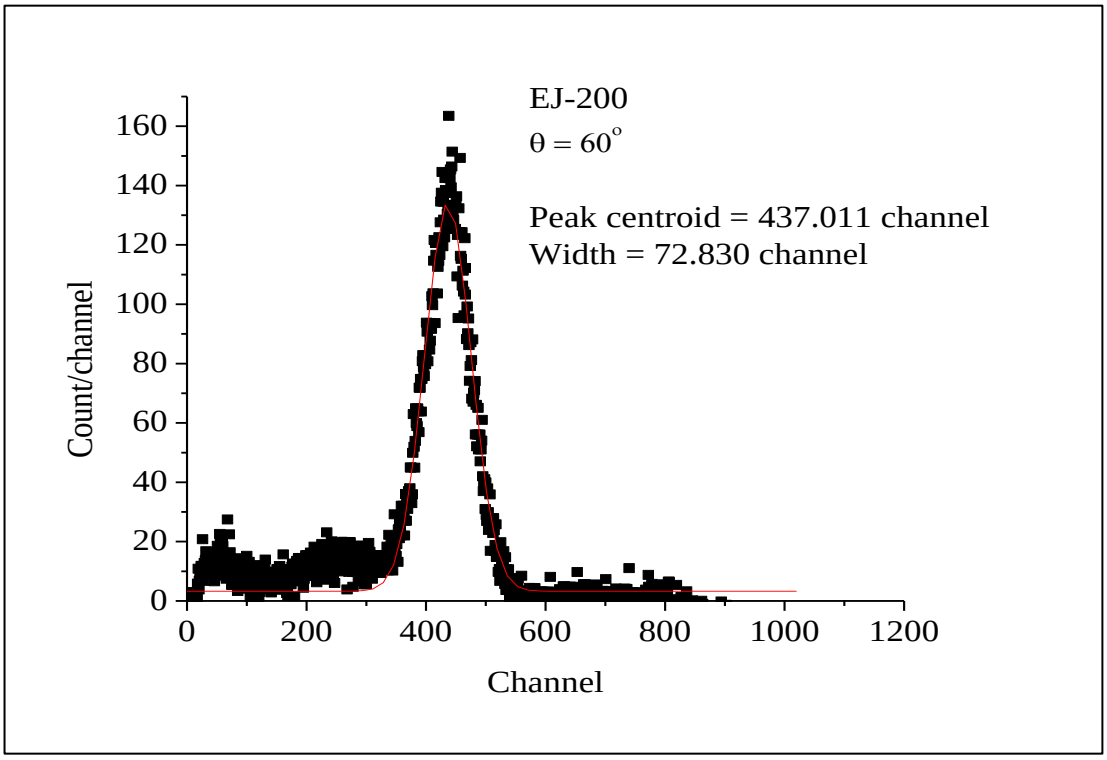

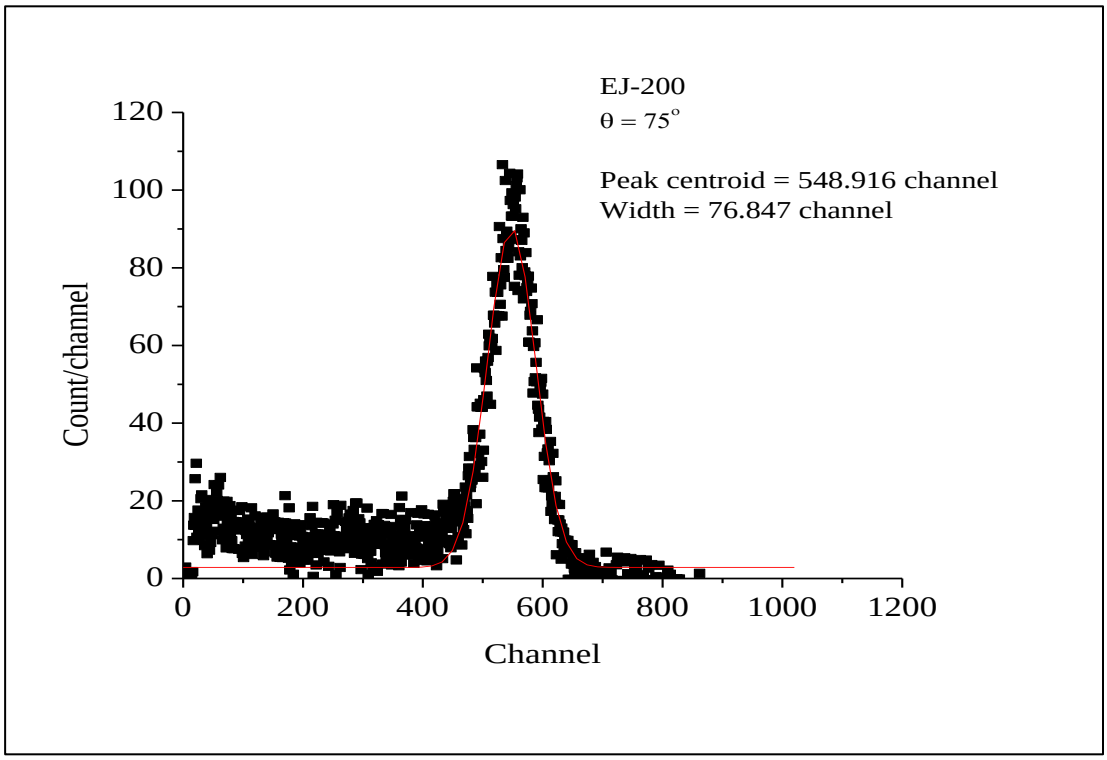

Fig.4.7.(d). The pulse height distribution from EJ-200 detector for the coincidence events with NaI(Tl) detector in CCT measurements.

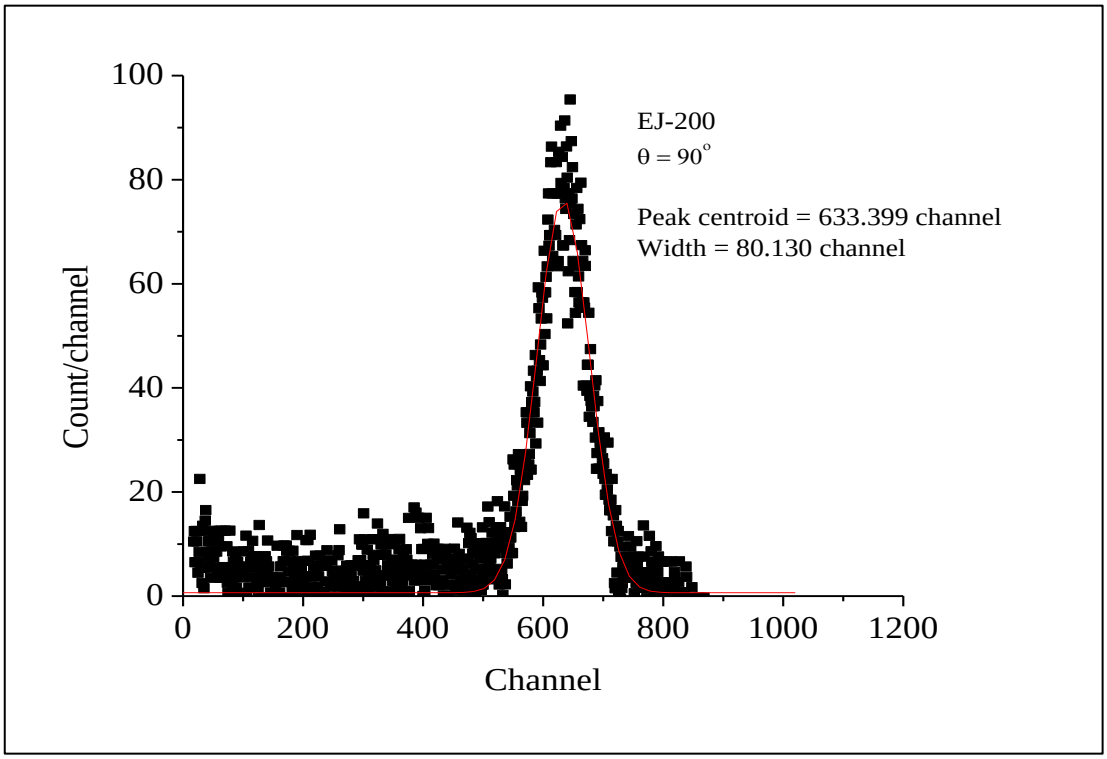

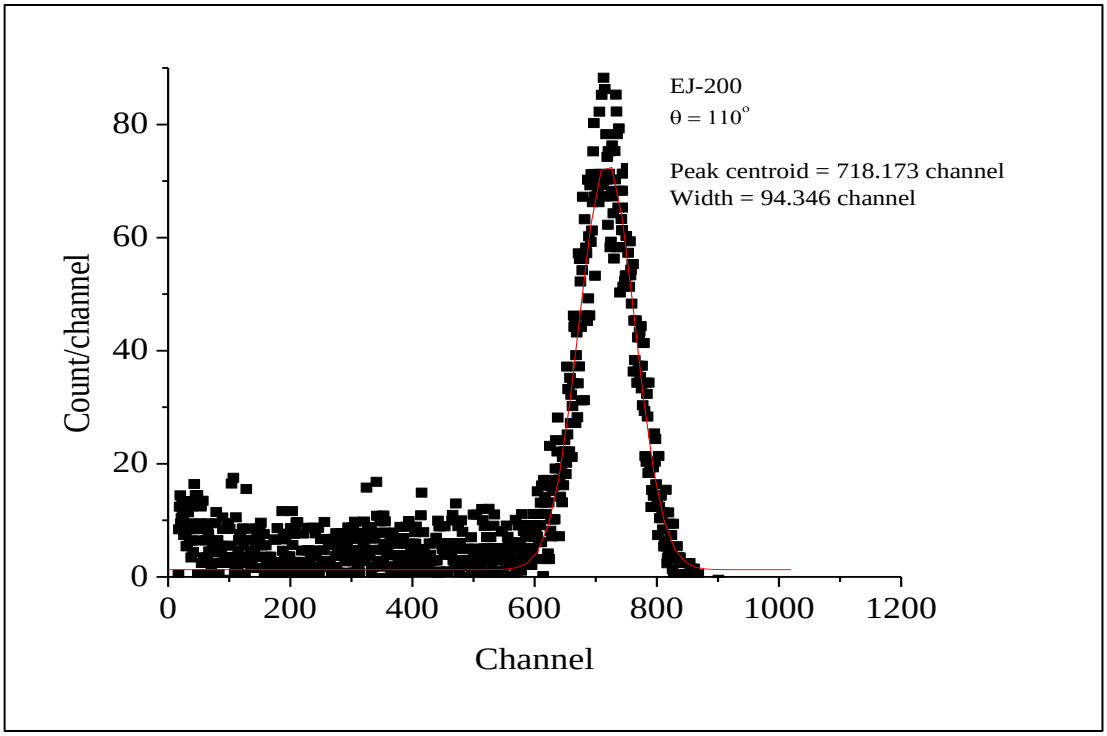

Fig.4.7.(e). The pulse height distribution from EJ-200 detector for the coincidence events with NaI(Tl) detector in CCT measurements.

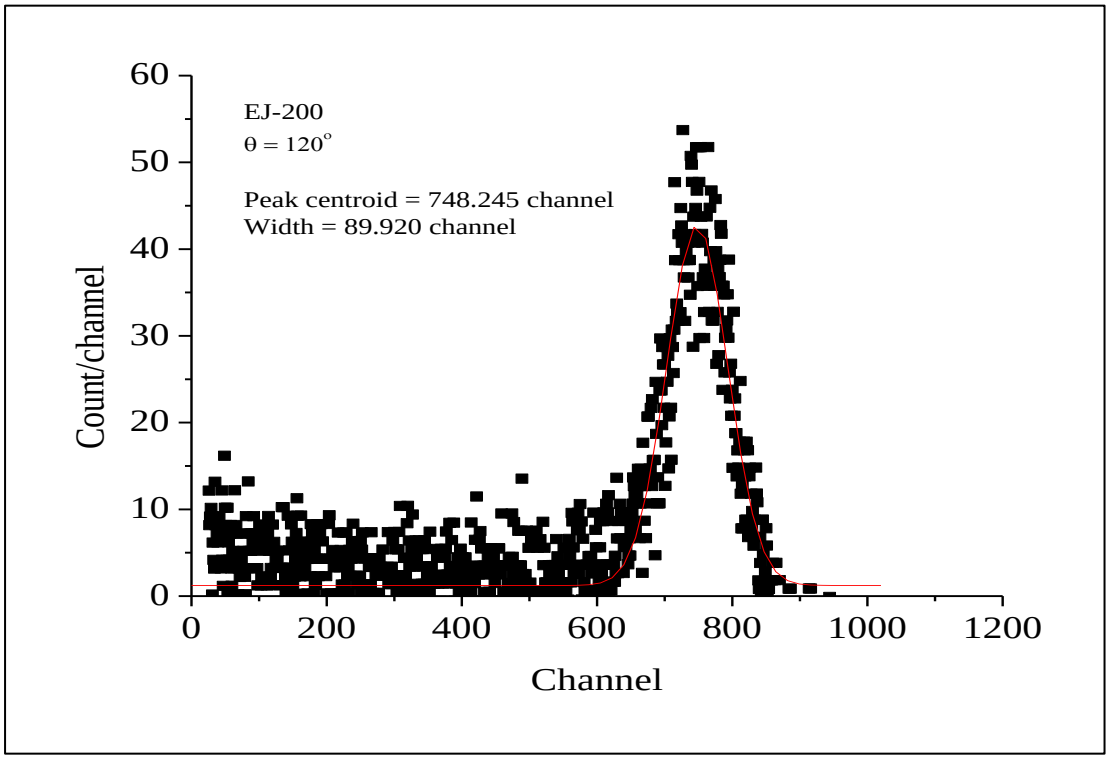

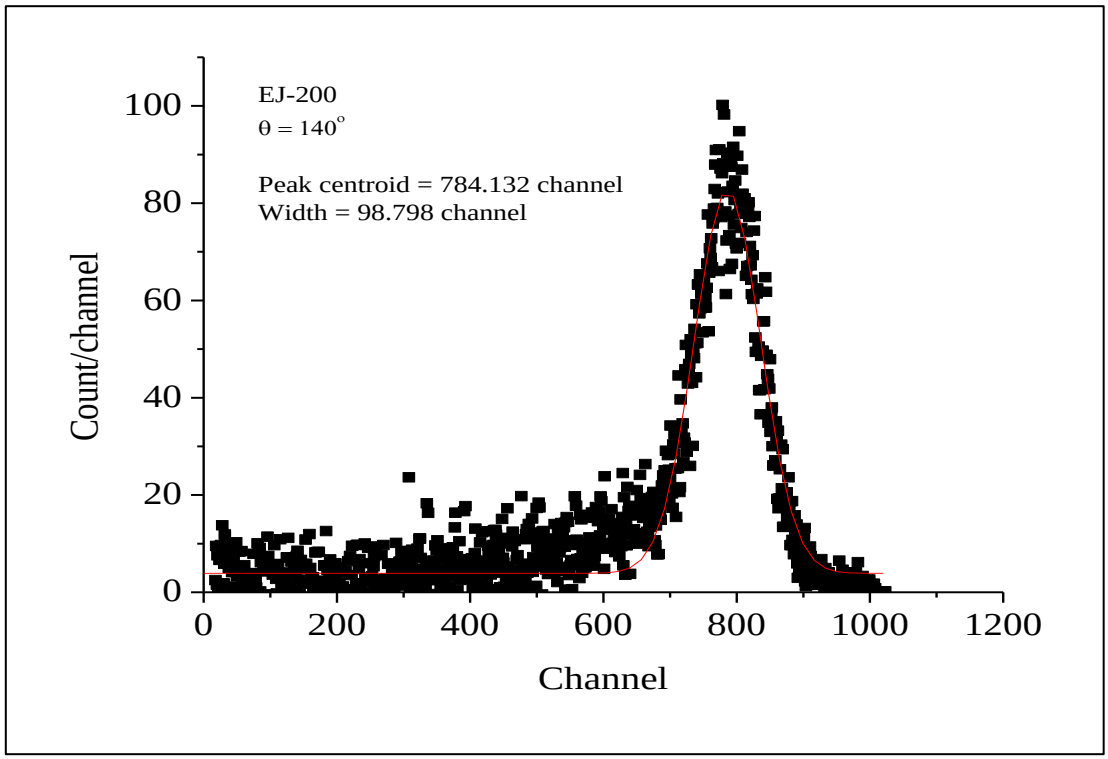

Fig.4.7.(f). The pulse height distribution from EJ-200 detector for the coincidence events with NaI(Tl) detector in CCT measurements.

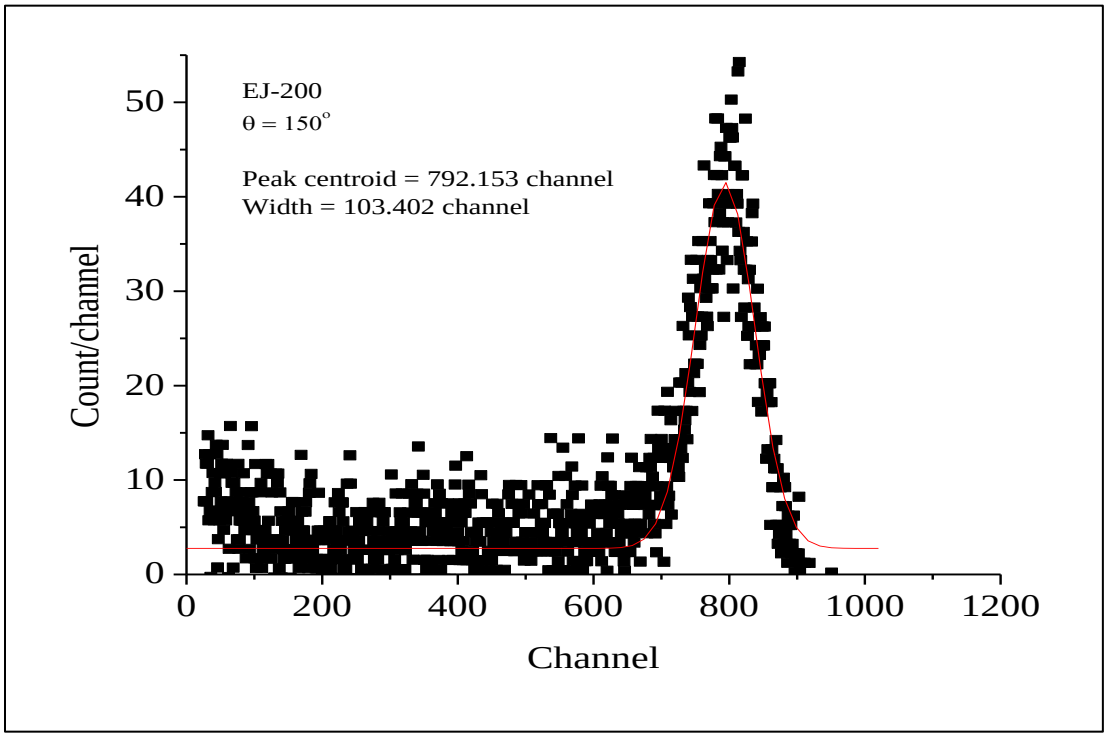

Fig.4.7.(g). The pulse height distribution from EJ-200 detector for the coincidence events with NaI(Tl) detector in CCT measurements.

lower than 150 keV. The electron response for 60-keV gamma ray from ^{241}Am is also plotted in the figure and is on the line showing a trend. This reduction is suggested being due to the quenching effects at high dE/dx where excited and ionized molecules are in high density and possibly lose their energy by collisions leading to the degradation in the light output [4]. This is suggested being related to the non-proportionality of light yield in plastic scintillators.

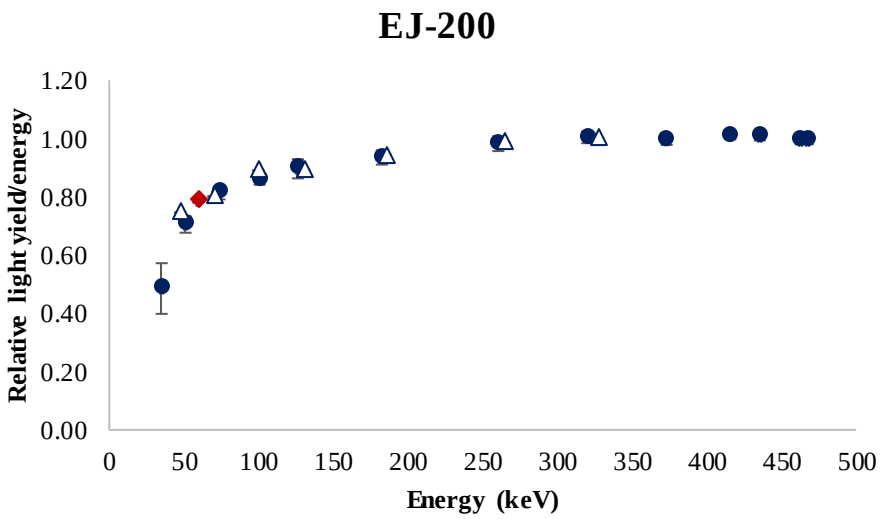

Fig.4.8. Electron response of EJ-200.
(Circle marks represent data points with NaI(Tl), triangle marks represent data points with HPGe, and diamond mark represents the data point for ^{241}Am).

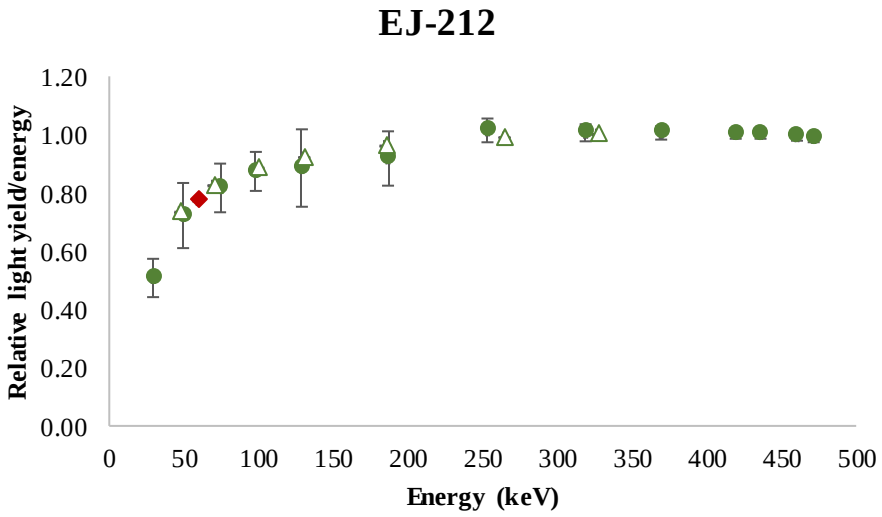

Fig.4.9. Electron response of EJ-212.
(Circle marks represent data points with NaI(Tl), triangle marks represent data points with HPGe, and diamond mark represents the data point for ^{241}Am).

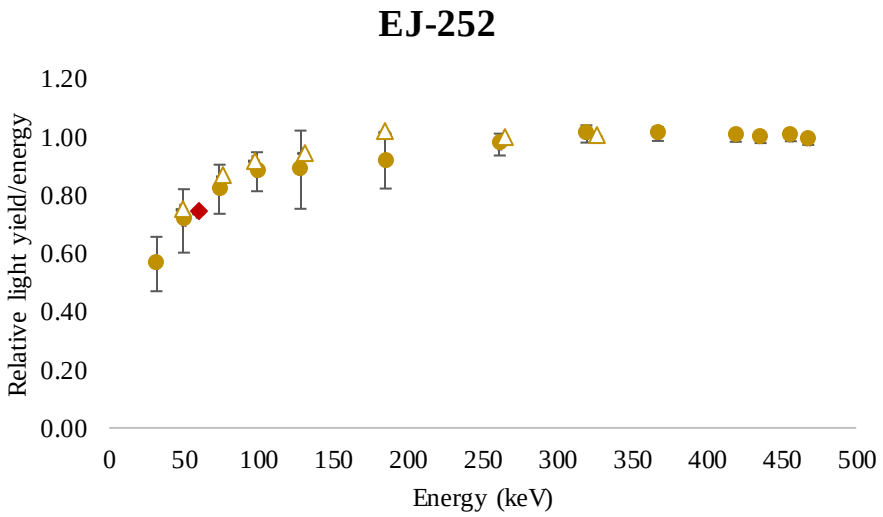

Fig.4.10. Electron response of EJ-252.
(Circle marks represent data points with NaI(Tl), triangle marks represent data points with HPGe, and diamond mark represents the data point for ^{241}Am).

The ambiguity in the measurements of electron response is determined by the contribution of the energy calibration for the reference detectors and the uncertainty of the peak centroid by the Gaussian fitting. As a result of error propagation, an ambiguity of 2% to 13% was evaluated for the electron response obtained by using the NaI(Tl) detector and about 0.2% for the electron response achieved by using the HPGe detector.

The electron response measured in this study was compared with data from other studies which is shown in Fig.4.11. These data are in agreement with each other in the energy range from 100 keV and above. In the lower energy region, electron responses in this study have lower values than other studies'. The electron response of the lowest energy (about 35 keV), which corresponds to the scattering angle of 15°, shows the highest amount of different from the others. Although the reason for this difference cannot be explained at present, one possibility is due to the high uncertainty in determining the peak centroid in the distribution of plastic scintillator detector at this angle. The Gaussian fitting was applied to get the peak centroid even though the peak did not has the full

Gaussian shape. It is due to the low pulse height obtained for plastic scintillator detector at the scattering angle of 15° which is too close to the discrimination level set for the ADC. Besides, the determination procedure for electron response in this study was not identical to other studies. The comparison cannot indicate that any of these studies is completely precise for plastic scintillators and vice versa.

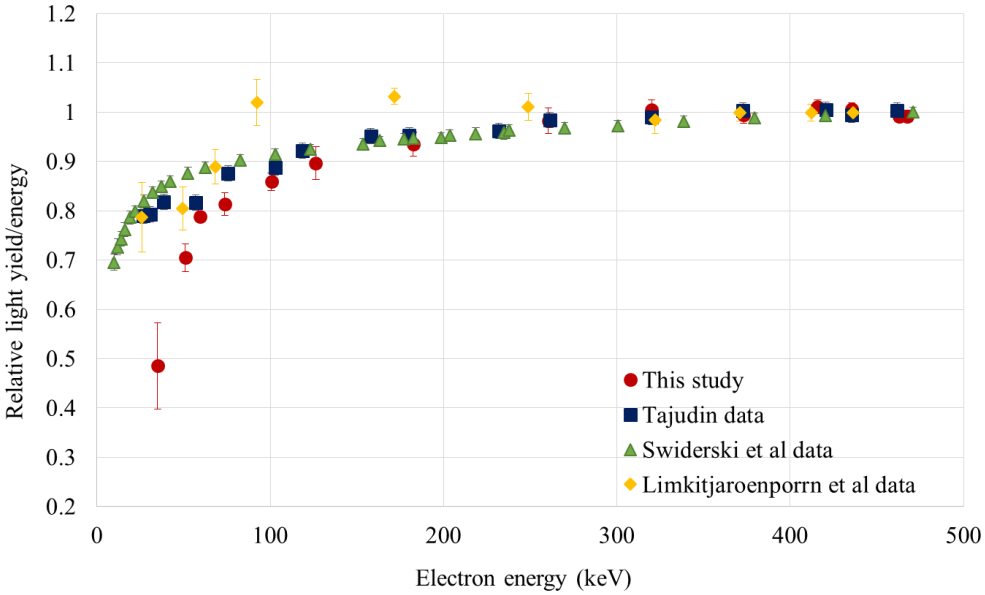

Fig.4.11. Comparison of electron response obtained in this study with other studies. Data of $2''\phi \times 2''L$ EJ-200 represents for electron response in this study, data of $2''\phi \times 2''L$ EJ-200 represents for electron response in Tajudin data [5], 40 mm $\phi \times 50$ mm L BC-408 represents for electron response in Swiderski et al. [6], and $1''\phi \times 1''L$ NE-102 represents for electron response in Limkitjaroenporrn et al. [7].

4.3. Energy resolution

EGS5 code [8] was used to calculate the geometrical component causing the spread in the energy of the electrons in CCT measurement.

The CCT measurement using plastic scintillators and NaI(Tl) detectors was simulated by EGS5 code. As a result of coincidence, the energy distribution spectra for recoil electrons in the plastic scintillator detector were obtained. The FWHM and the

centroid obtained from Gaussian fitting of the coincidence peaks. Then, δ_{CCT} of the plastic scintillator was evaluated as the ratio of the FWHM to the peak centroid.

The energy resolutions in three plastic scintillators EJ-200, EJ-212, and EJ-252, measured in the CCT measurements are shown in Figs.4.12, 4.13, and 4.14, respectively. In the low energy region, the influence of CCT geometric components on the resolution is remarkable.

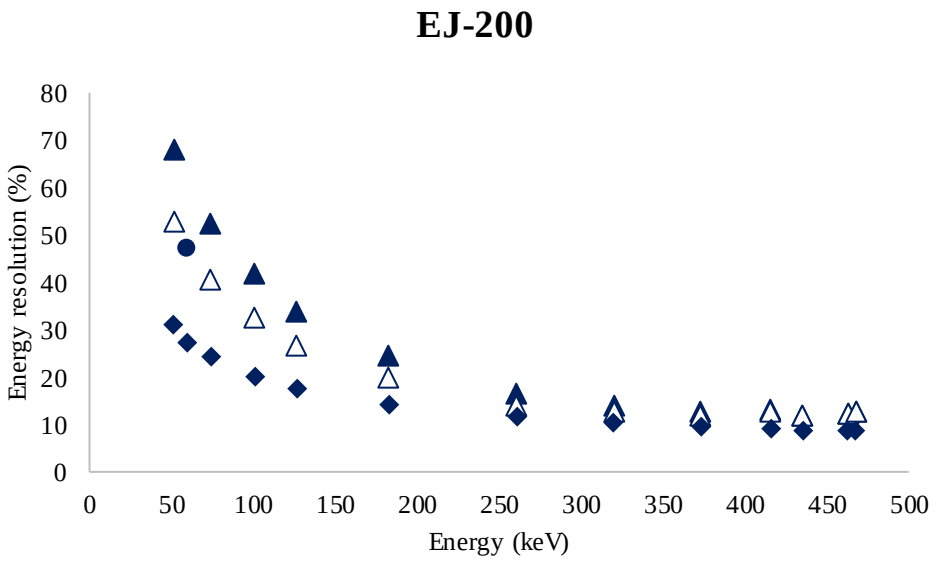

Fig.4.12. Energy resolution of EJ-200 as a function of electron energy; closed triangle marks represent the measured resolution from the CCT, open triangle marks represent the intrinsic resolution δ_{sc}, closed circle marks represent measured resolution for 60-keV gamma rays and diamond marks represent the statistical fluctuation δ_{st}.

The intrinsic resolution δ_{sc}, which includes the statistical fluctuation δ_{st} in the number of scintillation photons, obtained after eliminating δ_{CCT} is considered to be the energy resolution due to monochromatic electrons generated in the Compton effect. The intrinsic resolution is larger than the statistical fluctuation in the low energy region and becomes close as the electron energy increases. The trends are similar in three plastic scintillators. The intrinsic resolution of EJ-200, EJ-212, and EJ-252 in the energy range

around 450 keV is 13.0%, 11.2%, and 13.9%, respectively, where the statistical fluctuation is 8.7%, 8.3%, and 10.4%, respectively.

Since the trend in energy resolutions getting worse in the low energy region seems to be coincident with the reduction in the electron response below the energy of approximately 150 keV, the worse resolution is attributed to the fluctuation in scintillation efficiency due to secondary electrons generated by a monochromatic recoil electron. However, the explanation of the difference between δ_{sc} and δ_{st} in the low energy side is not made clear at this stage because of not having enough understandings of this mechanism.

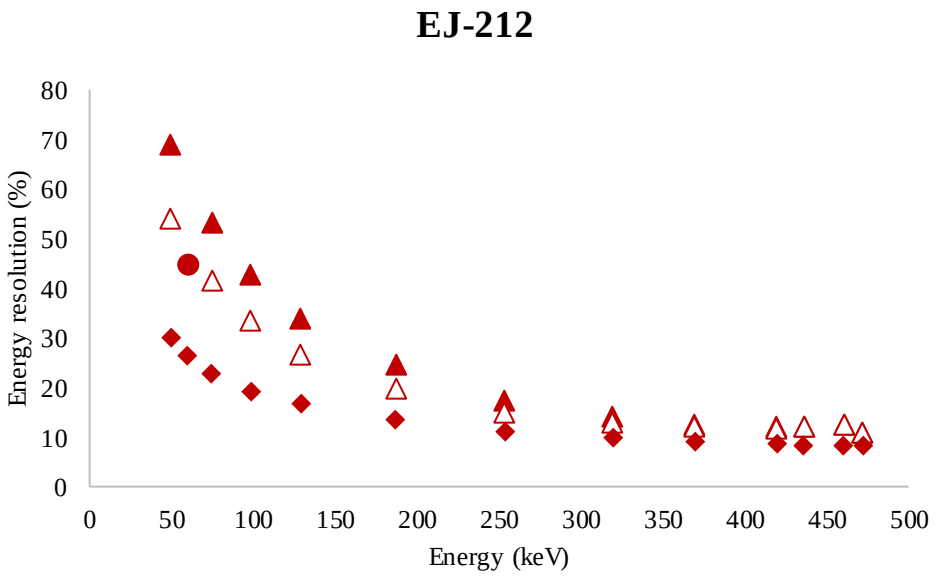

Fig.4.13. Energy resolution of EJ-212 as a function of electron energy; closed triangle marks represent the measured resolution from the CCT, open triangle marks represent the intrinsic resolution δ_{sc}, closed circle marks represent measured resolution for 60-keV gamma rays, and diamond marks represent the statistical fluctuation δ_{st}.

In the manner of the statistical fluctuation, EJ-252 has the highest W_s among three plastic scintillators (104 eV, 93 eV, and 146 eV in EJ-200, EJ-212, and EJ-252,

respectively) as mentioned previously. One possible contribution to the light yield of EJ-252 would be due to a small amount of arsenic component added in the plastic to realize a response close to air, while the other two plastic scintillators are composed of only hydrogen and carbon. The number of scintillation photons generated in EJ-252 due to the same deposited energy is the smallest and then, the statistics in the small number of scintillation photons cause the worse energy resolution of EJ-252 in comparison with the others.

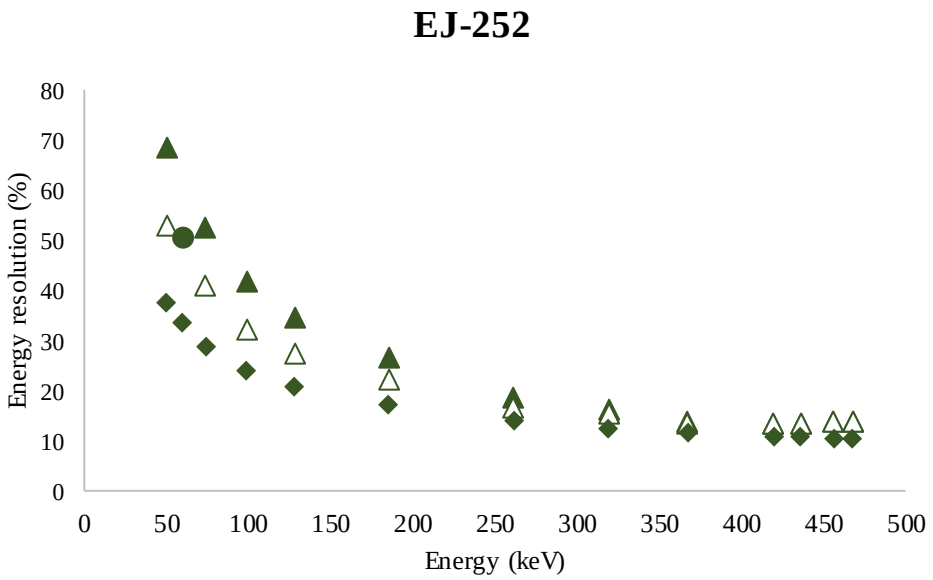

Fig.4.14. Energy resolution of EJ-252 as a function of electron energy; closed triangle marks represent the measured resolution from the CCT, open triangle marks represent the intrinsic resolution δ_{sc}, closed circle marks represent measured resolution for 60-keV gamma rays, and diamond marks represent the statistical fluctuation δ_{st}.

The energy resolution measured for a photopeak of 60-keV gamma rays from ^{241}Am is found to be on the trendline of the intrinsic resolution δ_{sc}. Furthermore, the scintillation efficiency measured for this photopeak shown in Fig.4.8 is also confirmed to be on the line interpolated in the electron response data. These results may lead to an idea that the photopeak of 60-keV gamma rays is mainly composed of electrons generated by the

photoelectric effect at the first interaction, while the most of 662-keV gamma rays undergo the Compton scattering several times before its termination due to photoelectric effect or escape from the scintillator.

The pulse height distribution for 60-keV gamma rays was measured by a $2''\phi \times 2''L$ plastic scintillator (EJ-200, EJ-212, or EJ-252) coupled to a $2''\phi$ PMT Hamamatsu R375. Although the response function of a plastic scintillator detector to gamma rays is a continuum distribution, the distribution for 60-keV gamma rays is assumed corresponding to the photopeak. After eliminating the influence of the background determined by fitting exponential functions, the peak centroid and FWHM for the photopeak were obtained with a Gaussian fitting, and its resolution R_{241Am} (%) was calculated. The typical pulse height distribution of 60-keV gamma rays measured with the EJ-200 detector is shown in Fig.4.15.

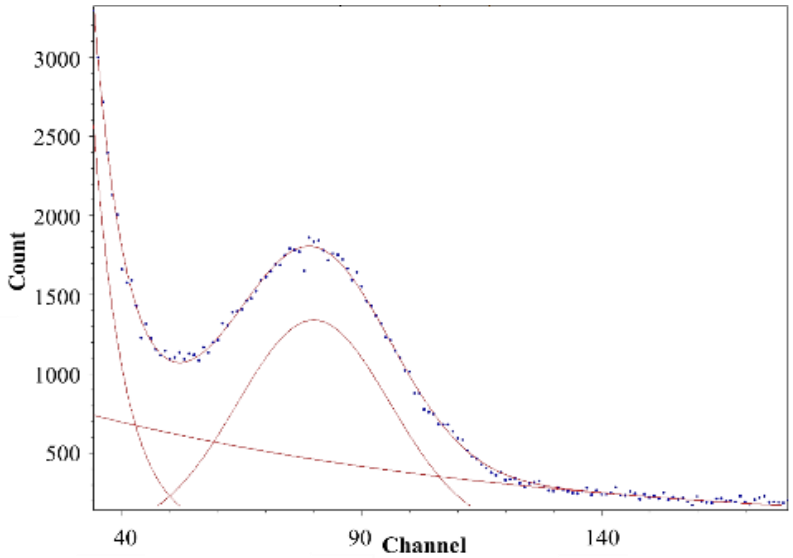

Fig.4.15. Pulse height distribution of 60-keV gamma rays measured with EJ-200 detector.

The measurement of 60-keV gamma rays by the plastic scintillator detector was simulated by EGS5 code. In this calculation, all processes that a photon experienced from

entering till terminating inside the scintillator were recorded. These processes were marked as Compton scattering or photoelectric absorption with their corresponding deposited energies in the scintillator. Based on the results of classified processes, the probability of occurrence for each type of processes was determined. Particularly, the probability of direct photoelectric absorption, photoelectric absorption following one or more Compton scattering was obtained. Besides, by the recorded deposited energy, the energy distribution spectrum was reconstructed.

The energy distribution spectrum was also re-examined with the influence of the electron response. For this purpose, firstly, the electron response for each deposited energy obtained from EGS5 needs to be determined. For the incident gamma rays is about 60 keV, the energy range of 35 – 73 keV in the electron response curve of EJ-200 was extrapolated to zero, and the threshold energy of about 15 keV corresponds to electron response equalling zero. The threshold energy is not a fixed value, it depends on the fitting curve of the electron response in the observed energy range. The extrapolating curve and the fitting equation is shown in Fig.4.16.

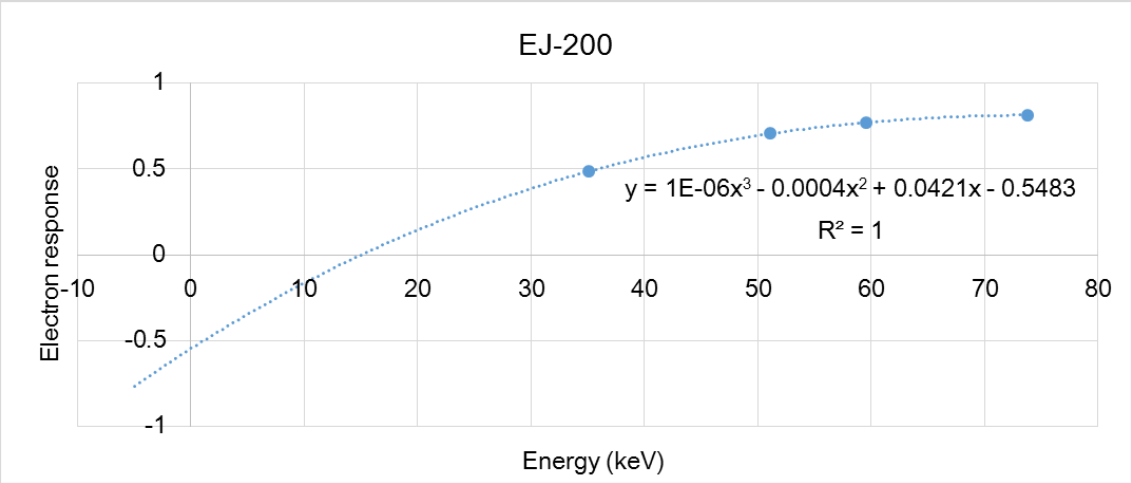

Fig.4.16. Electron response curve was extrapolating to zero to obtain the electron response corresponding to energies below 60 keV.

Then, the electron response for each deposited energy was calculated by substituting the energy into the obtained fitting equation. From the deposited energy influenced by the electron response, the pulse height distribution spectrum was re-constructed.

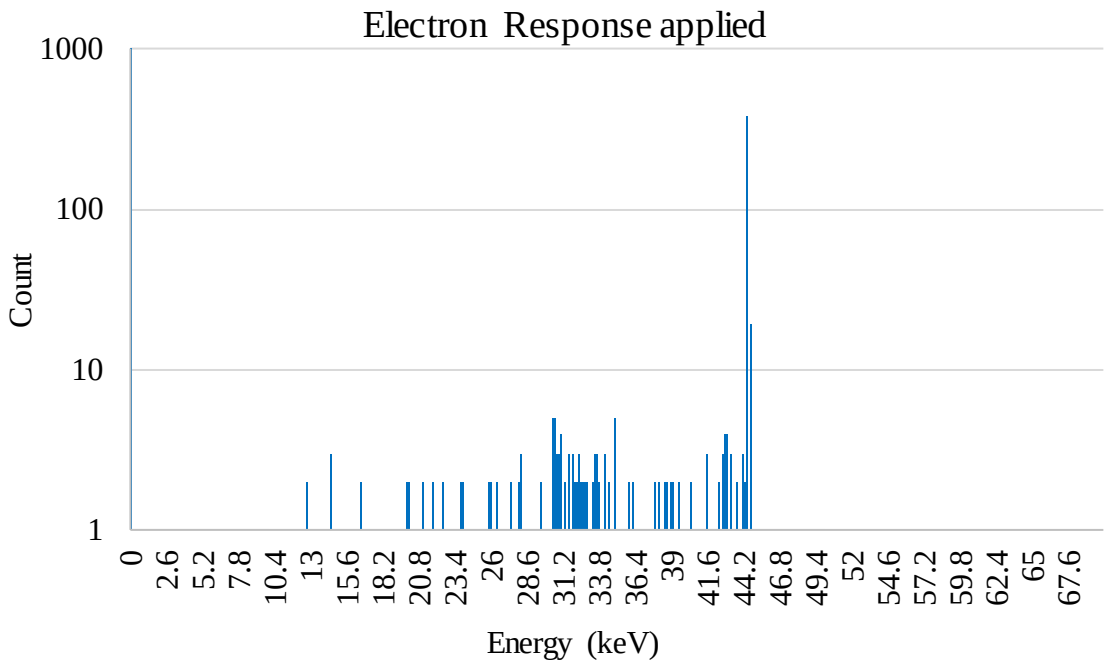

Fig.4.17. Pulse height distribution simulated by using EGS5 for 60-keV gamma rays in EJ-200. Under the influence of the electron response, there is a shift of the photopeak pulse height to a lower energy region.

Results from the EGS5 calculation indicate that the contribution to the photopeak of a 60-keV gamma ray includes (1) direct photoelectric absorption (60%), (2) photoelectric absorption following one Compton scattering (22%), and (3) photoelectric absorption following two or more Compton scatterings (18%). In the processes (2) and (3) mentioned here, however, the total light yields become smaller than that due to the process (1) by the influence of electron response. Namely, the pulse heights corresponding to the process (2) and (3) appear at far lower channels from the original position of the photopeak. Figure 4.17 shows the calculated results for 60-keV gamma

rays with EGS5 in which the electron response data were incorporated. As shown in the reconstructed distribution spectrum in Fig.4.17, it is proved that the process except the (1) direct photoelectric absorption may not contribute to the original peak. This indicates that the photopeak for 60-keV gamma rays is dominantly formed by 60-keV monochromatic photon, and is the possible evidence for the suitability for the data point of 60-keV gamma rays on the trendline of the electron response and the intrinsic resolution characterized by monochromatic recoil electrons.

4.4. Position sensitivity in plastic scintillator rod system

4.4.1. Measurement with alpha particles

The pulse height obtained from both end PMT as a function of source position for four rods are shown in Figs. 4.18, 4.19, 4.20, and 4.21. The data were normalized for the gain difference between both-end PMTs. The data of four rods were shown to examine the plastic scintillator rods have the similar tendency or not.

According to the results, pulse height distributions of both end PMTs have the similar tendency and close values in case of rod 2 and rod 4 shown in Figs 4.19 and 4.21. In the case of rod 1 and rod 3 shown in Figs. 4.18 and 4.20, it is suggested that the difference in pulse height distributions between both-end PMTs is due to the connection between the plastic scintillators and PMT was not good (position shifting of the rods with corresponding PMT channels or there were air bubbles in the optical grease as the interface between scintillators and PMT's window).

Then, the measurement was re-conducted. Unfortunately, the PMTs were destroyed due to the operation's mistakes. Thus, the rod system was kept the same, but a new pair of PMTs of the same model as the broken PMTs was used. The measurements were performed for one plastic scintillator rod in two cases: wrapped in aluminized mylar

reflector and bare scintillator. The variation in pulse height as the function of distance from the source to PMT for aluminized mylar wrapped rod and bare rod are shown in Figs.4.22 and 4.23.

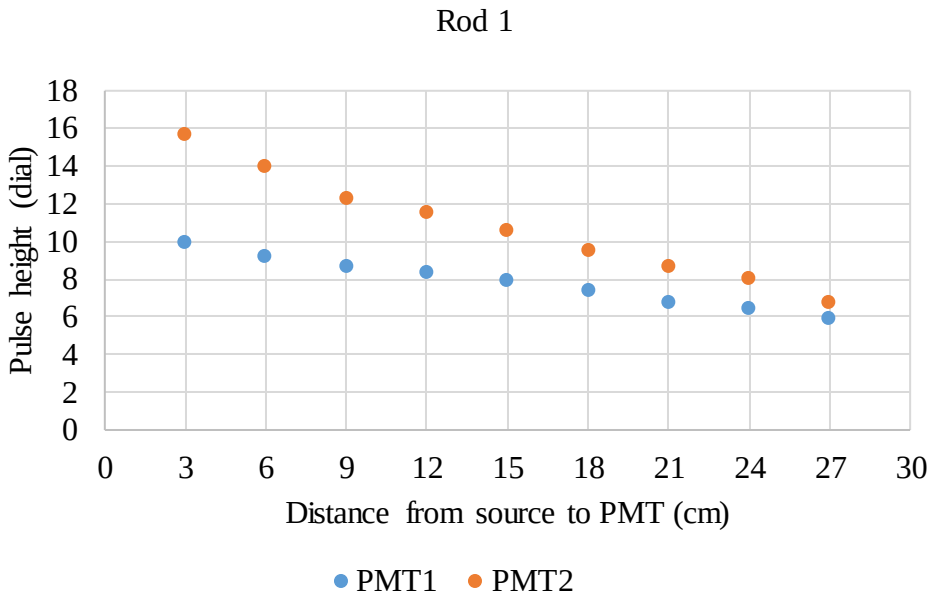

Fig.4.18. Variation in pulse height of both end PMTs as a function of rod 1.

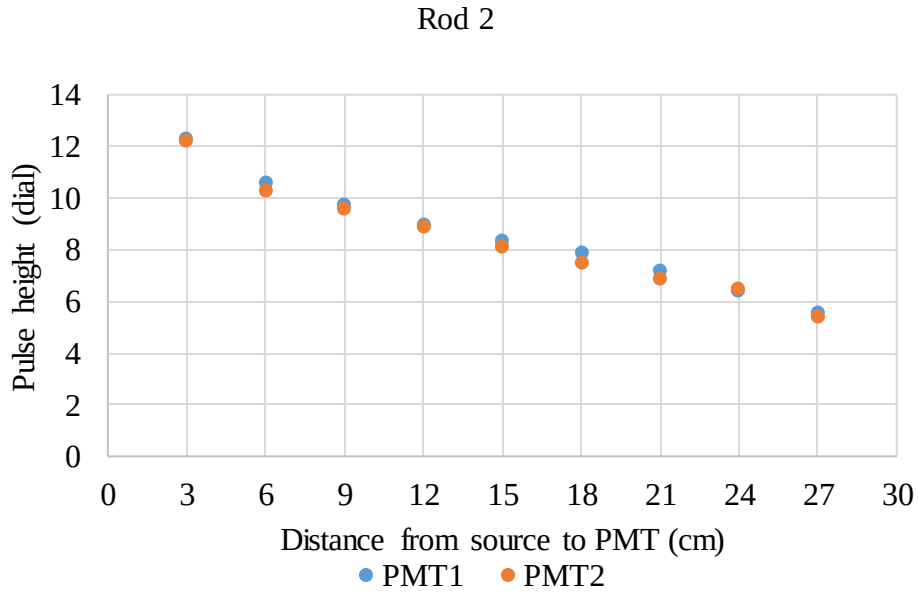

Fig.4.19. Variation in pulse height of both end PMTs as a function of rod 2.

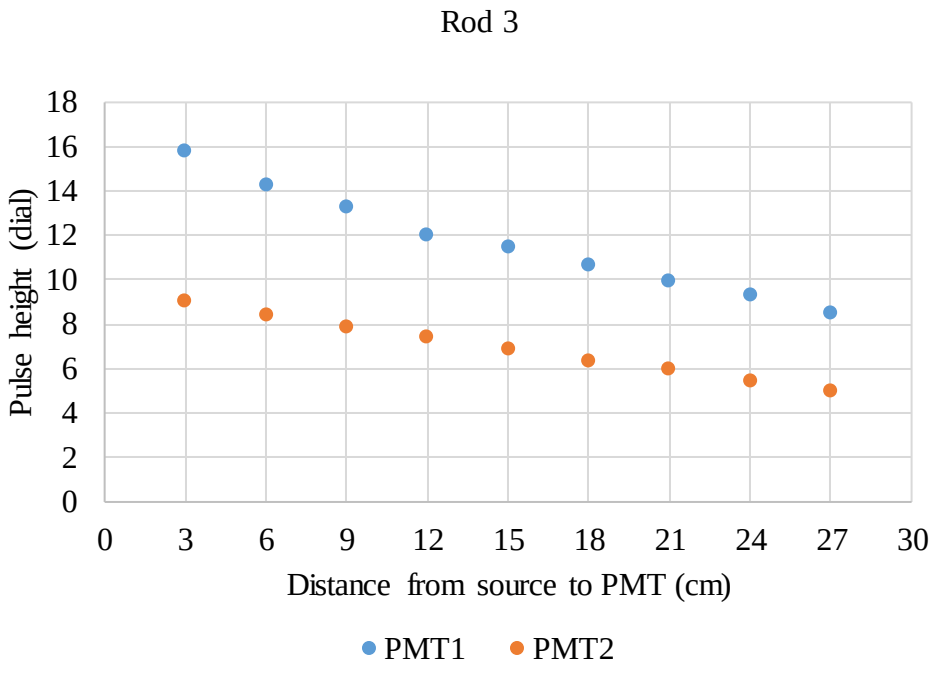

Fig.4.20. Variation in pulse height of both end PMTs as a function of rod 3.

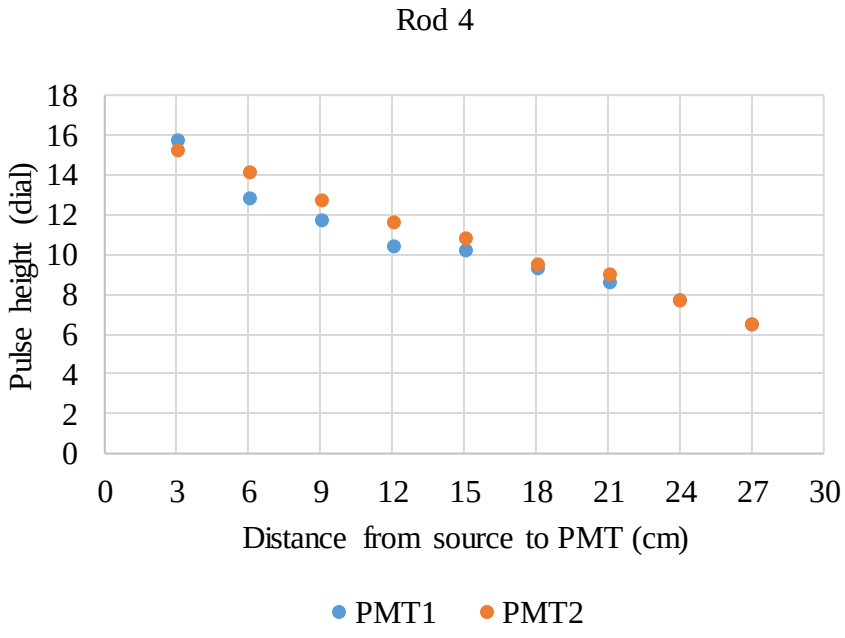

Fig.4.21. Variation in pulse height of both end PMTs as a function of rod 4.

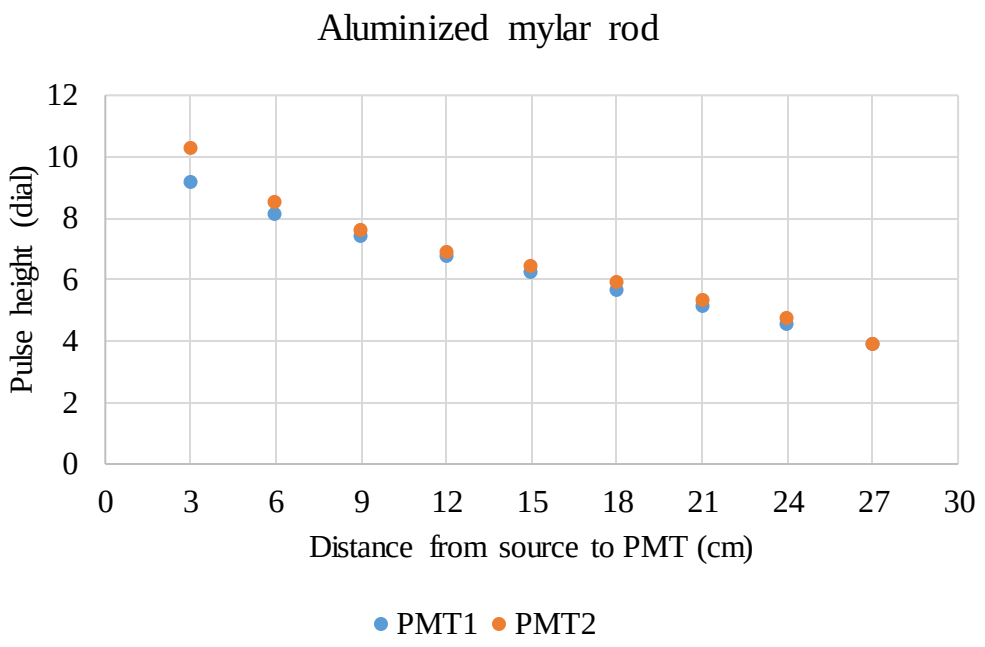

Fig.4.22. Variation in pulse height of both end PMTs as a function of an aluminized mylar wrapped rod in the measurement using a new pair of PMTs.

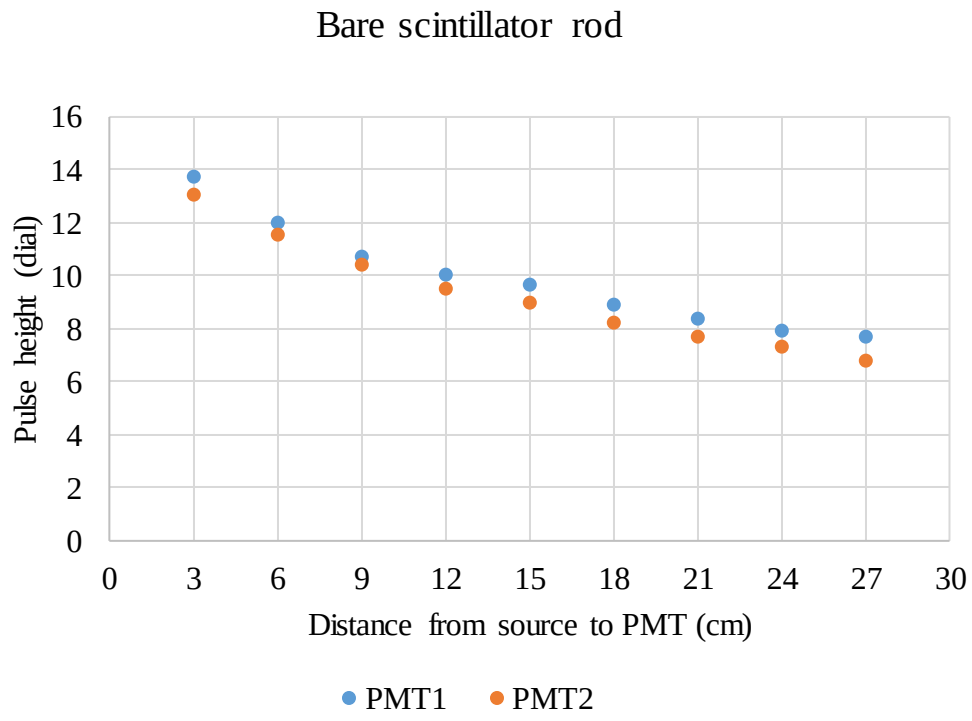

Fig.4.23. Variation in pulse height of both end PMTs as a function of a bare rod in the measurement using a new pair of PMTs.

Then, the pulse heights of aluminized mylar wrapped rod shown in Fig.4.22 were used to examine the nature of the transparency of light in the rod. Pulse height P as a function of the distance d from the PMT is sometimes explained by $P = Cexp(-Ad)$, where C and A are constant. Factor A^{-1} is the attenuation length of the photon in the scintillator rod; however, it is not the property of the scintillator but is affected by wrapping the rod.

In the measurements, most of the photons are detected by the PMT not directly, but after some reflections at the rod wall or wrapping material. Some of the photons produced at a point near the PMT might be directly detected. The ratio of the solid angle subtended by the end face of the rod $0.9 \times 0.9\ cm^2/4\pi d^2$, where d is the distance between the source and the PMT, expresses the probability of photons directly detected by the PMT. For the rod which is 30 cm length, the pulse height P as a function of d is shown in Fig.4.24, where the solid angle subtracted pulse height was plotted. The factor A was 0.033 corresponding to the attenuation length of 30 cm which is much shorter than the attenuation length denoted by the manufacturer (250 cm). Figure 4.24 shows the pulse height distribution well fitted with an exponential function after eliminating the solid angle effect of PMT 1 of the data shown in Fig.4.20. The solid angle corresponding to each position of alpha particles source was calculated, and the results showed that the solid angle mainly influences on the close positions of the source to PMT such as 3 cm or less. Thus, the pulse heights obtained as a function of positions along the rod can be expressed using only an exponential function.

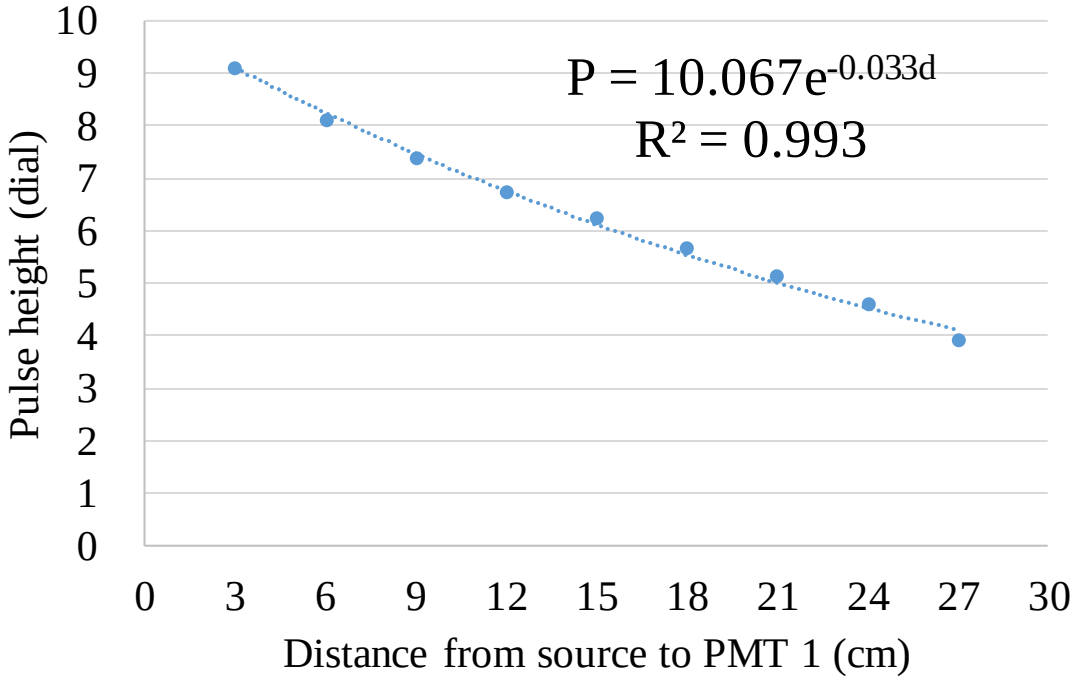

Fig.4.24. The pulse height distribution well fitted with an exponential function after eliminating the solid angle effect of PMT 1 of the data shown in Fig.4.22.

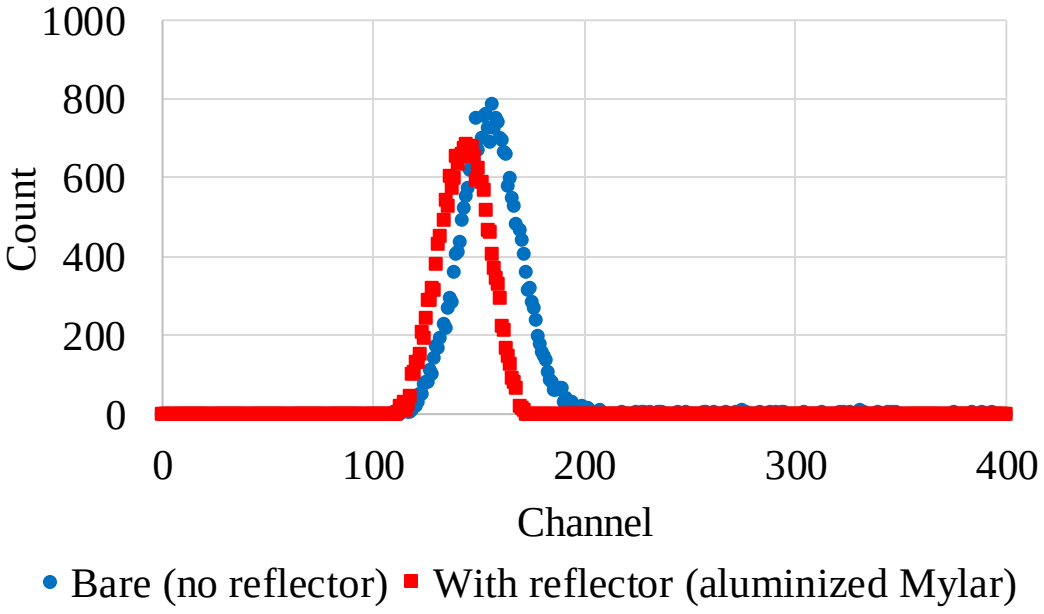

Fig.4.25. Pulse height obtained for the rod irradiated with alpha particle source placed at 15 cm from PMT.

The measured pulse height distribution is assumed to be a Gaussian-shaped peak as shown in Fig.4.25. By applying Gaussian fitting, the pulse height is obtained as the peak centroid. The ratio of the pulse height measured with PMTs at both ends of the rod with and without the aluminized mylar reflector is shown in Fig.4.26. The trends of pulse height ratio are in good agreement in the two cases.

The uncertainty in the pulse height ratio is determined by the standard deviation of the fitted Gaussian-shaped peaks (FWHM/2.35) and by using the error propagation method. The uncertainty ranges from ± 11.1% to ± 27.4% for the rod wrapped in aluminized mylar, and from ± 6.7% to ± 9.3% for the bare rod. The expectation in determining an incidence position was evaluated to be ± 2 ~ 4 cm for the bare rod and ±3 ~ 8 cm for the rod wrapped in aluminized mylar by multiplying the length of the rod 30 cm with the highest uncertainty of pulse height ratio for each case.

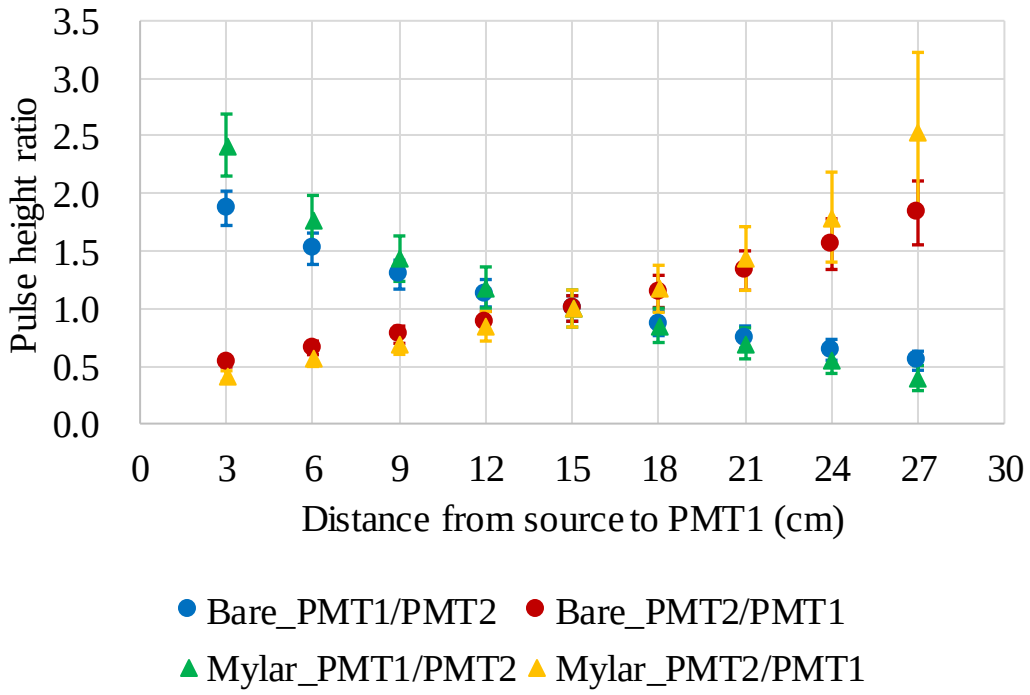

Fig.4.26. The variation of the pulse height ratio for two PMTs as a function of source position.

The reason why the resolution in the rod wrapped in aluminized mylar is worse than that in the bare rod is due to the fluctuation of incident alpha particle energy caused by the aluminized mylar layer. According to the data measured using a Si detector by the manufacturer [9], the average energy of approximately 0.32 MeV is lost in a layer of aluminized mylar for the incidence of 5.5 MeV alpha particles (^{241}Am), and the resolution becomes worse by a ratio of about 1.3 in existence of the reflector. Based on the measured data, at the middle position of plastic scintillator rod (namely at a distance of 15 cm from PMTs), the resolution becomes worse by a ratio of about 1.48 and 1.41 in existence of the reflector for PMT1 and PMT2, respectively, and shows the influence of the aluminized mylar layer on the resolution. Accordingly, the resolution measured in the bare rod is considered to indicate the actual resolution for alpha-particles in the rod wrapped in aluminized mylar.

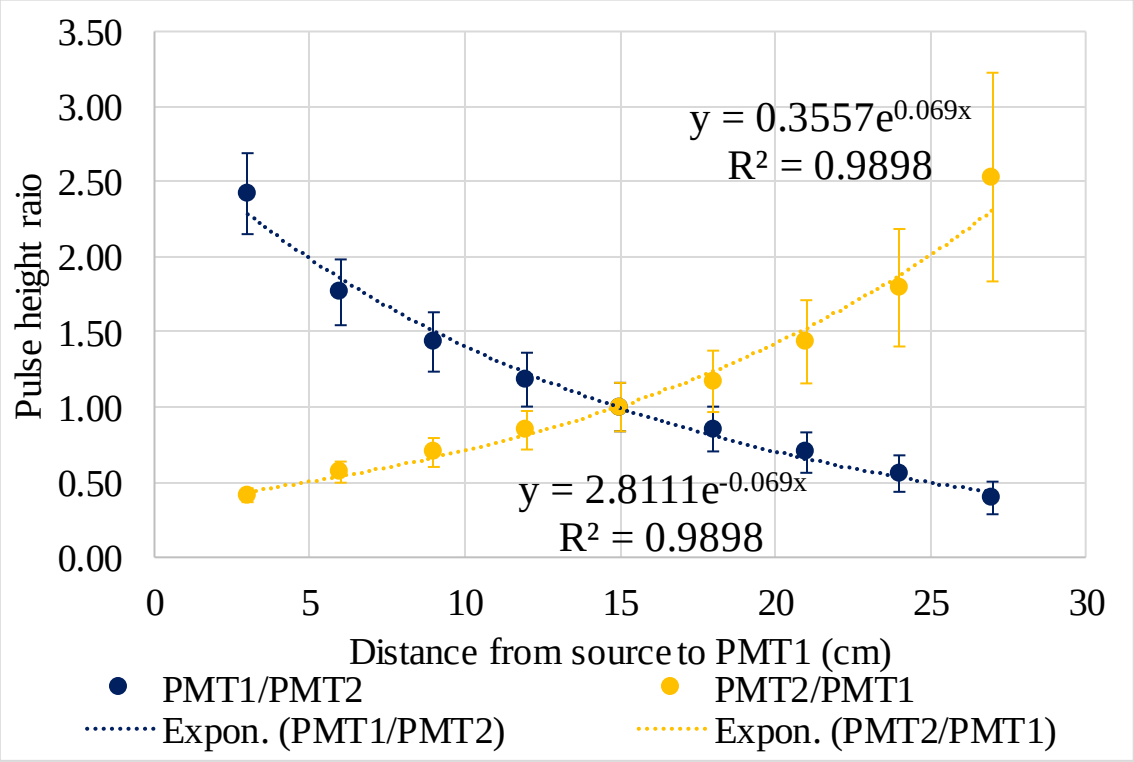

Fig.4.27. The variation of the pulse height ratio for two PMTs as a function of source position for aluminized mylar wrapped rod with fitting exponential function.

Then, the ratio of the pulse height measured with PMTs at both ends of the aluminized mylar reflector rod is shown in Fig.4.27 with the exponential function fitting to show the attenuation along the rod.

4.4.2. Measurements with beta particles

The pulse height distribution obtained from one end PMT as a function of source position with three different reflectors is shown in Fig.4.28, the data were normalized for the gain difference between both end PMTs.

The pulse height at which the source is closer to the PMT is higher because more scintillation photons can reach the PMT.

The ratio of pulse heights measured at both end PMTs for one plastic scintillator rod is shown in Figs.4.29, 4.30 and 4.31. The data are normalized to the measured value at a distance of 5 cm from a specific PMT at one end (PMT 1), which is in the middle of the rod and are given as a function of distance from PMT 1.

In case that the transparency of light in the rod is contributed by the attenuation expressed as an exponential function only:

$$PH1 = A \times exp(-B \times d), \qquad (4.1)$$

$$PH2 = A \times exp[-B \times (L - d)], \quad (4.2)$$

where *PH1* and *PH2* are the pulse height of each PMT, *A* (relating to the total scintillation yield) and *B* are the fitting parameters, *L* is the length of the rod, and *d* is the distance from the source to PMT.

The ratio of pulse heights, which is expressed as equation 4.3 or 4.4, does not depend on the number of scintillation photons generated initially.

$$\frac{PH_1}{PH_2} = exp(30B)exp(-2Bx) \qquad (4.3)$$

$$\frac{PH_2}{PH_1} = exp(-30B)exp(2Bx) \qquad (4.4)$$

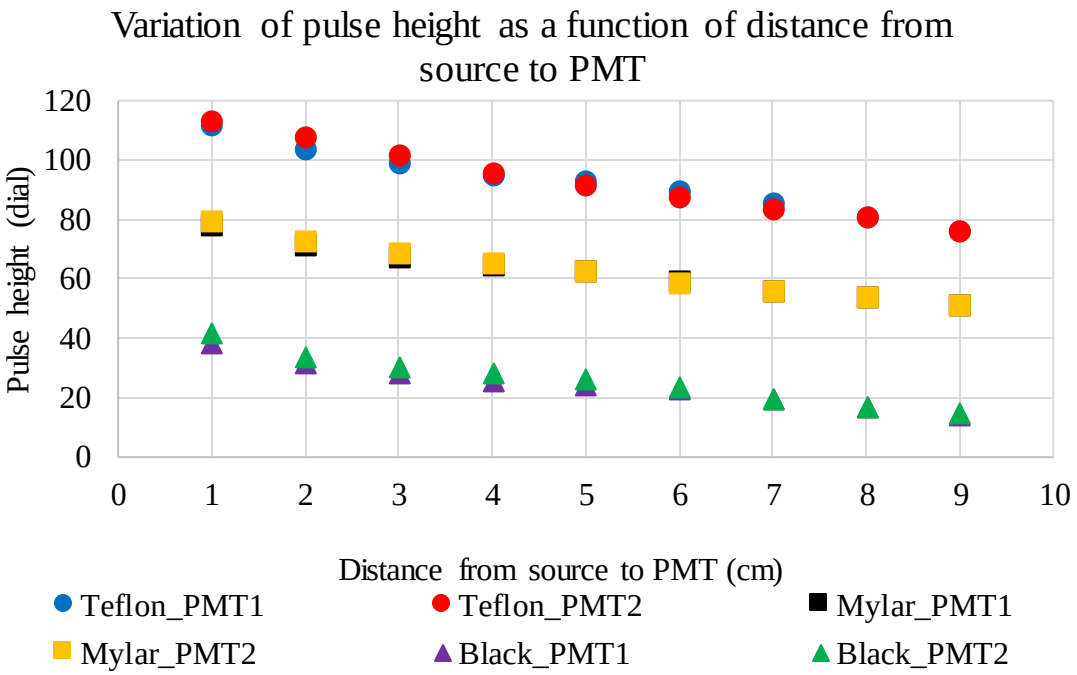

Fig.4.28. The variation of pulse height obtained for both end PMTs as a function of source position with three different reflectors.

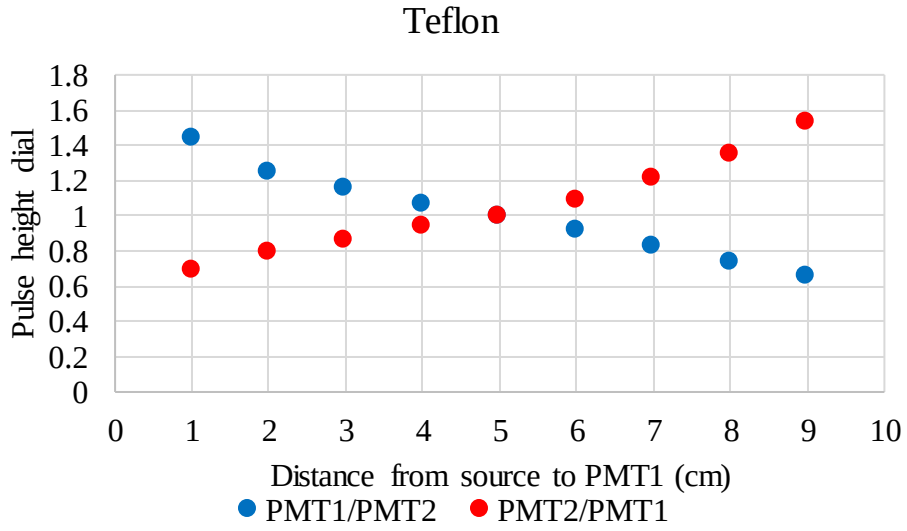

Fig.4.29. The variation of pulse height ratio between two PMTs as a function of source position with teflon reflector.

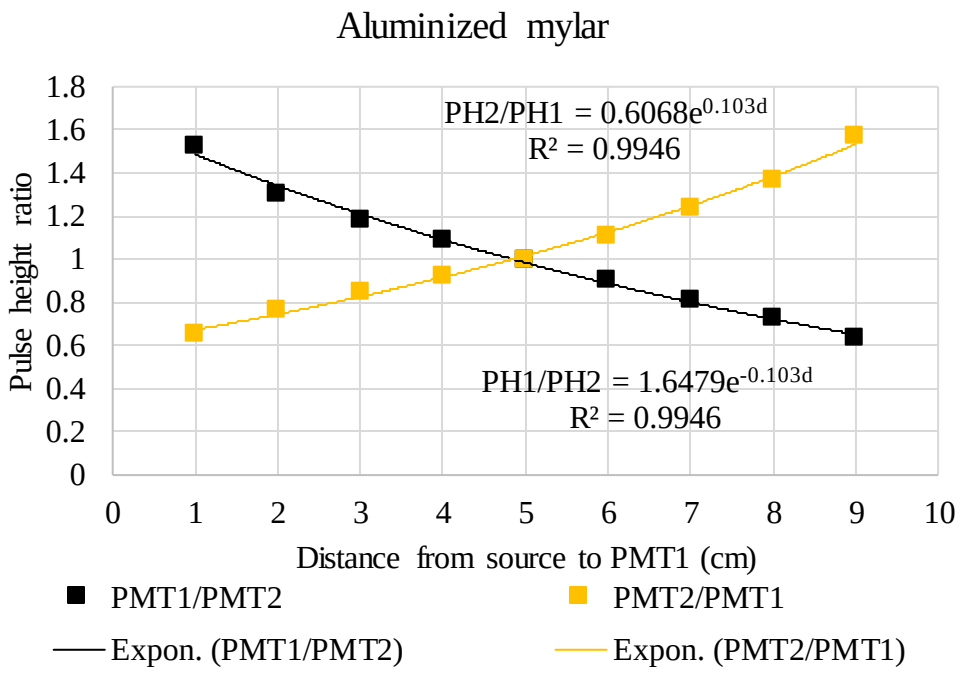

Fig.4.30. The variation of pulse height ratio between two PMTs as a function of source position with aluminized mylar reflector.

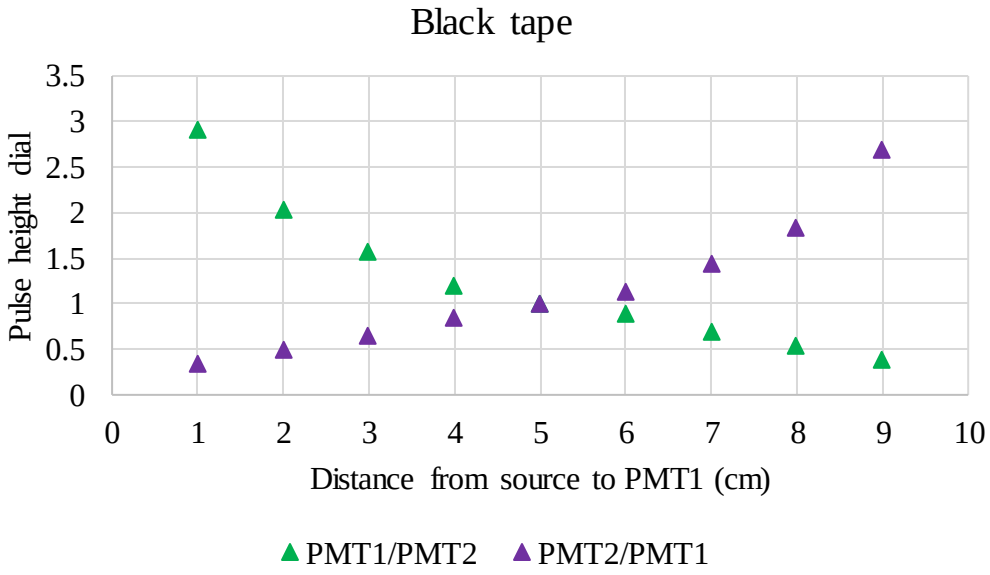

Fig.4.31. The variation of pulse height ratio between two PMTs as a function of source position with black reflector.

For 10 cm plastic scintillator rod, pulse height ratio indicates that aluminized mylar sheet and teflon tape are reflectors of interest due to the approximately good linear

tendency. According to Figure 4.28, the highest pulse heights were obtained with teflon reflector while the black tape's data show the lowest values. However, the observed pulse heights for three different reflectors cannot be compared directly because of the different deposited energy in the plastic scintillator rod by beta particles after passing through the reflector.

For the plastic scintillator rod whose length is around 5 cm and shorter, black tape is a suitable reflector due to high variance in pulse height ratio between each position of the source. Comparing teflon tape and aluminized mylar, the difference in pulse height ratio is larger. Additionally, because aluminized mylar reflector will be used in practical measurement case, data measured with the aluminized mylar reflector is used to evaluate the position sensitivity for beta irradiation, and the fitting with exponential function is shown in Fig.4.30. Then, for the same detector system, the incident position of radiations can be evaluated from the pulse height ratio.

4.5. Response of plastic scintillator for heavy charged particles

The light outputs for H (230 MeV/u) and Si (800 MeV/u) in the plastic scintillator rod system were measured by changing absorbers set in front of the rod systems. The pulse height distributions measured are shown in Figs.4.32 and 4.33. Besides, Fig.4.34 shows the pulse height distribution spectrum of C (400 MeV/u) measured by plastic scintillator rod with the changing of beam incident position in the rod.

The measured pulse height distribution is assumed to be a Gaussian-shaped peak. By applying Gaussian fitting, the pulse height is obtained from the peak centroid, and the FWHM of the peak was also determined. The amount of deposited energies ΔE were calculated using the SRIM2008 code and are presented in Table.4.8. and Table.4.9.

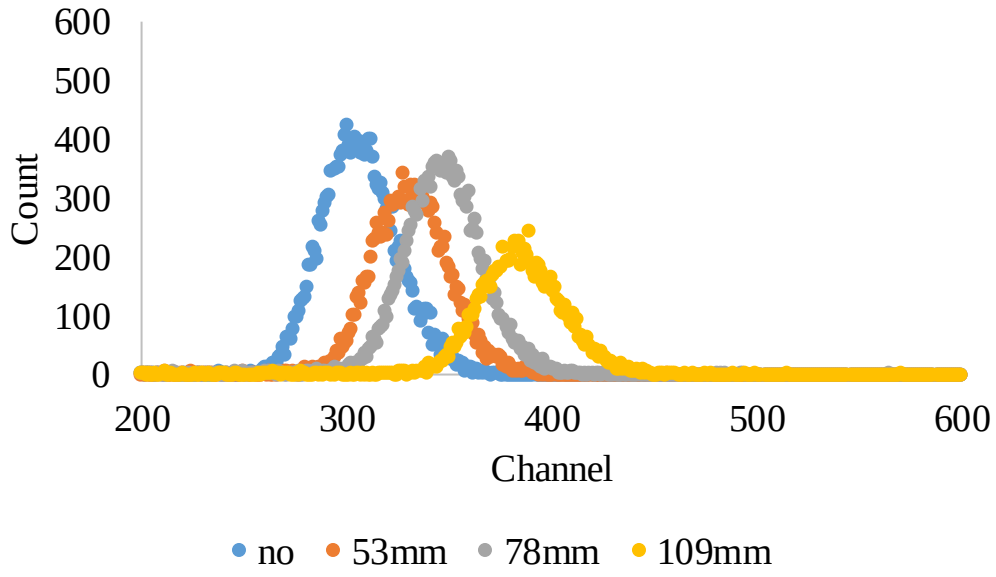

Fig.4.32. Pulse height distribution spectrum of H measured by plastic scintillator rod and the beam incident to the middle of the rod.

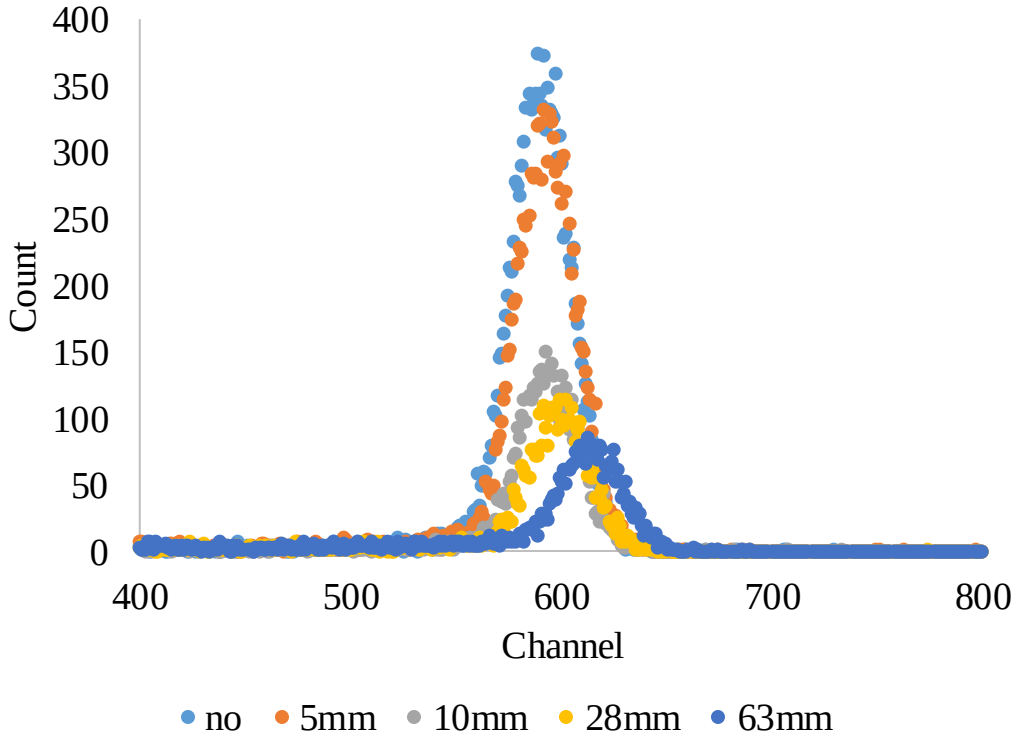

Fig.4.33. Pulse height distribution spectrum of Si measured by plastic scintillator rod and the beam incident to the middle of the rod.

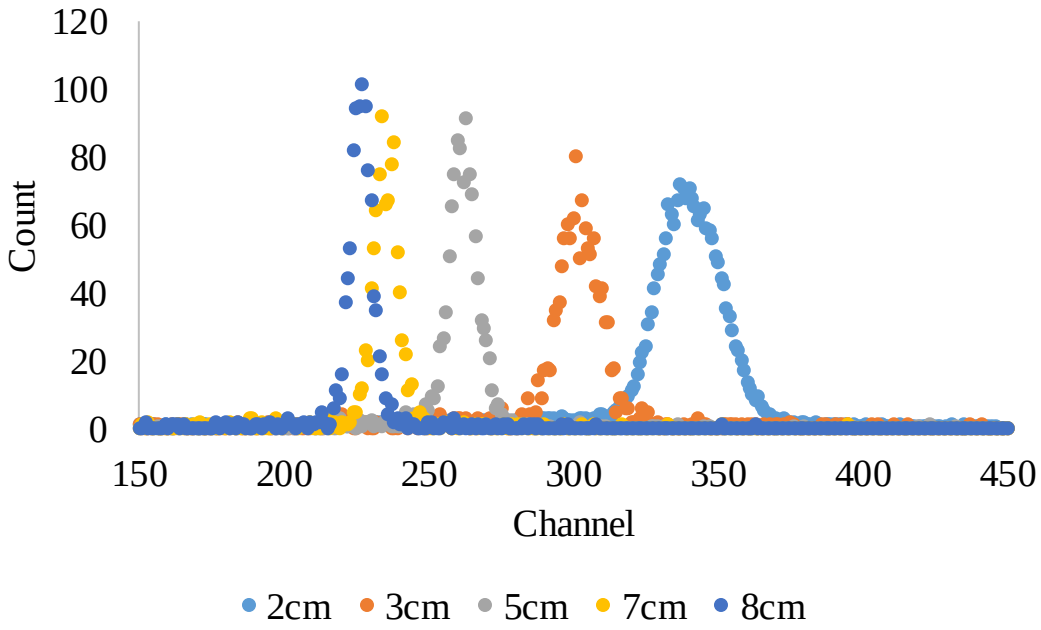

Fig.4.34. Pulse height distribution spectrum of C measured by plastic scintillator rod with the changing of beam incident position in the rod.

Table.4.8. Deposited energy and FWHM (%) in plastic scintillator rod (PMT 1) measuring H.

	Thickness of Al absorber (mm)	Rod 1			Rod 4		
		Incident E (MeV/u)	ΔE (MeV)	FWHM (%)	Incident E (MeV/u)	ΔE (MeV)	FWHM (%)
H	0	230	3.79	11.94	226	3.83	11.11
	53	184	4.38	11.00	179	4.44	10.33
	78	162	4.76	10.22	157	4.85	9.85
	109	135	5.40	10.25	130	5.55	9.70

Table.4.9. Deposited energy and FWHM (%) in plastic scintillator rod (PMT 1) measuring Si.

	Thickness of Al absorber (mm)	Rod 1			Rod 4		
		Incident E (MeV/u)	ΔE (MeV)	FWHM (%)	Incident E (MeV/u)	ΔE (MeV)	FWHM (%)
Si	0	793	415.43	4.76	778	417.95	3.98
	5	776	418.40	4.71	761	420.92	4.01
	10	758	421.28	4.70	743	423.89	3.85
	28	695	432.90	4.70	680	436.32	4.03
	63	573	463.78	4.74	556	469.37	3.84

Measured light yield as a function of LET ($MeVcm^2/g$) of different radiations (beta particle, proton, silicon, and carbon) incident to the middle of the aluminized mylar wrapped rod is shown in Fig.4.35. The LET was determined as the ratio of the deposited energy calculated by SRIM2008 code to the thickness of one rod (9 mm) because these observed radiations passed through one rod. The measured data were compared and in agreement with data obtained in Matsufuji et al. [10].

Besides the light yield, measurements of 10 cm aluminized mylar wrapped rod irradiated by carbon were used for position sensitivity at five incident positions (2cm, 3cm, 5cm, 7cm, and 8cm from the PMT 1). The variation of pulse height ratio as a function of distance from the source to PMT 1 is shown in Fig.4.36 compared with data obtained from beta particles which shown in section 4.1.2. Pulse height ratios obtained with carbon agree well those of beta particles except at position of 2 cm from PMT 1. However, this difference is within 10% which can be accepted for assuming these ratios

have a similar tendency. This agreement in pulse height ratios between two types of radiation confirms the feasibility of using plastic scintillator to determine the position of radiation incidence.

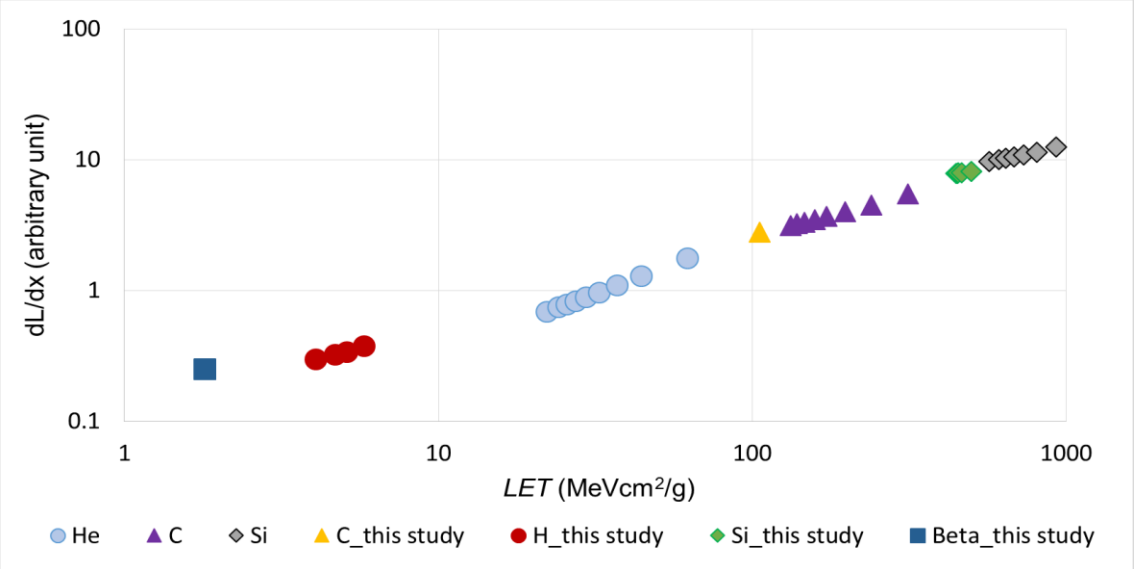

Fig.4.35. Light yield as a function of LET (MeVcm^2/g) of different radiations incident to the middle of the aluminized mylar wrapped rod. The measured data were compared with data in Matsufuji et al. [10].

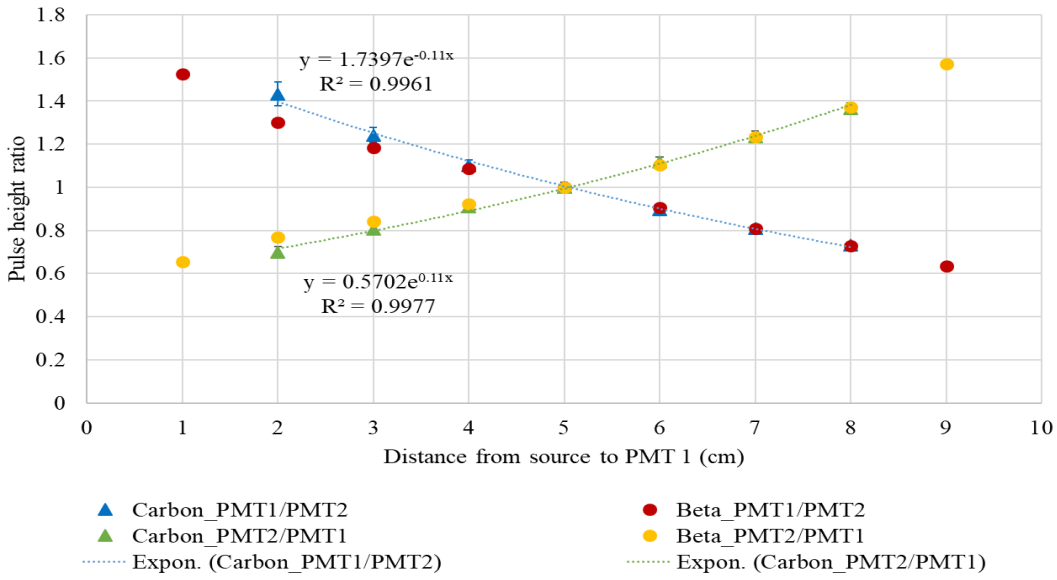

Fig.4.36. Variation of pulse height ratio as a function of distance from source to PMT 1 of 10 cm aluminized mylar wrapped rod.

Similarly to alpha particles case, the ambiguity in the pulse height ratio for carbon ions' data is determined from the standard deviation of the fitted Gaussian-shaped peaks (FWHM/2.*35*) and by using the error propagation method. The ambiguity ranges from ±1.9% to ±3.8%. Then, the expectation in determining an incidence position (position resolution) was evaluated to be ±3.84 mm at the position close to PMT (2 cm), ±2.17 mm at the center position (5 cm), and ±1.88 mm at the furthest position close to PMT (8 cm). The position resolution evaluated with carbon ions' data is much better compared with the one obtained for alpha particles because of the better FWHM (or better energy resolution).

References

[1] S. Sasaki, H. Tawara, K. Saito, M. Miyajima, and E. Shibamura, Average Energies Required per Scintillation Photon and Energy Resolutions in NaI(Tl) and CsI(Tl) Crystals for Gamma Rays, Japanese Journal of Applied Physics 45 (8A), 2006, 6420–6430.

[2] Doke, E. Shibamura, S. Kubota, and K. Terasawa, Maximum scintillation yields in NaI(Tl) and CsI(Tl) crystals estimated from the scintillation model for liquid rare gases, Nuclear Instruments and Methods in Physics Research B 266, 2008, 5063–5066.

[3] J. D. Valentine, D. K. Wehe, G. F. Knoll, C. E. Moss, Temperature Dependence of CsI(Tl) Absolute Scintillation Yield, IEEE Transactions on Nuclear Science 40 (4), 1993, 1267 –1274.

[4] G. Zanella, R. Zannoni, "Absolute light yield of plastic scintillators and cerium scintillating glasses under low energy X-ray excitation, Nuclear Instruments and Methods in Physics Research A 302, 1991, 352 – 354.

[5] Suffian B.M. Tajudin, The Development of Detector and Calibration Field as an Approach of Low Energy Photon Dosimetry, Ph.D. thesis, Department of Accelerator Science, School of High Energy Accelerator Science, The Graduate University for Advanced Studies, Japan, 2015.

[6] L. Swiderski, R. Marcinkowski, M. Moszynski, W. Czarnacki, M. Szawlowski, T. Szczesniak, G. Pausch, C. Plettner, K. Roemer, Electron response of some low-Z scintillators in wide energy range, Journal of Instrumentation 7, 2012, 1 – 10.

[7] P. Limkitjaroenporrn, J. Kaewkhao, P. Limsuwan, W. Chewpraditkul, Nonproportionality of electron response using CCT: Plastic scintillator, Applied Radiation and Isotopes 68, 2010, 1780 – 1784.

[8] H. Hirayama, Y. Namito, A.F. Bielajew, S.J. Wilderman and W.R. Nelson: SLAC-R-730 (2005), KEK Report 2005-8.

[9] Private communication with Oyo Koken Kogyo Co., Ltd.

[10] N. Matsufuji, T. Kanai, H. Komami, T. Kohno, The response of a NE-102 scintillator to passing-through relativistic heavy ions, Nuclear Instruments and Methods in Physics Research A 437, 1999, 346 – 353.

CHAPTER 5 A CONCEPTUAL DESIGN AND OPERATION PRINCIPLES OF THE TISSUE-EQUIVALENT LET SPECTROMETER USING PLASTIC SCINTILLATORS

In this chapter, the conceptual design is shown for a tissue-equivalent LET spectrometer using plastic scintillators. Then, the operation principles of this system are proposed.

5.1. Conceptual design

5.1.1. Design Criteria

A design of a LET spectrometer is performed as the following conditions;

1) In order to realize a dosimeter based on LET spectrometry, a tissue equivalent LET spectrometer will be constructed where plastic scintillators are used a tissue equivalent material.

2) In energy measurements for a variety of heavy charged particles, by way of compensation for ion response in plastic scintillators, a second detector having a flat response for ion species and a good linearity for energy must be introduced. The candidates of a second detector are like a rare gas scintillator, a silicon semiconductor detector (SSD), a rare gas ionization detector, etc.

3) It is appropriate if a second detector has position sensitivity, like a time projection chamber, a proportional counter with resistive wires, etc.

4) It is to be desirable that the spectrometer can detect radiation with a solid angle close to 4π directions.

In this study, the LET spectrometer composed of two layers of three sets of four plastic scintillator rods and a 2-dimensional silicon position sensitive detector (where double-sided Si detector; DSSD is considered) are settled in a sandwich structure will be designed, and the operational principles are discussed. The conceptual illustration of the LET spectrometer is shown in Fig.5.1.

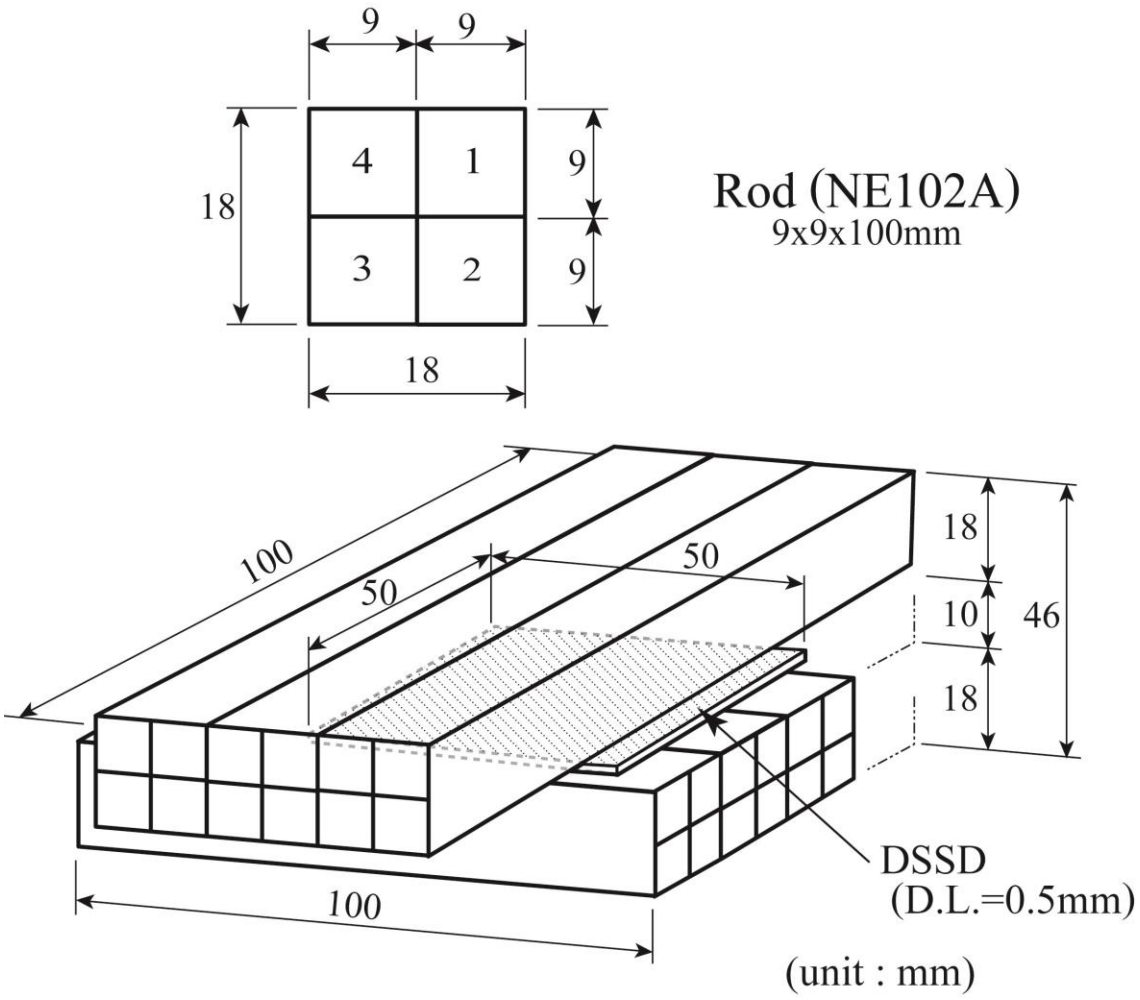

Fig.5.1. Conseptual drawings for the LET spectrometer designing in this study.

5.1.2. Spectrometer Design

In the front and the side views, schematic designs for the spectrometer are shown in Figs.5.2, and 5.3. As described previously, the spectrometer consists of two systems of plastic scintillators aligned perpendicular to each other, and the distance between them is 1 cm where a 2-dimensional silicon position sensitive detector (double-sided Si detector; DSSD is considered) is placed in the middle. The distance of 1 cm is set in consideration of 4π detection for the whole system.

Each plastic scintillator system includes two layers, and there are six plastic scintillator rods in each layer. Thus, there are twelve scintillators in total for each system. $S_{A1} - S_{A6}$ and $S_{B1} - S_{B6}$ denote the plastic scintillators in the first and second layers of the horizontal system (x-axis). Similarly, $S_{C1} - S_{C6}$ and $S_{D1} - S_{D6}$ denote the plastic scintillators in the first and second layers of the vertical system (y-axis). Each plastic scintillator rod, which is NE-102, is 9 mm x 9 mm x 100 mm in dimension. The plastic scintillator rods have polished surfaces and each rod is wrapped in one layer of aluminized mylar sheet (thickness of 1.5 μm). Both ends of each scintillator rod are coupled to photomultiplier tubes.

A double-side SiPSD (DSSD) is 5 cm x 5 cm in dimension and has a thickness of 500 μm. Each side has 16 read-outs corresponding to 16 strips. At this stage, the electronic circuit, as well as data recorded system, were not described in detail.

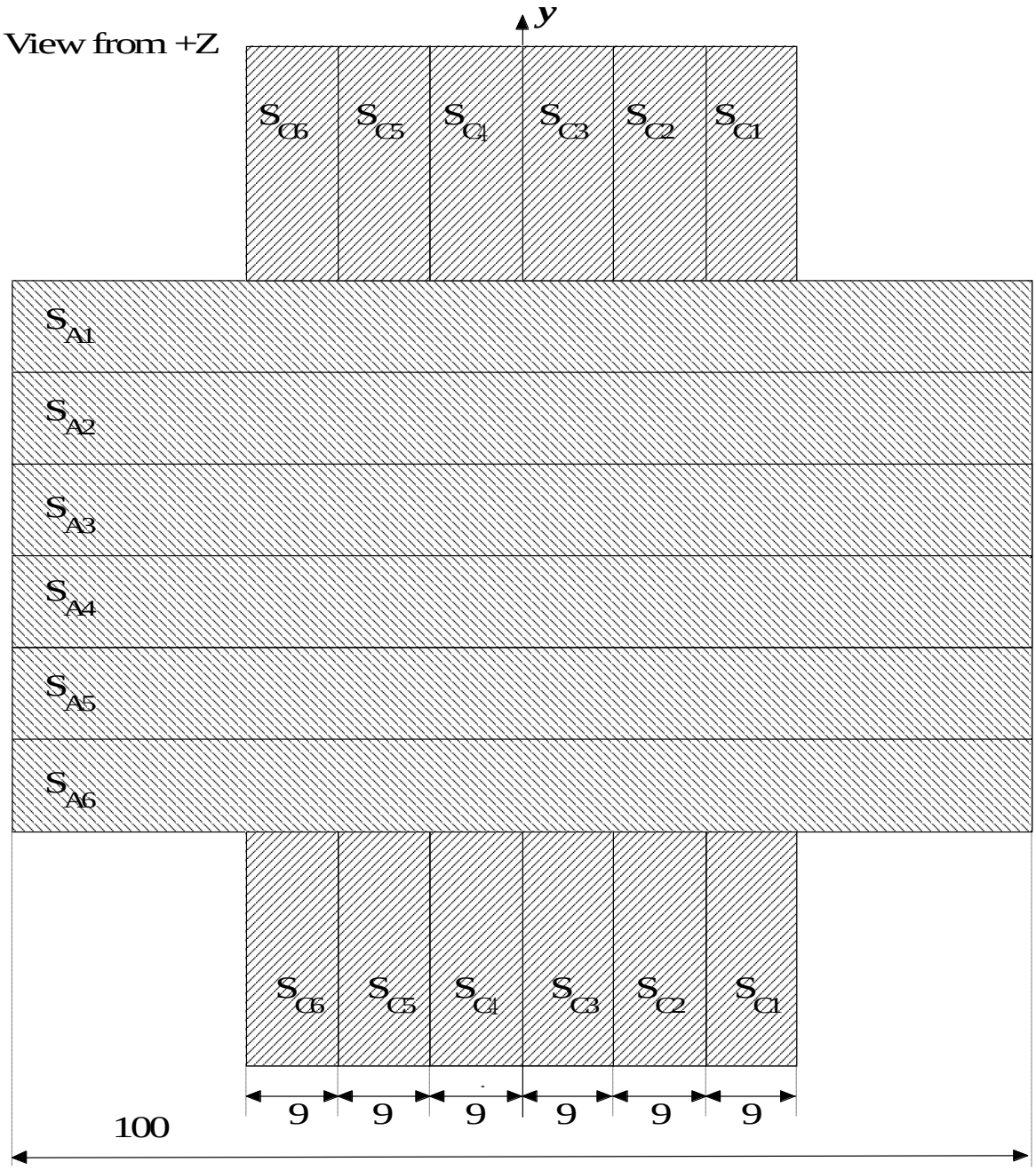

Fig.5.2. The front view of the schematic design of the LET spectrometer.

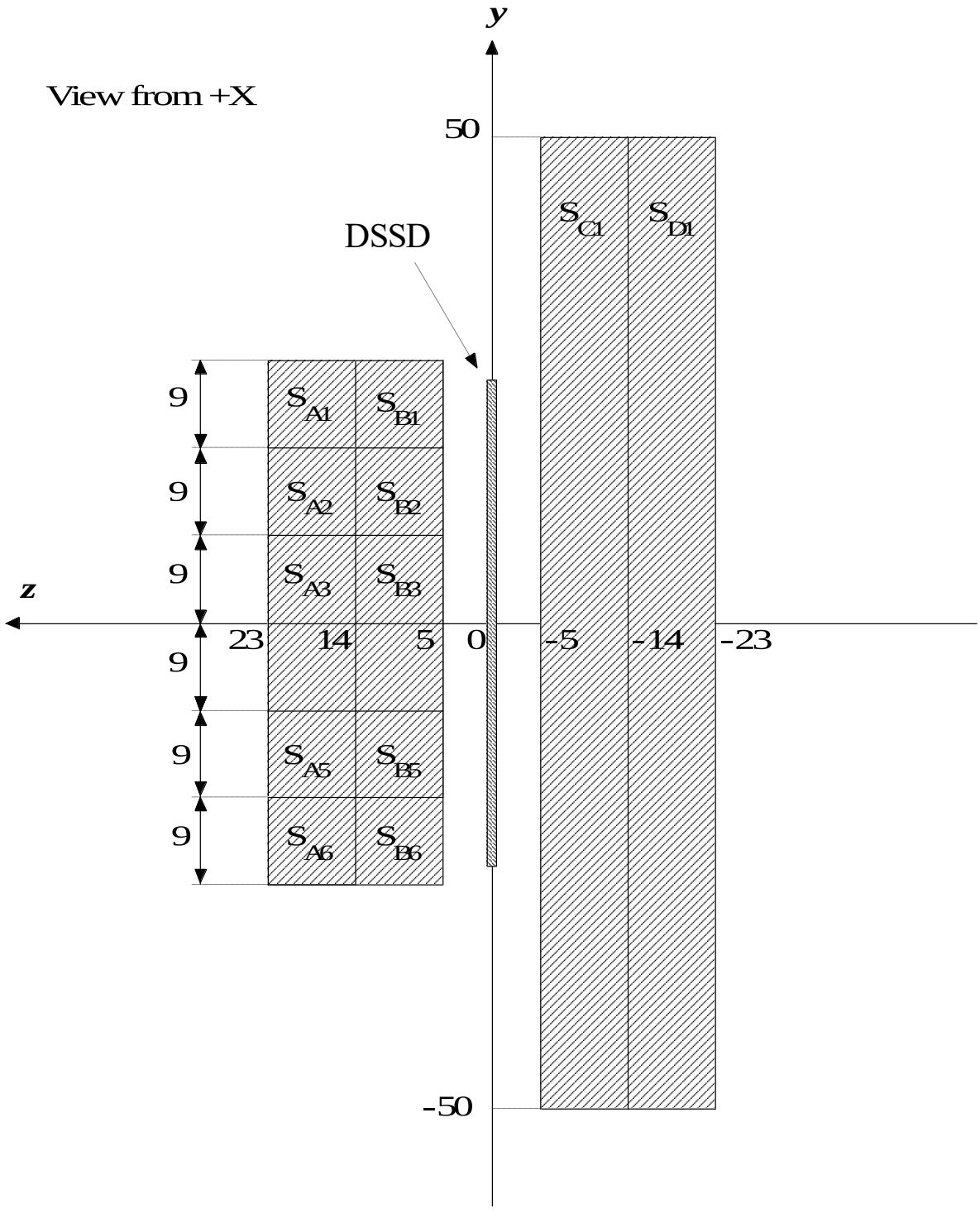

Fig.5.3. The side view of the schematic design of the LET spectrometer.

5.2. Operation principles

5.2.1. Determing the deposited energy

The position sensitivity measurement is performed for the plastic scintillator by the ionizing radiation, and the relationship between the output signals and the irradiated position can be established for each plastic scintillator rod in the system.

The energy calibration is performed for the DSSD. Then, for any radiation incident to the DSSD, the deposited energy can be obtained.

For ionizing radiation with known species and energies, the energy depositions in the front (1^{st}) plastic scintillator system E_1 and in the rear (2^{nd}) plastic scintillator system E_2 can be determined from the SCRIM2008 code. The corresponding output signals O_1, O_2, and O_{Si} of plastic scintillators and DSSD are measured. Then, the energy ratio E_1/E_{Si} and E_2/E_{Si}; and output signal ratio O_1/O_{Si} and O_2/O_{Si} are determined.

For unknown ionizing radiation, the deposited energies E_1 and E_2 can be obtained from the deposited energy E_{Si} measured with the DSSD by calculating the ration E_1/E_{Si} and E_2/E_{Si}. In addition, it is noted that approximate species of ionizing radiation are possibly known from the relation of O_1/E_1 or O_2/E_2 and the LET, by using data obtained by Matsufuji et al. [1]. Furthermore, the incident energy of ionizing radiation E_0 might be evaluated from the information of both the species of radiation and the LET.

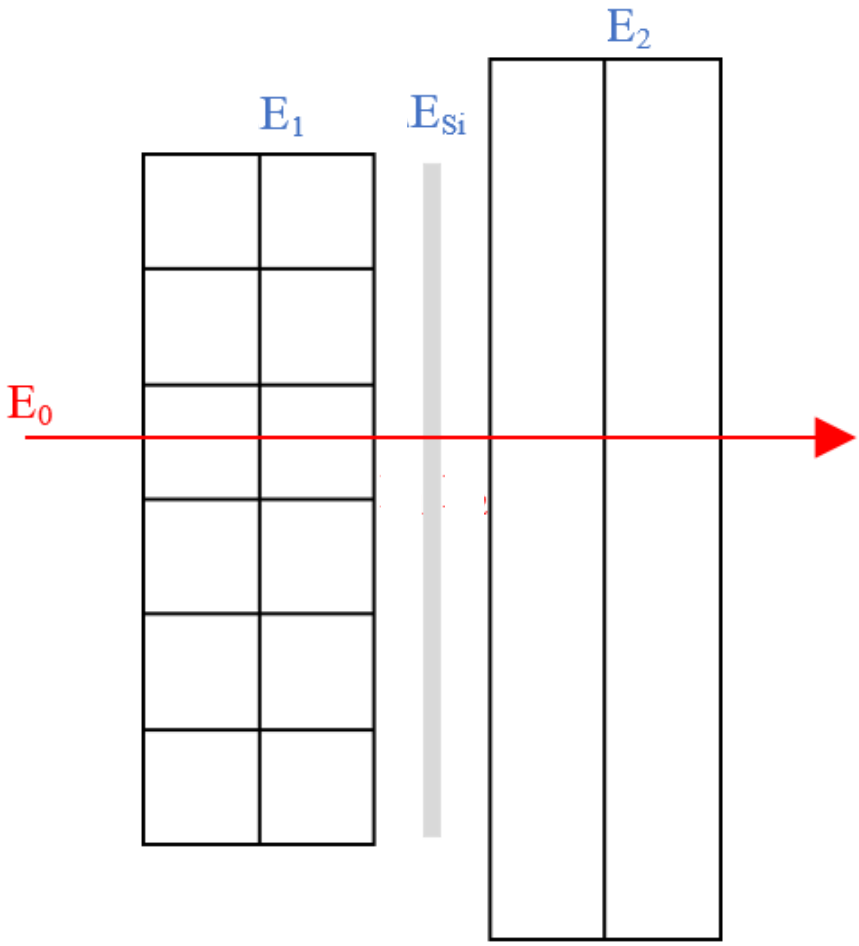

Fig.5.4. The energy determination in the LET spectrometer irradiated with energy E_0.

5.2.2. Determining the track length

Considering one example of track length corresponding to one ion which enters the dosimeter at a point (X = 27, Y = 27, Z = 23) and exits at (X = -27, Y = -27, Z = -23) as shown as the red arrow in Figs 5.5, 5.6, and 5.7.

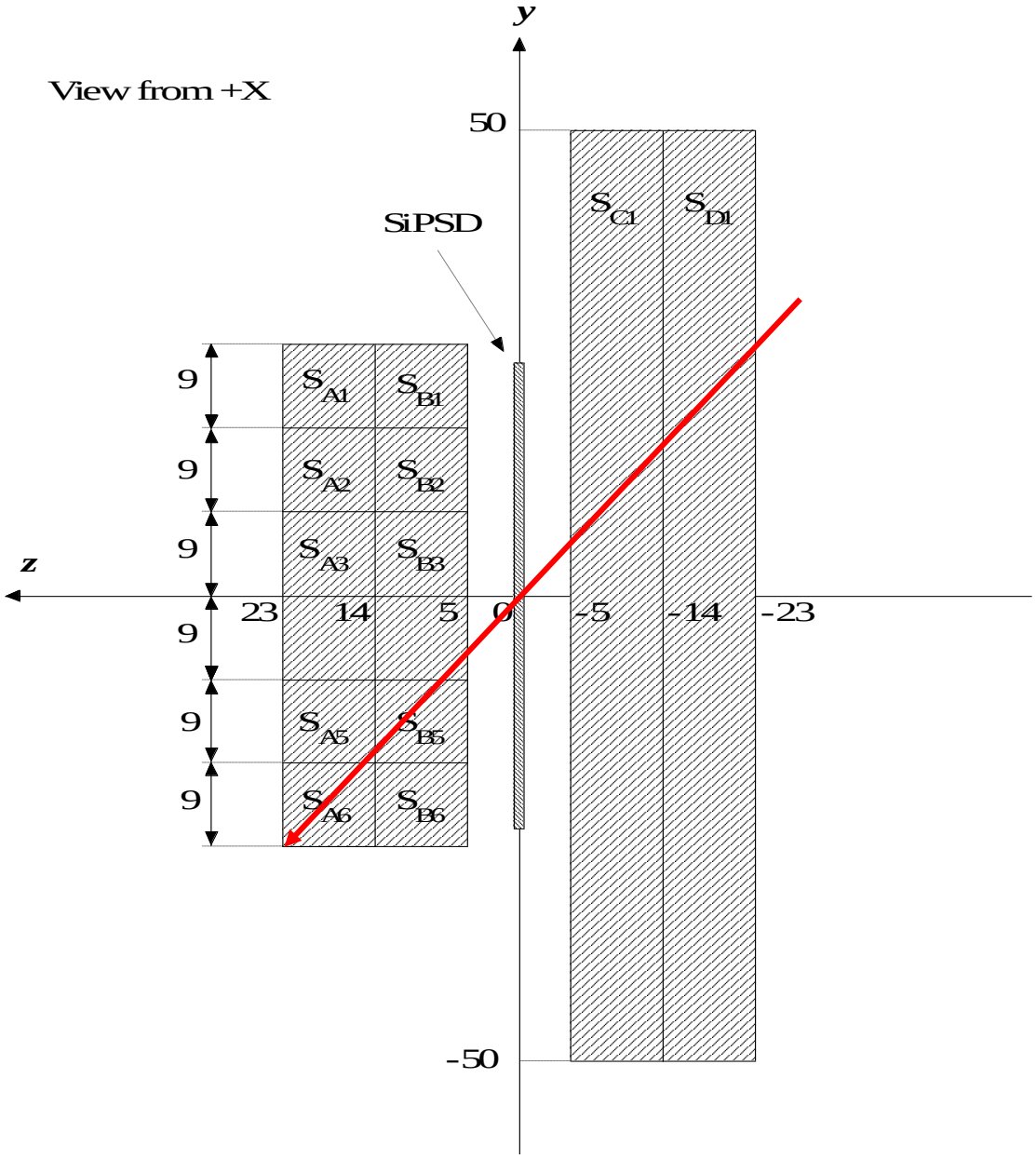

Fig.5.5. The front view of the schematic design of the LET spectrometer with ion's track.

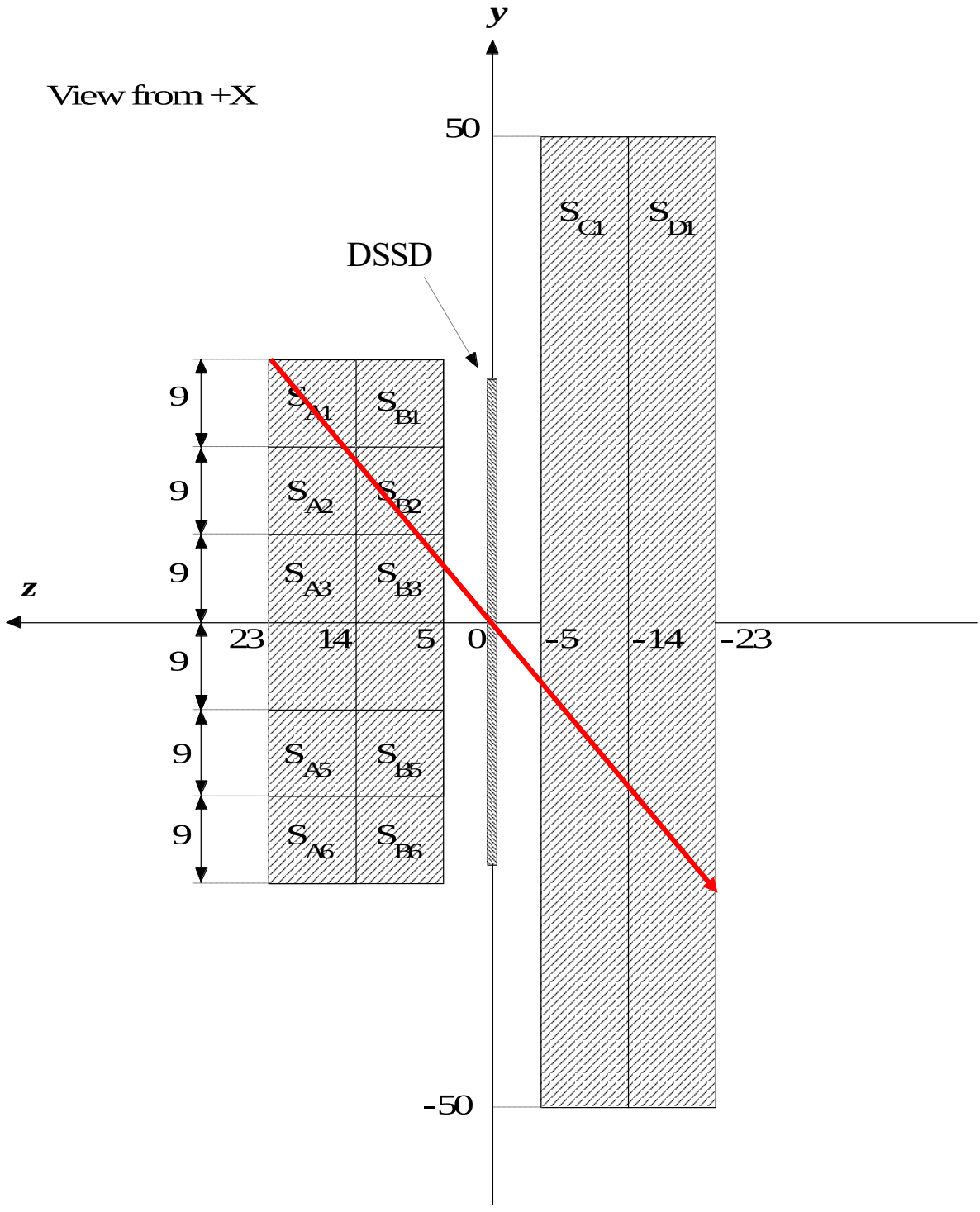

Fig.5.6. The side view of the schematic design of the LET spectrometer with ion's track.

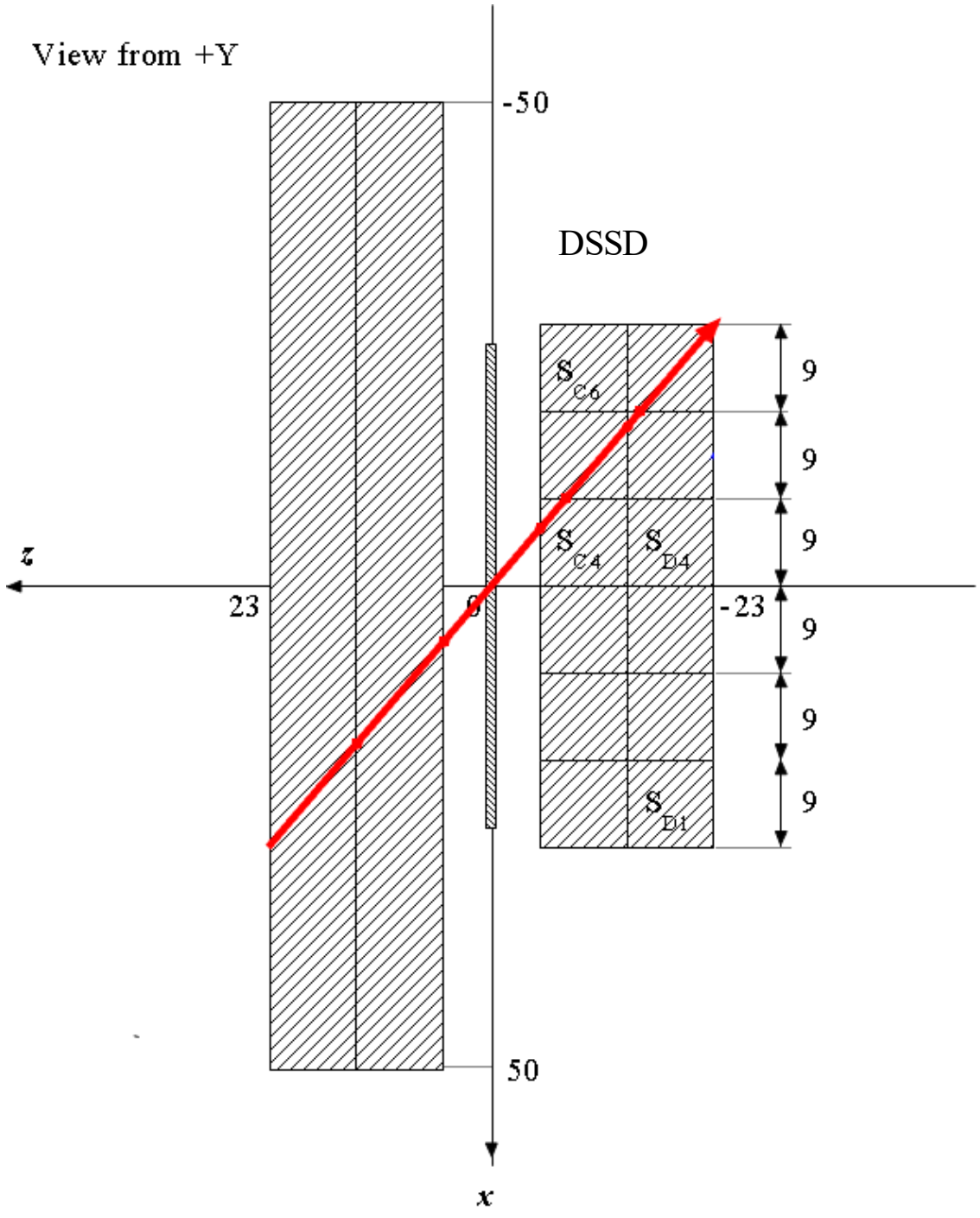

Fig.5.7. The side view of the schematic design of the LET spectrometer with ion's track.

According to the illustration, the track passes through plastic scintillators A1, A2, B2, B3, C4, C5, D5, D6, and DSSD; and track lengths in A1, B2, C5, and D6 are the dominant contribution. Firstly, the coincidence events between A1, B2, C5, D6, and DSSD are recorded.

With the first plastic scintillator system which consists of A and B layers, it is assumed that the interaction point of radiation in each plastic scintillator is at the center of the rod such as plastic scintillator A1 (X1, 22.5, 18.5), B2 (X2, 13.5, 9.5). The X positions are determined by referred the measured pulse height ratio to the exponential function obtained with carbon data. The uncertainties for X, Y, Z are considered as $\sigma_X = \pm 1.88\ mm$ (best position resolution determined from carbon ions' data), $\sigma_Y = \sigma_Z = \pm\, 4.5/\sqrt{3} = \pm 2.60\ mm$ determined from the rod's width 9 mm.

Similarly, with the second plastic scintillators system which consists of C and D layers, it is assumed that the interaction point of radiation in each plastic scintillator is at the center of the rod such as plastic scintillator C5 (-13.5, Y1, -9.5), D6 (-22.5, Y2, -18.5). The Y positions are determined by referred to the measured pulse height ratio to the exponential function obtained with carbon data. The uncertainties for X, Y, Z are considered as $\sigma_Y = \pm 1.88\ mm$, $\sigma_x = \sigma_Z = \pm\, 4.5/\sqrt{3} = \pm 2.60\ mm$ determined from the rod's width 9 mm.

Based on these interaction points, the track length L of radiation in spectrometer and uncertainty σ_L are calculated.

$$L = \sqrt{L_X^2 + L_Y^2 + L_Z^2}\,, \tag{5.1}$$

$$\sigma_L = \sqrt{\left(\frac{dL}{dL_X}\right)^2 \sigma_{L_X}^2 + \left(\frac{dL}{dL_Y}\right)^2 \sigma_{L_Y}^2 + \left(\frac{dL}{dL_Z}\right)^2 \sigma_{L_Z}^2}\,, \tag{5.2}$$

where L_X, L_Y, L_Z and $\sigma_{L_X}, \sigma_{L_Y}, \sigma_{L_Z}$ are the length and uncertainty in X, Y, and Z dimension.

Then, with the information about the deposited energy E and the track length L, the LET and uncertainty σ_{LET} are calculated.

$$LET = \frac{E}{L}. \quad (5.3)$$

$$\sigma_{LET} = LET \sqrt{\left(\frac{\sigma_E}{E}\right)^2 + \left(\frac{\sigma_L}{L}\right)^2}. \quad (5.4)$$

Reference

[1] N. Matsufuji, T. Kanai, H. Komami, T. Kohno, The response of a NE102 scintillator to passing-through relativistic heavy ions, Nuclear Instruments and Methods in Physics Research A 437, 1999, 346 – 353.

CHAPTER 6 CONCLUSION

In this study, properties of plastic scintillators were examined to use this material in designing a tissue-equivalent LET spectrometer. The properties of three plastic scintillators EJ-200, EJ-212, and EJ-252 are studied.

EJ-200 and EJ-212 are commercially available, both of them have the density and the effective atomic number close to those of water and human tissues. Besides, EJ-252 is an air-equivalent scintillator and is a potential candidate for developing an air-equivalent dosimeter. The three plastic scintillators were examined to check whether there are any differences in their behaviors or not.

The absolute light yields of plastic scintillators measured as W_s are 104 ± 9, 93 ± 8, and 146 ± 13 eV in EJ-200, EJ-212, and EJ-252, respectively.

The scintillation efficiency defined as "electron response" are determined for plastic scintillators by the CCT measurement. The electron response of plastic scintillators approaches a saturated value in the high energy region, while indicates a reduction in the energy region lower than 150 keV. This reduction is suggested being caused by the quenching effects at high dE/dx where excited and ionized molecules are in high density and possibly lose their energy by collisions leading to the degradation in the light output.

The electron response measured in this study is compared with data from other studies. These data are in agreement with each other in the energy range from 100 keV and above. In the lower energy region, electron responses measured in this study have lower values than other studies'. The electron response of the lowest energy (about 35 keV), which corresponds to the scattering angle of 15°, shows the highest amount of different from the others. Although the reason for this difference cannot be explained at present, the electron response in this study was measured by two ways using NaI(Tl) and

HPGe detectors and the results are consistent.

The energy resolution of plastic scintillators is evaluated from the CCT measurement. The intrinsic resolution of EJ-200, EJ-212, and EJ-252 in the energy range around 450 keV is 13.0%, 11.2%, and 13.9%, respectively, where the statistical fluctuation is 8.7%, 8.3%, and 10.4%, respectively. Since the trend in energy resolutions getting worse in the low energy region seems to be coincident with the reduction in the electron response below the energy of approximately 150 keV, the worse resolution is attributed to the fluctuation in scintillation efficiency due to secondary electrons generated by a monochromatic recoil electron. However, the explanation of the difference between δ_{sc} and δ_{st} in the low energy side is not made clear at this stage because of not having enough understandings of this mechanism.

The position sensitivity is examined by using 10cm and 30 cm long plastic scintillator rods. The nature of light transparency in the rod is studied by using data obtained with 30 cm aluminized mylar wrapped rod irradiated with alpha particles. As a result, the attenuation of light along the rod is expressed as an exponential function. Data obtained with 10 cm rod, which was wrapped in the aluminized mylar reflector, irradiated with beta particles are used to examine the position sensitivity.

The response of plastic scintillators to heavy charged particles (proton, silicon and, carbon) are examined. The position sensitivity of plastic scintillator is confirmed with another data of carbon with the position resolution is evaluated to be from ± 1.88 mm to ± 3.84 mm.

Based on the results of energy and position sensitivity measurements in this study, a conceptual design and operation principles of a tissue-equivalent LET spectrometer using plastic scintillators are proposed.

The spectrometer consists of two systems of plastic scintillators aligned perpendicular to each other, and the distance between them is 1 cm where a 2-dimensional silicon position sensitive detector (double-sided Si detector – DSSD is considered as a second detector) is placed in the middle.

The deposited energy, as well as the ambiguity, can be determined from the calibration of the plastic scintillators or from the measured energy by the second detector.

The X positions are determined by referred to the measured pulse height ratio to the exponential function obtained with carbon data (X-axis is the horizontal which is along the length of the plastic scintillator rod). The uncertainties for X, Y, Z are considered as $\sigma_X = \pm 1.88\ mm$ by using the best position resolution obtained for carbon data, $\sigma_Y = \sigma_Z = \pm 2.60\ mm$ determined from the rod's width of 9 mm.

Based on the present consideration, it is possible to turn the conceptual design of a tissue-equivalent LET spectrometer into a prototype. Then, several tests would be performed to have detailed examinations of the deposited energy and the track length of the incident radiation for this LET spectrometer.

List of Academic works

[1] **Ngan N. T. Tran**, Shinichi Sasaki, Toshiya Sanami, Yuji Kishimoto, Eido Shibamura, "Measurements of Electron Response and Average Energy Required per Scintillation Photon in Plastic Scintillators for Gamma Rays", Oral presentation at the 77th JSAP Autumn Meeting, 13 – 16 September 2016, Niigata, Japan.

[2] **Ngan N. T. Tran**, S. Sasaki, T. Sanami, Y. Kishimoto, and E. Shibamura, "Scintillation Efficiency in Plastic Scintillators Measured as a Function of Electron Energy", Oral presentation at the 31st Workshop on Radiation Detectors and Their Uses, 23 – 25 January 2017, KEK Tsukuba, Japan.

[3] **Ngan N. T. Tran**, Shinichi Sasaki, Toshiya Sanami, Yuji Kishimoto, Eido Shibamura, "Measurements of Electron Response and Average Energy Required per Scintillation Photon in Plastic Scintillators for Gamma Rays (II)", Oral presentation at the 64th JSAP Spring Meeting, 17 – 20 March 2017, Yokohama, Japan.

[4] **Ngan N. T. Tran**, Shinichi Sasaki, Toshiya Sanami, Yuji Kishimoto, Eido Shibamura, "Characterizing the Position Sensitivity in Plastic Scintillators", Oral presentation at the 78th JSAP Autumn Meeting, 5 – 8 September 2017, Fukuoka, Japan.

[5] **Ngan N. T. Tran**, S. Sasaki, T. Sanami, Y. Kishimoto, and E. Shibamura, "Scintillation Efficiency and Position Sensitivity for Radiation Events in Plastic Scintillators", Poster presentation at 14th International Conference on Scintillating Materials and Their Applications, 18 – 22 September 2017, Chamonix, France.

[6] **Ngan N. T. Tran**, Shinichi Sasaki, Toshiya Sanami, Yuji Kishimoto, Eido Shibamura, "Characterizing the Electron Response and Position Sensitivity for Radiation in

Plastic Scintillators", Poster presentation at 2017 IEEE Nuclear Science Symposium and Medical Imaging Conference, 21 – 28 October 2017, Atlanta, USA.

[7] **Ngan N. T. Tran**, Shinichi Sasaki, Toshiya Sasami, Yuji Kishimoto, and Eido Shibamura, "Some Properties of Plastic Scintillators to Construct a LET Spectrometer", Oral presentation at the 2nd International Symposium on Radiation Detectors and Their Uses, 23 – 26 January 2018, KEK Tsukuba, Japan.

List of publications

[1] Eido Shibamura, Shinichi Sasaki, **Ngan N. T. Tran**, "Systematic Study of Inorganic and Organic Scintillator Light Yields," Proceedings of the International Symposium on Radiation Detectors and Their Uses, JPS Conf. Proc. 11, 020004, 1 (2016).

[2] **Ngan. N. T. Tran**, S. Sasaki. T. Sanami, Y. Kishimoto and E. Shibamura, "Scintillation Efficiency in Plastic Scintillators Measured as a Function of Electron Energy," Proceedings of the 31st Workshop on Radiation Detectors and Their Uses, Japan, KEK Proceedings 2017-9, 1 (2017).

[3] **Ngan N. T. Tran**, Shinichi Sasaki, Toshiya Sanami, Yuji Kishimoto, Eido Shibamura, "Characterizing the Electron Response and Position Sensitivity for Radiation in Plastic Scintillators," Conference record of 2017 IEEE Nuclear Science Symposium and Medical Imaging Conference, 21-28 October 2017, Atlanta, Georgia, USA, 1 (2017).

[4] **Ngan. N. T. Tran**, S. Sasaki. T. Sanami, Y. Kishimoto and E. Shibamura, "Scintillation Efficiency and Position Sensitivity for Radiation Events in Plastic Scintillators," IEEE Transactions on Nuclear Science, 65, 2178 (2018).

[5] **Ngan. N. T. Tran**, Shinichi Sasaki. Toshiya Sanami, Yuji Kishimoto and Eido Shibamura, "Some Properties of Plastic Scintillators to Construct a LET Spectrometer," Proceedings of the 2nd International Symposium on Radiation Detectors and Their Uses (2018) (to be published on JPS Conf. Proc.).